Max L. Porter Robert J. Guinn Jr. Andrew L. Lundy
Dustin D. Davis John G. Rohner

Investigation of Glass Fiber Composite Dowel Bars For Highway Pavement Slabs

June 2001

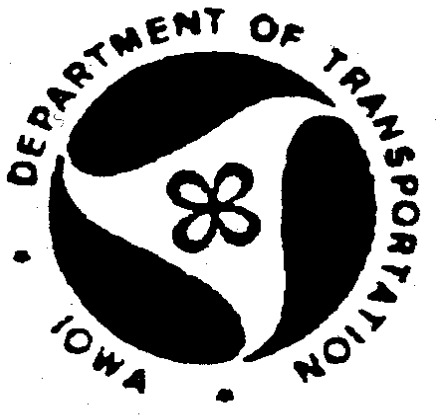

Submitted to:

Highway Division of the
Iowa Department of Transportation
and
Iowa Highway Research Board

Project Number: TR-408

final

report

Max L. Porter Robert J. Guinn Jr. Andrew L. Lundy
Dustin D. Davis John G. Rohner

Investigation of Glass Fiber Composite Dowel Bars For Highway Pavement Slabs

Project Number: TR-408

June 2001

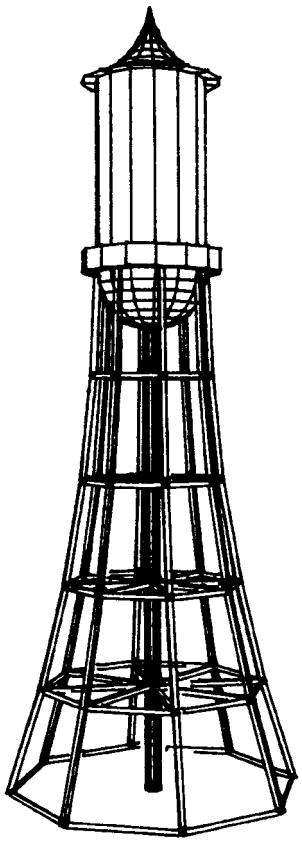

Engineering Research Institute

Iowa State University

Disclaimer

The contents of this report do not represent a warranty of the products used on behalf of the State of Iowa, Iowa State University, Iowa Department of Transportation, Highway Research Board, or the authors. The opinions, findings, and conclusions expressed in this publication are those of the authors and not necessarily those of the Highway Division of the Iowa Department of Transportation. Engineering data, designs, and suggested conclusions should not be used without first securing competent advice with respect to the suitability for any given application. The responsibility for the use of information in this report remains with the user. This report is for information purposes and is made available with the understanding that it will not be cited without the permission of the authors.

TABLE OF CONTENTS

LIST OF FIGURES

List of Tables

1.0 INTRODUCTION

1.1 Background

America's roadways are in serious need of repair. According to the American Society of Civil Engineers (ASCE) one third of the nation's roads are in poor or mediocre condition [1]. In the latest report prepared by ASCE, these conditions were estimated to cost American drivers $5.8 billion and as many as 13,800 fatalities a year from 1999 to 2001 [1]. A considerable amount of the damage is due to the premature deterioration of concrete resulting from the corrosion of steel reinforcement. Fabricating this reinforcement using a material and/or shape conducive to transferring wheel loads will help to aid in minimizing roadway damage.

Load transfer within a series of concrete slabs takes place across the joints. For a typical concrete paved road, these joints are approximately 1/8" gaps between two adjacent slabs. Dowel bars are located at these joints and used to transfer load from one slab to an adjacent slab. After a significant number of vehicles have passed over the joint an oblonging where the dowel bar contacts the concrete can occur. This oblonging creates a void space. This void space is formed due to a stress concentration where the dowel contacts the concrete at the joint face directly above and below the dowel. Over time, the repeated process of traffic traveling over the joint crushes the concrete surrounding the dowel bar and causes a void in the concrete. This void inhibits the dowels ability to effectively transfer load across the joint.

Possible corrosion of the dowel bar can potentially bind or lock the joint. When locking of the joint occurs no thermal expansion is allowed and new cracks parallel to the joint are formed directly behind the dowel bars in the concrete. As temperature

decreases, contraction of the concrete will occur resulting in the new cracks becoming wider and a resulting load transfer failure. Once there is no longer load transferred across the joint all the load is then transferred to the subgrade and differential settlement of the adjacent slabs occurs. Differential settlement of the slabs creates a vertical discontinuity at the joints, making vehicle travel uncomfortable, and requires that the slab be repaired or replaced.

A majority of the dowel bars used today for load transfer are epoxy coated. This epoxy coating aids in the reduction of the exposure to corrosive agents. However, many times this coating is nicked or scraped before installation leaving the uncoated steel susceptible to deterioration.

As was mentioned previously, a void around a dowel bar is formed by stress concentrations crushing the concrete directly in contact with the dowel. When a wheel load is applied to the concrete slab the force is supported only by the top or bottom of the dowel bar, not the sides. Since the stress concentration region lies on the top or bottom of the dowel bar, the smaller the dowel the higher the stress concentration. The sides of the dowel bar do not aid in the distribution of the wheel load from the concrete. Therefore, the top and bottom of the dowel bar at the face of the joint is where the stress concentration is located and is directly related to the width and/or shape of the dowel bar. While round dowel bars handle these stress concentrations relatively well, other shapes and materials may provide a better distribution.

1.2 Experimental and Analytical Investigation

Before a change can even be considered, contractors, engineers, owners and manufacturers want to be certain that a new product or procedure will yield beneficial

results when compared to the current method of construction. The following research was conducted in order to compare the performance of epoxy coated dowel bars to dowel bars of alternative shapes and materials such as stainless steel and glass fiber reinforced polymer (GFRP). Research was also done on the effect that dowel bar spacing has on the performance of concrete pavements. Four phases of this research are described in this report.

1.2.1 Objective

The objectives of Phases I - IV were:

1. to determine the material properties of all the GFRP dowel bars,
2. to investigate the behavioral parameters of aged GFRP dowel bars under elemental static testing,
3. to investigate the behavioral parameters of unaged GFRP dowel bars under elemental static testing,
4. to investigate the behavior of aged GFRP dowel bars under elemental fatigue loading (0.5 to 1 million cycles),
5. to investigate the behavior of unaged GFRP dowel bars under elemental fatigue loading (0.5 to 1 million cycles) in a full-scale test,
6. to investigate the fatigue behavior of GFRP dowel bars under an accelerated partial design life number of cycles (3-5 million),
7. to determine the bond characteristics of both aged and unaged GFRP dowel bars,
8. to evaluate the condition of dowel bars placed in actual highway joints,
9. to investigate the failure modes and adequacy of alternate dowel bar parameters,
10. to develop a finite element model of a jointed concrete highway pavement, and

11. to compile the results of the study into a final report and possible standards.

1.2.2 Scope

The scope of Phase I included the following tasks:

1. the investigation of fatigue behavior of unaged GFRP and steel dowel bars in the modified AASHTO test set up,
2. the investigation of the direct shear strength of unaged GFRP and steel dowel bars in the Iosipescu test set up,
3. the investigation of failure modes of the dowel concrete system using altered cross-sectional parameters of unaged GFRP and steel dowel bars in the Iosipescu test set up,
4. the investigation of bond strength of unaged GFRP and steel dowel bars in the elemental pullout format,
5. the investigation of mechanical and material properties of GFRP through burnout, flexure and tensile testing and compare values with manufacturer specifications,
6. the development of a finite element model of the dowel concrete pavement joint system based on the results obtained from Tasks 2 and 5 above, and
7. the aging of specimens for Phase II.

The scope of Phase II included:

1. the investigation of fatigue behavior of aged GFRP and steel dowel bars in the modified AAHSTO test set up,
2. the investigation of the direct shear strength of aged GFRP and steel dowel bars in the Iosipescu test set up,

3. the investigation of bond strength of aged GFRP and steel dowel bars in the elemental pull-out format,
4. a finite element model to verify the laboratory test arrangement for implementation in Phase III, and
5. a theoretical model to investigate dowel bar spacing, diameter, and shape.

The scope of Phase III included:

1. the investigation of the fatigue behavior of GFRP and steel dowel bars in a full-scale test setup at a high number of cycles. Two test slabs were designed from the elemental testing and analysis conducted in Phases I and II, and
2. the investigation of the behavior of dowel bars placed in Highway 30 by subjecting joints to service loading and measuring deflections.

The scope of Phase IV included:

1. the development of comprehensive design criteria for using GFRP dowel bars as load transfer devices in transverse highway pavement joints, the criteria was a product of the entire scope of GFRP research conducted at Iowa State University and relevant material from outside sources,
2. the recommendation of a test standard to determine the shear properties of the dowel-concrete system for both GFRP and steel products; the recommendations are proposed for an ASTM or AASHTO standard, and
3. comprising a final report that summarizes and coordinates the results of all four phases of the project.

1.3 Literature Review

The literature review included theoretical modeling of dowel bars, highway pavement dowel bars, finite analysis of pavement slabs, pavement design and performance evaluation, and bar spacing. A discussion of the references can be found throughout the report. The appropriate references can be found under the discussion of the associated topic.

2.0 THEORETICAL INVESTIGATION

2.1 Dowel Bar Load Distribution

2.1.1 Joint Effectiveness

The effectiveness of a joint is determined by its ability to transfer part of an applied load across the joint to the adjacent slab. There are several methods available for determining the efficiency of a joint. One measure of joint effectiveness is given by Equation 2.1 [Ioannides et al. 1990 as cited in 2].

$$TLE = \frac{P_t}{P_w} \times 100\% \tag{2.1}$$

where,

TLE = transferred load efficiency (%)
P_t = load transferred across the joint (lbs)
P_w = applied wheel load (lbs)

If a joint were fully effective in transferring load, half of the applied wheel load would be transferred to the subgrade while the other half would be transferred through the dowels to the adjacent slab. Therefore, the maximum permissible value for transferred load efficiency is 50 percent. Brown and Bartholomew [3] consider a TLE of 35 to 40 percent adequate for heavy truck traffic.

AASHTO and ACPA use deflection measurements to determine the efficiency of a joint. Equation 2.2 is given by ACPA as a means of rating joint effectiveness.

$$E = \frac{2\,d_U}{d_L + d_U} \times 100\% \tag{2.2}$$

where,

E = joint effectiveness (%)
d_U = deflection of the unloaded side of a joint (in.)
d_L = deflection of the loaded side of a joint (in.)

A joint effectiveness of 75 percent or more is considered adequate for medium to heavy truck loadings [4]. AASHTO gives Equation 2.3 for determining joint effectiveness associated with a 9000 lb wheel load.

$$LTE = \frac{d_U}{d_L} \times 100\% \tag{2.3}$$

where,

LTE = deflection load transfer efficiency (%)

When the value of LTE is between 70 and 100 percent, the joint provides sufficient load transfer. Deflection measurements for use in Equations 2.2 and 2.3 should be taken at the location of the outside wheel path [5].

2.1.2 Thickness Design

Pavement design involves selecting the appropriate thickness of pavement to limit the flexural stresses in the pavement slab so fatigue cracking will not affect the serviceability of the pavement over its intended design life. The major criterion in the selection of a pavement thickness is the flexural stress in the bottom of the pavement slab. Depending on the load transfer characteristics of the dowel bars, the critical flexural stress for thickness design occurs at one of two locations. If dowel bars provide adequate load transfer, an edge load placed at midslab produces the critical stress and cracking will occur at the bottom edge of the slab, as shown in Figure 2.1. If dowel bars are inadequate in transferring load, joint loading causes the critical stress and longitudinal cracking will initiate in the wheel paths at the transverse joints, as shown in Figure 2.1. Another possibility exists if the joint locks or freezes then a crack can occur across the slab in the vicinity immediately behind the row of dowels, as shown in Figure 2.1.

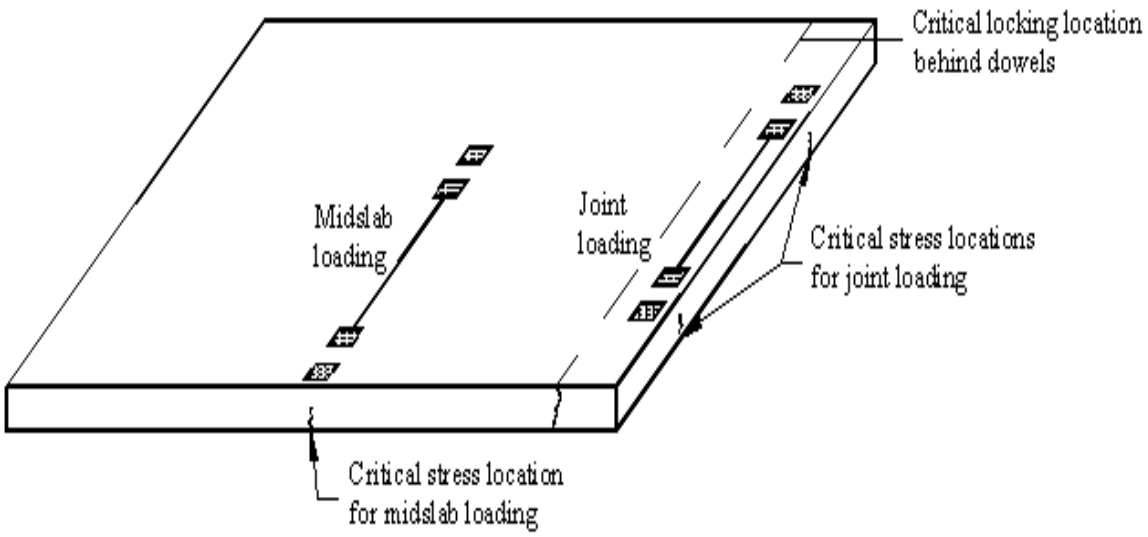

Figure 2.1 Load positions for critical stress

In the thickness design of pavements, the ACPA or AASHTO method is commonly used. In the current ACPA method, the thickness of the pavement is based on the edge stress at midslab. Axle loads are divided into groups, and the flexural stress induced in the bottom of the slab is determined for each group. Based on the ratio between the flexural stress and the modulus of rupture, an allowable number of load repetitions is determined for each group. A damage ratio, defined as the ratio between the predicted and allowable number of load repetitions, is then calculated for each group. Failure is assumed to occur when the sum of the damage ratios for all groups exceeds a value of 1 [6]. Therefore, if the damage ratio for the anticipated design life is greater than one, a thicker pavement is required.

The required thickness of pavement determined by the AASHTO method is based on an empirical equation derived from data obtained from the AASHO Road Test and further modified to incorporate additional knowledge gained from theory and experience. In the AASHTO method, each axle load is converted to an 18 kip equivalent single axle load (ESAL) through the use of equivalency factors. For the anticipated number of ESALs and a specified terminal serviceability index, the empirical equation obtained from the AASHO Road Test is solved to give the required thickness of pavement. The serviceability index is a measure of the performance of the pavement and is based on pavement roughness [5].

2.2 Dowel Bar Theory

2.2.1 Introduction

A transverse joint represents a plane of weakness in a concrete pavement. Without load transfer across the joint, stresses and deflections due to joint loading are substantially higher than those due to interior loading. A dowel bar's function is to transmit part of an applied wheel load from the loaded slab across the joint to the adjacent unloaded slab. Therefore, load transfer, through the use of dowel bars, significantly reduces stresses and deflections resulting from joint loading, thus, minimizing faulting and pumping. Faulting is the difference in elevation across the joint of the two slabs, while pumping is defined as the expulsion of subgrade material through joints and along the edges of the pavement. A slab constructed between two army camps near Newport News, Virginia between 1917 and 1918 is thought to be the first concrete pavement to use steel dowels as load transfer devices [7].

2.2.2 Analytical Model

The theoretical model used to predict the behavior of a dowel bar embedded in concrete is based upon the work presented by Timoshenko and Lessels [8] for the analysis of beams on an elastic foundation. According to Timoshenko and Lessels, the differential equation for the deflection of a beam on an elastic foundation is written as follows:

$$EI\frac{d^4y}{dx^4} = -ky \tag{2.4}$$

where k is a constant usually called the modulus of foundation and y is the deflection. The modulus of foundation denotes the reaction per unit length when the deflection is equal to unity.

The solution to this differential equation is given by:

$$y = e^{\beta x}(A\cos\beta x + B\sin\beta x) + e^{-\beta x}(C\cos\beta x + D\sin\beta x) \tag{2.5}$$

where,

$\beta = \sqrt[4]{\frac{k}{4EI}}$ = relative stiffness of the beam on the elastic foundation (in^{-1})
k = modulus of foundation (psi)
E = modulus of elasticity of the beam (psi)
I = moment of inertia of the beam (in^4)

The constants A, B, C, and D are determined from the boundary conditions for a particular problem. For a semi-infinite beam on an elastic foundation subject to a point load and moment applied at its end, as shown in Figure 2.2, constants A and B are equal to zero and Equation 2.5 becomes

$$y = \frac{e^{-\beta x}}{2\beta^3 EI}[P\cos\beta x - \beta M_o(\cos\beta x - \sin\beta x)] \tag{2.6}$$

Loads P and M_o are shown in their positive sense in Figure 2.2. The positive direction for deflection is downward. Differentiating Equation 2.6 with respect to x gives the slope, dy/dx, of the beam anywhere along its axis.

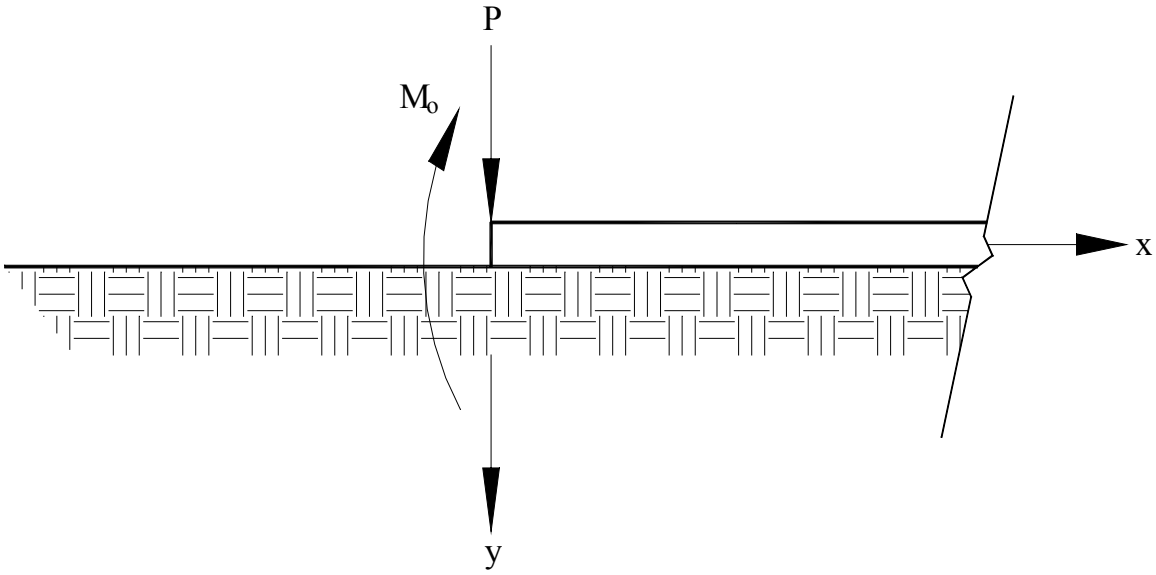

Figure 2.2 Semi-infinite beam on an elastic foundation

$$\frac{dy}{dx} = \frac{e^{-\beta x}}{2\beta^2 EI}\left[(2\beta M_o - P)\cos \beta x - P \sin \beta x\right] \qquad (2.7)$$

Applying the solution for a semi-infinite beam on an elastic foundation to dowel bars, Friberg [9] developed equations for determining the slope and deflection of a dowel at the face of a joint as shown in Figure 2.3. Assuming that an inflection point exists in the dowel at the center of the joint, the forces acting on the portion of the dowel within the width of the joint, z, are as shown in Figure 2.4. Substituting $-Pz/2$ for M_o and setting x equal to zero in Equations 2.6 and 2.7, Friberg arrived at Equations 2.8 and 2.9 for the slope, dy_o/dx, and the deflection, y_o, of the dowel at the face of the joint.

$$\frac{dy_o}{dx} = \frac{-P}{2\beta^2 EI}(1 + \beta z) \qquad (2.8)$$

$$y_o = \frac{P}{4\beta^3 EI}(2 + \beta z) \qquad (2.9)$$

where,

$$\beta = \sqrt[4]{\frac{K_o b}{4EI}} = \text{relative stiffness of the dowel bar encased in concrete } (in^{-1})$$

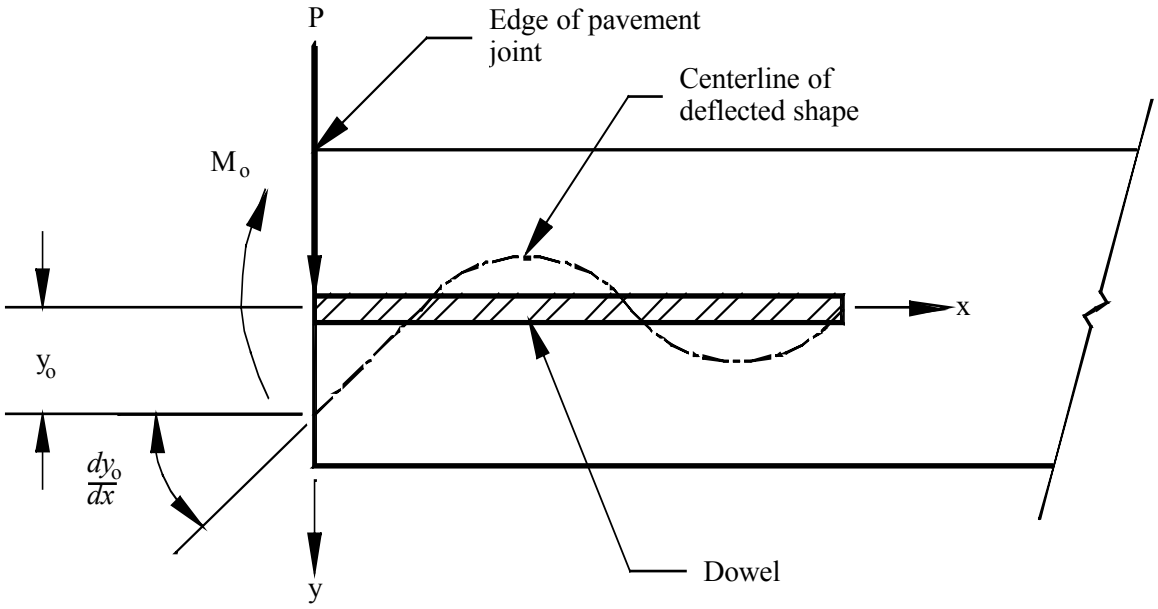

Figure 2.3 Slope and deflection of dowel at joint face

K_o = modulus of dowel support (pci)
b = dowel bar width (in.)
E = modulus of elasticity of the dowel bar (psi)
I = moment of inertia of the dowel bar (in^4)
P = load transferred through the dowel (lbs)
z = joint width (in.)

In Friberg's analysis, he replaced the modulus of foundation, k, with the expression $K_o b$. The modulus of dowel support, K_o, denotes the reaction per unit area when the deflection is equal to unity. Further discussion on the modulus of dowel support can be found in Section 2.2.3.

Friberg's equations were derived assuming a dowel bar of semi-infinite length. Dowel bars used in practice are of finite length; therefore, this equation would not apply. However, Albertson and others [10,11] has shown that this equation can be applied to dowel bars with a βL value greater than or equal to 2 with little or no error. The length of the dowel bar embedded in one side of the slab is denoted as L.

Bradbury [12] also developed equations for predicting the response of a dowel bar encased in concrete. However, Friberg's work is viewed by many engineers as the authoritative analysis on the behavior of dowel bars to date. Therefore, Friberg's equations were used in accomplishing the theoretical work associated with this research project.

2.2.3 Modulus of Dowel Support

The modulus of dowel support is an important parameter in Friberg's design equations presented in Section 2.2.2. Before a design engineer can use these equations, a value for the modulus of dowel support for the given dowel-concrete system is needed. Since no sound theoretical procedure exists for the determination of this value, the modulus of dowel support must be determined experimentally.

Results from experimental testing indicate a wide range of values for the modulus of dowel support. Researchers at ISU [11, 13, 14] have determined values for the modulus of dowel support ranging anywhere from 132,790 pci to 2,139,000 pci. Experimental tests conducted by Friberg [15] yielded modulus of dowel support values ranging from 200,000 pci to 5,000,000 pci.

There is also disagreement amongst researchers on what value should be used for the modulus of dowel support in the design of doweled joints. For steel dowel bars Friberg [9] believed that the modulus of dowel support would seldom be less than 25 percent of the modulus of elasticity of the concrete; therefore, he recommended a value of 1,000,000 pci for the modulus of dowel support. Grinter [16] selected values of 300,000 and 1,500,000 pci for use in his work. Yoder and Witczak [17] state that values

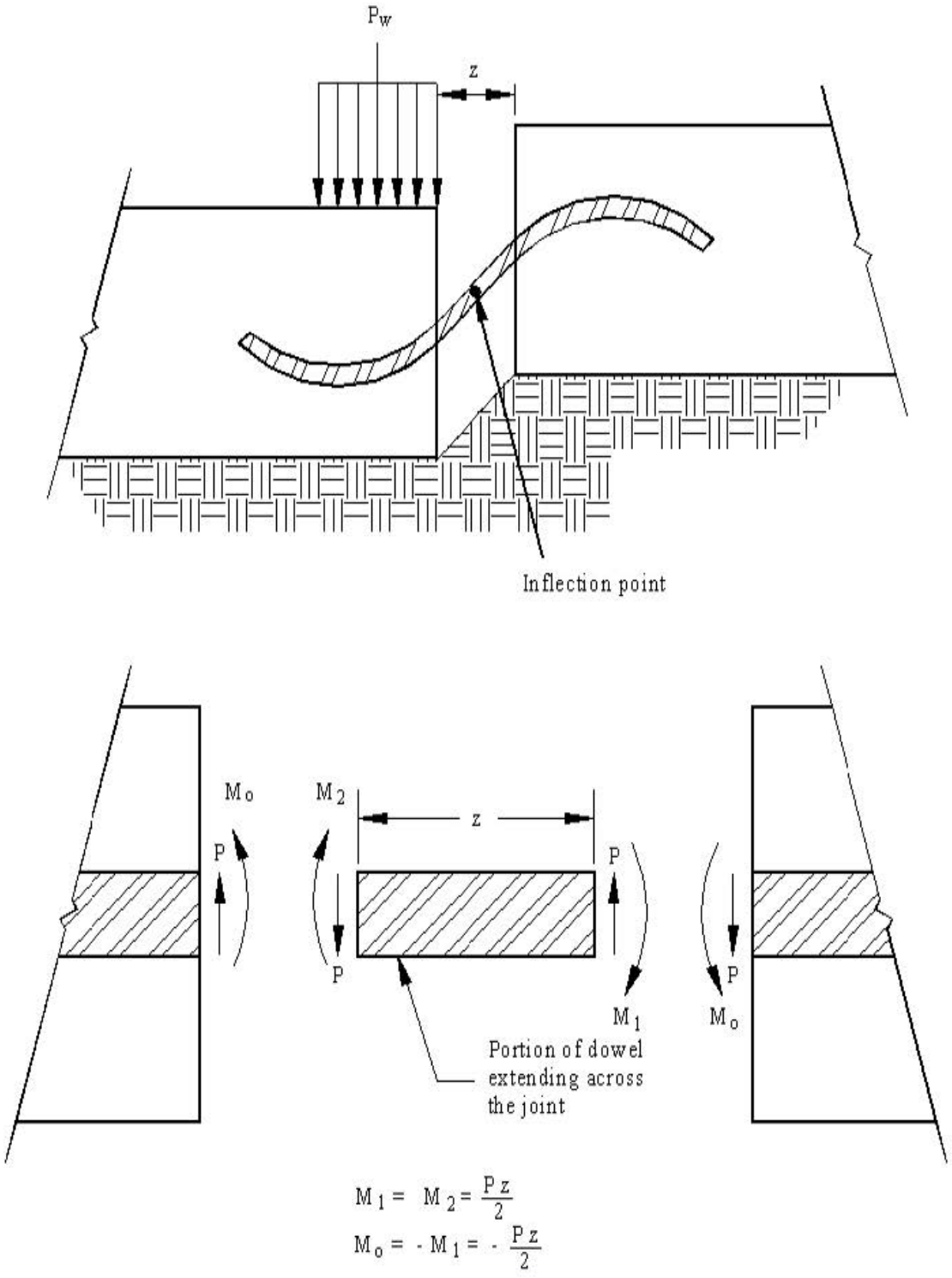

$$M_1 = M_2 = \frac{Pz}{2}$$

$$M_o = -M_1 = -\frac{Pz}{2}$$

Figure 2.4 Forces acting on dowel

for the modulus of dowel support range between 300,000 and 1,500,000 pci and recommend a value of 1,500,000 pci for use in design.

Although values of the modulus of dowel support are highly variable and researchers tend to disagree on the correct value to be used in design, researchers do agree that the modulus of dowel support increases with increased concrete strength, decreases with increased concrete depth below the dowel, and decreases with increased dowel bar diameter [15, 18].

2.2.4 Load Transfer Across a Joint

If 100 percent efficiency is achieved in load transfer by the dowel bars, 50 percent of the wheel load would be transferred to the subgrade while the other 50 percent would be transferred through the dowels to the adjacent slab. However, repetitive loading of the joint results in the creation of a void directly above or beneath the dowel at the face of the joint. According to Yoder and Witczak [17], a 5 to 10 percent reduction in load transfer occurs upon formation of this void; therefore, a design load transfer of 45 percent of the applied wheel load is recommended.

$$P_t = 0.45P_w \tag{2.10}$$

where,

P_t = load transferred across the joint (lbs)
P_w = applied wheel load (lbs)

Not all dowels are active in transferring the applied wheel load across the joint. Friberg [9] was the first to examine the distribution of transferred load to the dowels within a transverse joint. He assumed that dowel bars close to the load were more effective in transferring load than those farther away. For transverse joints containing 0.75 or 0.875-inch diameter dowel bars spaced from 12 to 20 inches apart, Friberg postulated that only the dowels contained within a distance of 1.8 ℓ_r from the load are

active in transferring the load where ℓ_r is the radius of relative stiffness, defined by Westergaard [19] as follows:

$$\ell_r = \sqrt[4]{\frac{E_c h^3}{12(1-\mu^2)K}} \tag{2.11}$$

where,

E_c = modulus of elasticity of the pavement concrete (psi)
h = pavement thickness (in.)
μ = poisson's ratio for the pavement concrete
K = modulus of subgrade reaction (pci)

Friberg also proposed a linear distribution of the load transferred across the joint as shown in Figure 2.5. For transverse joints containing dowel bars having a larger diameter or closer spacing, the stiffness of the joint increases and a distance of $1.8\ell_r$ no longer applies.

Finite element modeling of doweled joints by Tabatabaie et al. [20] showed that an effective length of $1.0\ell_r$ from the applied wheel load is more appropriate for dowels used in practice today. A linear approximation was also shown to exist with the maximum dowel shear occurring directly beneath the load and decreasing to a value of zero at a distance $1.0\ell_r$ from the load.

If the force transferred by a dowel located directly beneath the wheel load is designated as P_c, then the shear force in any other active dowel can be determined by multiplying the height of the triangle below that particular dowel by P_c. A value of 1.0 is assumed for the height of the triangle directly below the load as shown in Figure 2.5. The shear force in the dowel directly under the load is obtained by dividing the transferred load, P_t, by the number of effective dowels, as shown by Equation 2.12.

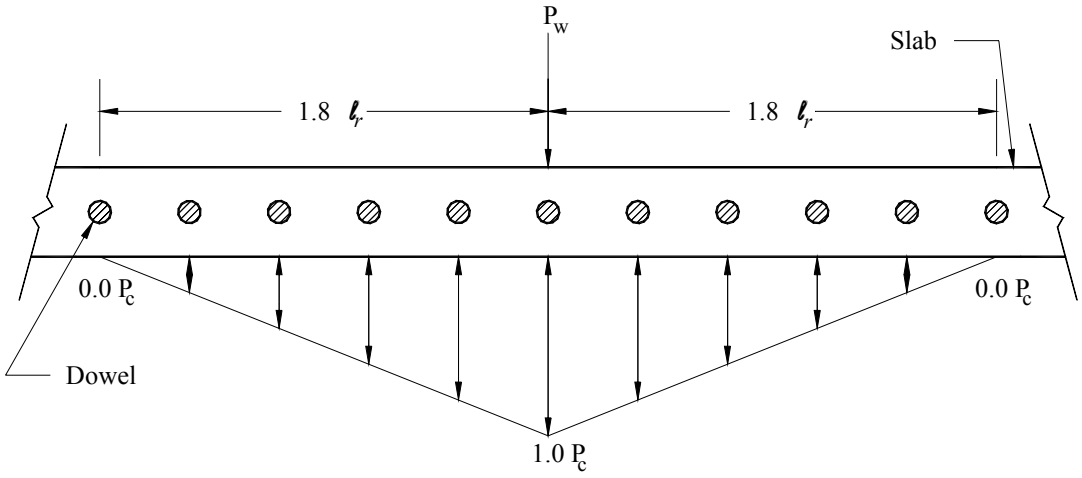

(a)

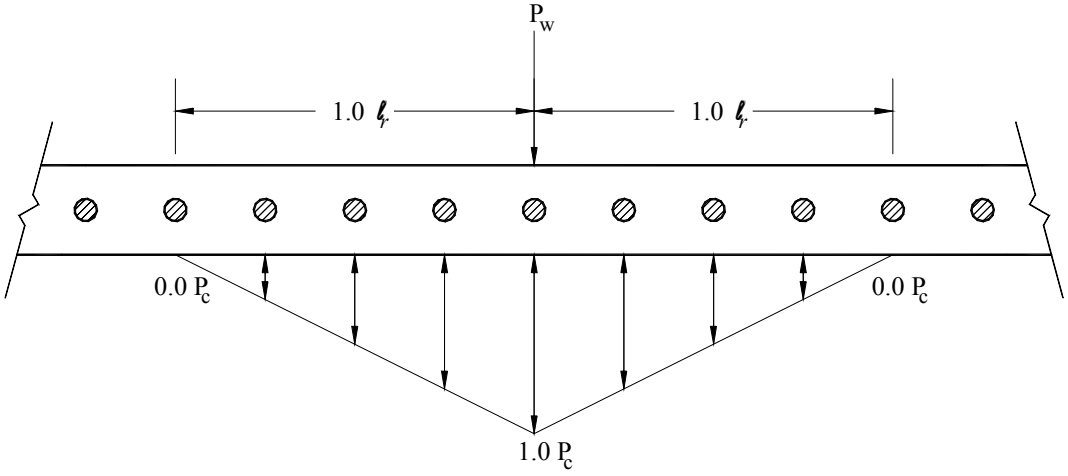

(b)

Figure 2.5 Load transfer distribution proposed by (a) Friberg and (b) Tabatabaie et al.

$$P_c = \frac{P_t}{\text{number of effective dowels}} \tag{2.12}$$

The sum of the heights of the triangle under each dowel gives the number of effective dowels.

2.2.5 Relative Deflection Between Adjacent Pavement Slabs

The relative deflection between adjacent pavement slabs, shown in Figure 2.6, consists of the following quantities:

1. twice the deflection of the dowel at each joint face, $2y_o$;
2. the deflection due to the slope of the dowel, $z\left(\frac{dy_o}{dx}\right)$;
3. shear deflection, δ; and
4. flexural deflection, $\frac{Pz^3}{12EI}$.

Considering all of these quantities, the relative deflection between adjacent pavement slabs, Δ, is given by the following equation:

$$\Delta = 2y_o + z\left(\frac{dy_o}{dx}\right) + \delta + \frac{Pz^3}{12EI} \tag{2.13}$$

where,

$\delta = \frac{\lambda Pz}{AG}$
λ = form factor, equal to 10/9 for solid circular section
A = cross-sectional area of the dowel bar (in^2)
G = shear modulus (psi)

For small joint widths, like the 1/8-inch joint formed in the test specimens of this study, the deflection due to the slope of the dowel is approximately zero since the width of the joint and the slope of the dowel are small. Also, the deflection due to flexural stresses in the dowel within the width of the joint is extremely small since load is transferred across

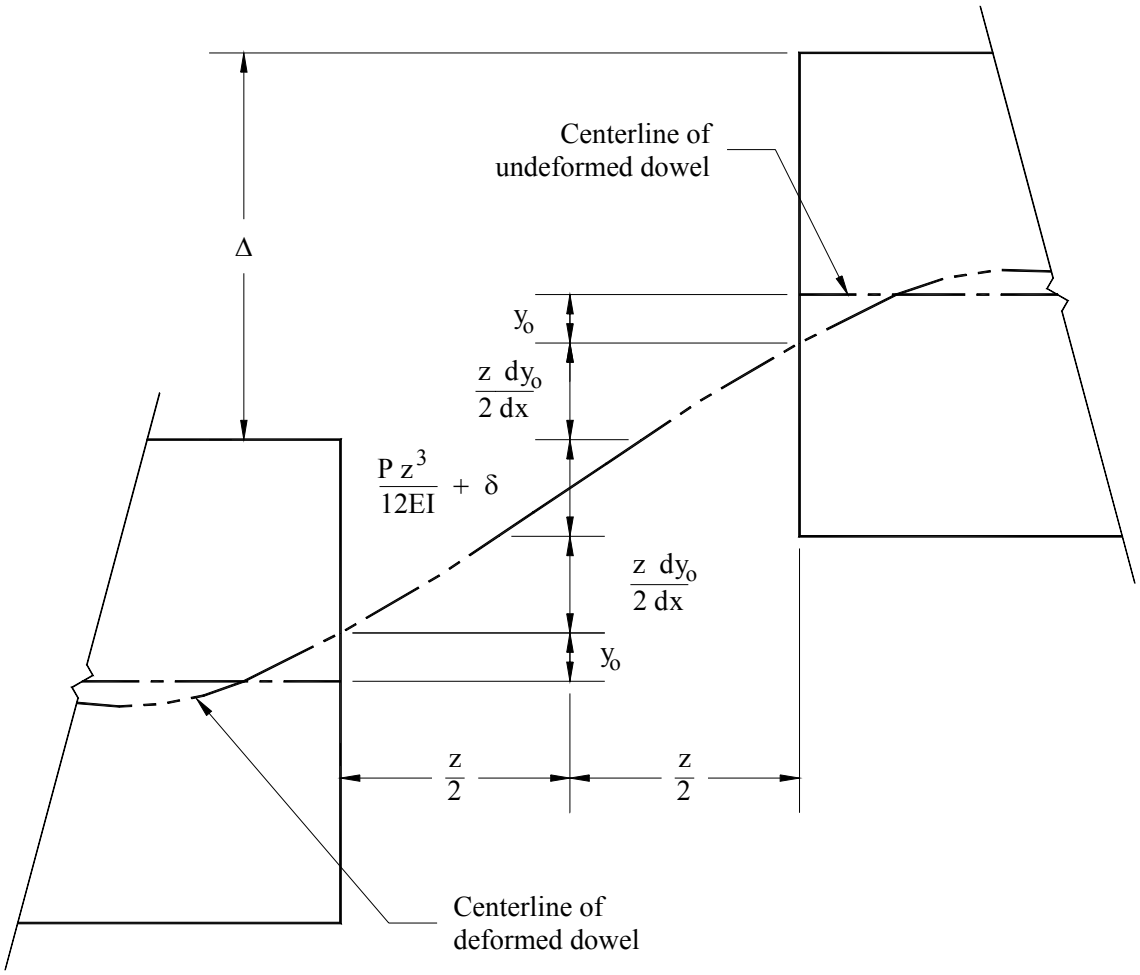

Figure 2.6 Relative deflection between adjacent pavement slabs

the joint predominantly by shear. Therefore, for small joint widths, the deflection due to the slope of the dowel and flexural stresses can be ignored and the relative deflection between adjacent pavement slabs, Δ, can be expressed as follows:

$$\Delta = 2y_o + \delta \tag{2.14}$$

For larger joint widths, the deflection due to the slope of the dowel and flexural stresses is significant and should be considered in computing the relative deflection between adjacent pavement slabs.

2.2.6 Bearing Stress

The load acting on a dowel is transferred to the supporting concrete through bearing. The magnitude of the resulting bearing stresses is critical to the performance of the joint and is the greatest at the face of the joint. Under repetitive loading, high bearing stresses lead to the deterioration of concrete around the dowel, which results in the formation of a void between the dowel and the surrounding concrete. This void is often referred to as dowel looseness. When a load is applied to a slab containing loose dowels, the slab will deflect an amount equal to the dowel looseness before the dowels become active. This looseness results in the loss of load transfer and subsequent faulting of the pavement.

Assuming the dowel behaves as a beam on an elastic foundation, the bearing stress at the face of the joint, σ_o, is directly proportional to the deformation of the concrete at this location and is given by [9]:

$$\sigma_o = K_o y_o = \frac{K_o P}{4\beta^3 EI}(2 + \beta z) \tag{2.15}$$

To ensure adequate joint performance, the bearing stress should not exceed an allowable value. Equation 2.16 gives recommended values for the allowable bearing stress.

$$\sigma_a = \left(\frac{4 - b}{3}\right) f'_c \tag{2.16}$$

where,

σ_a = allowable bearing stress (psi)
b = dowel bar diameter (in.)
f'_c = compressive strength of concrete (psi)

Equation 2.16 was developed by the American Concrete Institute's (ACI) Committee 325 [18] to provide a factor of safety of approximately three against bearing failures, signified by the formation of cracks in the concrete around the peripheral of the dowel.

3.0 COMPUTER MODELING

3.1 Jointed Plain Concrete Pavements

3.1.1 Introduction

Because of the lack of field data for the specific conditions of this research, a 2-D computer model for analyzing jointed plain concrete pavement (JPCP) was developed using the commercial finite element software program ANSYS. The model was used to obtain data on the behavior of concrete highway pavements and to verify that the laboratory test setup simulated these conditions. The JPCP model was similar to an earlier pavement model developed at ISU [11]. However, for the model created in this study, improvements were made to the way in which the behavior of the dowel was modeled.

3.1.2 Idealization

3.1.2.1 Pavement

The rigid pavement was assumed to behave as a plate on an elastic foundation. Based on this assumption, the pavement was modeled using element Shell 63, which is a plate element capable of handling both in-plane and out-of-plane loads. The element has 6 degrees of freedom per node: translations in the x, y, and z directions and rotations about the x, y, and z axes. The geometry, node locations, and coordinate system for this element are shown in Figure 3.1. The element input data includes four nodes, four thicknesses, an elastic foundation stiffness, and the material properties. If the element has a constant thickness, only the thickness at Node j needs to be entered. The elastic foundation stiffness is equivalent to the modulus of subgrade reaction for the soil [21].

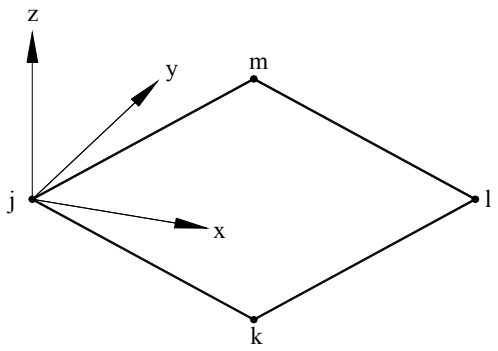

Figure 3.1 Shell 63

3.1.2.2 Subgrade

The subgrade beneath the pavement was modeled as a bed of springs, where the stiffness of each spring is equal to the modulus of subgrade reaction for the soil. This type of idealization is often referred to as a Winkler foundation. The springs are incorporated into the model by entering a value for the elastic foundation stiffness in the input for element Shell 63.

3.1.2.3 Dowel Bars

Since concrete is not a perfectly rigid material, the dowel will rotate and deflect in the concrete as shown in Figure 2.3. Two new elements were developed in an attempt to model this behavior. These two elements, referred to as Dowel 1 and Dowel 2, are depicted in Figure 3.2. An element entitled Matrix 27 was employed to incorporate these two elements into the model. Matrix 27 is an arbitrary 12 x 12 stiffness matrix relating two nodes with six degrees of freedom each. Translations in the x, y, and z directions and rotations about the x, y, and z axes constitute the degrees of freedom per node. The degrees of freedom are ordered as shown in Figure 3.3 [21]. The dowel bars were

incorporated into the computer model by simply determining the terms in the stiffness matrix for each element and inserting these terms in their proper position in the 12 x 12 stiffness matrix.

Figure 3.4 shows the degrees of freedom for element Dowel 1. The corresponding stiffness matrix for this element is of order 2 x 2 and is given by[1]

$$\mathbf{S} = \begin{matrix} \\ 3 \\ 9 \end{matrix} \begin{matrix} \begin{matrix} 3 & 9 \end{matrix} \\ \begin{bmatrix} k & -k \\ -k & k \end{bmatrix} \end{matrix} \tag{3.1}$$

The spring stiffness, k, is given by Equation 3.2.

$$k = \frac{P}{\Delta} \tag{3.2}$$

One nice feature about this element is that the effects of fatigue can be considered in the analysis by simply adjusting the stiffness of the spring.

Figure 3.5 shows the degrees of freedom for element Dowel 2. The stiffness matrix for this element is a 4 x 4 stiffness matrix and is given by

$$\mathbf{S} = \begin{bmatrix} \mathbf{S}_{jj} & \mathbf{S}_{jk} \\ \mathbf{S}_{kj} & \mathbf{S}_{kk} \end{bmatrix} \tag{3.3}$$

A technique which involves the flexibility method, matrix inversion, and translation-of-axes is employed to obtain this stiffness matrix. The flexibility method is used to obtain the submatrix $\mathbf{F}_{kk}$, which is given by

$$\mathbf{F}_{kk} = \begin{matrix} \\ 9 \\ 11 \end{matrix} \begin{matrix} \begin{matrix} 9 & 11 \end{matrix} \\ \begin{bmatrix} \frac{z^3}{3EI} + \frac{\lambda z}{GA} + \frac{2}{k_1} + \frac{z^2}{k_2} & \frac{-z^2}{2EI} - \frac{z}{k_2} \\ \frac{-z^2}{2EI} - \frac{z}{k_2} & \frac{z}{EI} + \frac{2}{k_2} \end{bmatrix} \end{matrix}$$

[1] Bold face type will be used to distinguish matrices from scalars.

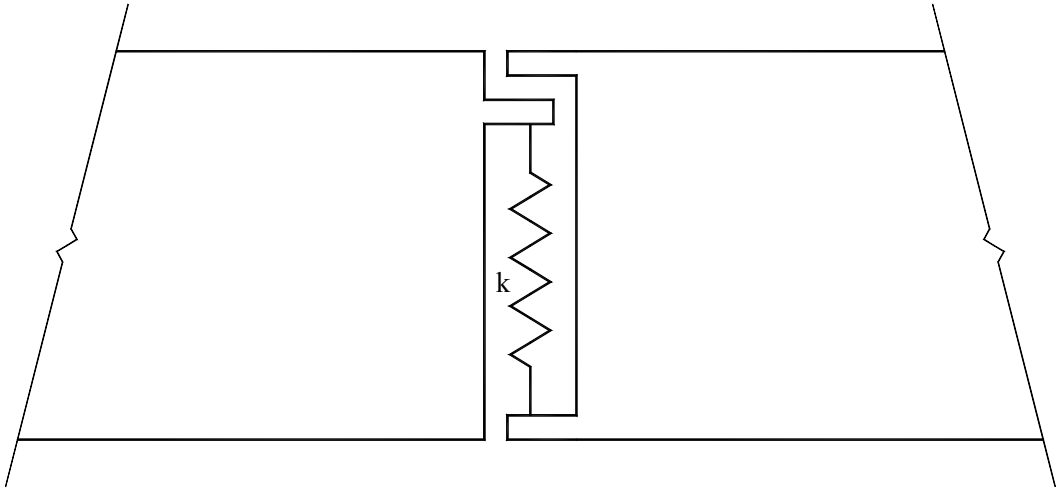

(a)

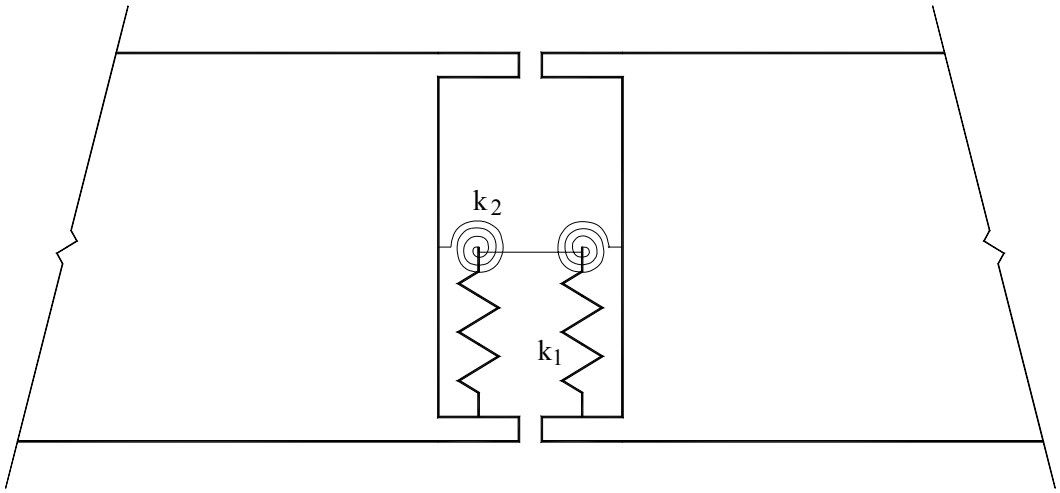

(b)

Figure 3.2 Dowel elements: (a) Dowel 1 and (b) Dowel 2

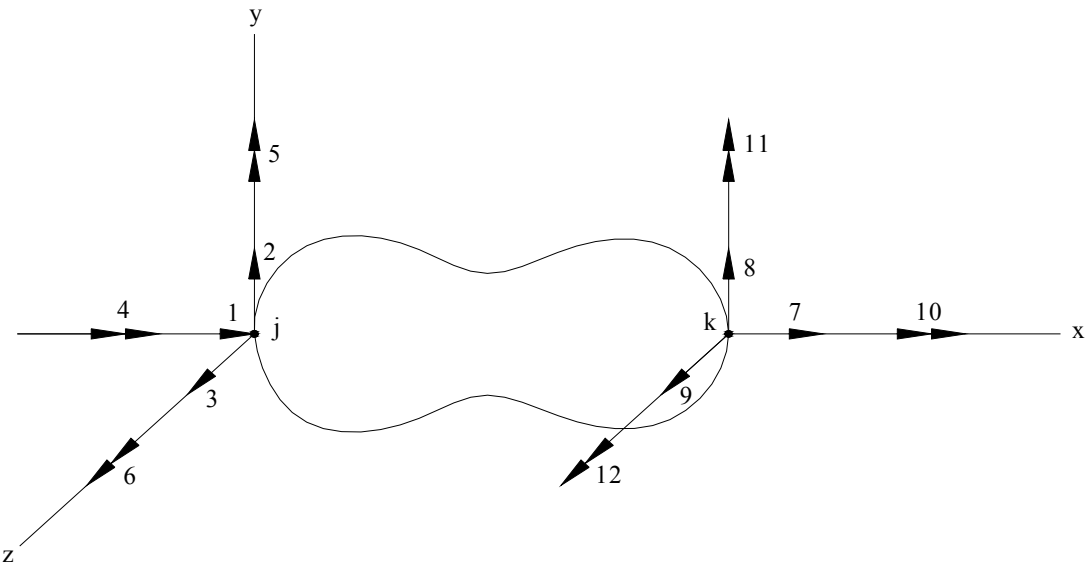

Figure 3.3 Degrees of freedom for Matrix 27

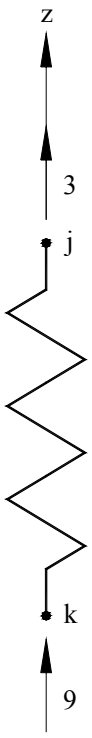

Figure 3.4 Degrees of freedom for Dowel 1

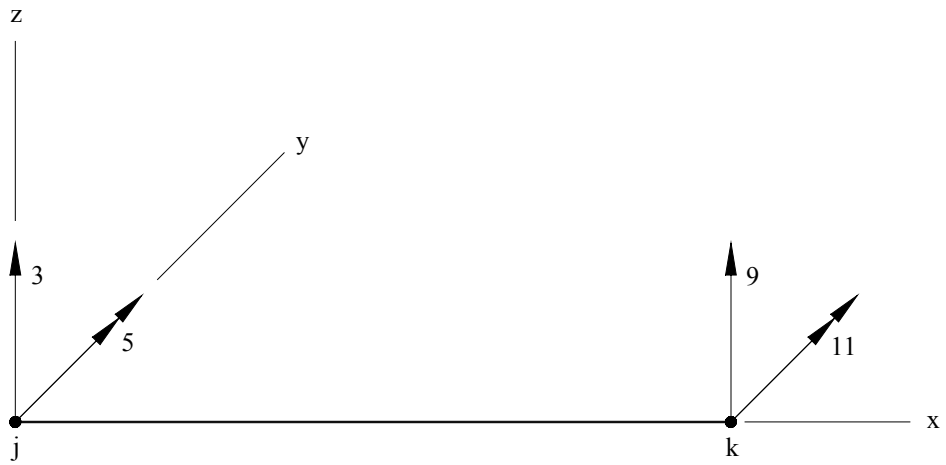

Figure 3.5 Degrees of freedom for Dowel 2

The terms in $\mathbf{F}_{kk}$ represent the displacements at the k end due to unit actions at the same end. The vertical spring stiffness, k_1, is given by Equation 3.5.

$$k_1 = \frac{P}{y_o} \tag{3.5}$$

The stiffness of this spring can also be adjusted to consider the effects of fatigue in the analysis. Equation 3.6 will yield the rotational spring stiffness, k_2.

$$k_2 = \frac{M}{dy_o/dx} \tag{3.6}$$

Inversion of $\mathbf{F}_{kk}$ yields the stiffness submatrix $\mathbf{S}_{kk}$, whose terms represent the actions at the k end due to unit displacements at the same end.

$$\mathbf{S}_{kk} = \mathbf{F}_{kk}^{-1} \tag{3.7}$$

Translation-of-axes can be used to obtain the submatrix $\mathbf{S}_{jk}$ as given in Equation 3.8.

$$\mathbf{S}_{jk} = \mathbf{T}_{jk}\mathbf{S}_{kk} \tag{3.8}$$

The matrix $\mathbf{T}_{jk}$ is a translation-of-axes transformation matrix and is given by Equation 3.9.

$$\mathbf{T}_{jk} = \begin{bmatrix} -1 & 0 \\ z & -1 \end{bmatrix} \tag{3.9}$$

Equations 3.10 and 3.11 give the remaining stiffness submatrices.

$$\mathbf{S}_{kj} = \mathbf{S}_{jk}^{T} \quad (3.10)$$

$$\mathbf{S}_{jj} = \mathbf{T}_{jk}\mathbf{S}_{kj} \quad (3.11)$$

The symbol $\mathbf{S}_{jk}^{T}$ in Equation 3.10 represents the transpose of the submatrix $\mathbf{S}_{jk}$.

Although Dowel 2 is a more accurate portrayal of the conditions that exist, finite element runs performed for both dowel elements yielded identical results (within less than 3.2 percent) with respect to shear and slab deflections. Therefore, Dowel 1 was selected to model the dowel bars since the stiffness matrix for this element was the easiest to determine.

3.1.2.4 Loading

An axle load is transmitted to the pavement through the tires of a truck. The tires of the truck distribute this load over a contact area; therefore, to properly represent the loading on the pavement, a surface pressure should be applied to a plate element having the same dimensions as the contact area of the tire. However, for concrete pavements, this distributed load can be represented by a concentrated force with little or no significant error [22]. Therefore, two point loads separated by a distance of 6 feet were used to represent an axle load on the pavement.

3.1.3 Sensitivity Study

A sensitivity study was performed to determine the appropriate mesh density. From this study the Jointed Plain Concrete Pavement (JCPC) mesh shown in Figure 3.6 was selected.

3.1.4 Model Verification

To verify the accuracy of the computer model, the solution found for a typical highway pavement problem was compared to available theoretical and numerical solutions. The problem consisted of a 12-foot wide jointed concrete pavement with contraction joints every 20 feet. Epoxy-coated steel dowels 1.5 inches in diameter and spaced at the standard 12 inches had a modulus of dowel support equal to 650,000 pci, which is a reasonable value for 1.5-inch diameter steel dowels based upon experimental test results [11]. The concrete pavement had a 28-day compressive strength of 6,000 psi and was subjected to an 18 kip axle load. The modulus of subgrade reaction for the soil was 100 pci, which is a typical value used in the design of pavements [*14*].

Results obtained from the computer model for load transfer were compared to those determined by the computer program KENSLABS [6] and the theoretical linear distribution suggested by Tabatabaie et al. [20]. The comparison is shown in Figure 3.7. The relative deflection between adjacent pavement slabs at the location of the applied wheel load was compared to a theoretical solution as well as that obtained from KENSLABS. This comparison is shown in Table 3.1. As can be seen from the figure and table, the results from the computer model are in close agreement with available theoretical and numerical solutions.

3.2 Laboratory Test Setup

3.2.1 Introduction

The test setup used in the laboratory for the fatigue testing of concrete pavement slabs is shown in Figure 3.8. As shown in Figure 3.8, steel beams were used to support the slab

during testing. The beams were designed to represent a soil having a modulus of subgrade reaction equal to 100 pci [11]. To determine the size of beams required, previous investigators created a finite element model that consisted of a concrete slab supported by six lines of vertical springs. Although the model was rather crude, it was the most efficient model for design purposes. To determine the actual value of the modulus of subgrade reaction for the steel beams, which was needed for the calculations of Section 5.2.2.2, a more refined model was developed.

3.2.2 Idealization

3.2.2.1 Steel Support Beams

The webs and flanges of the steel support beams were modeled using the Shell 63 element described in Section 3.1.2.1.

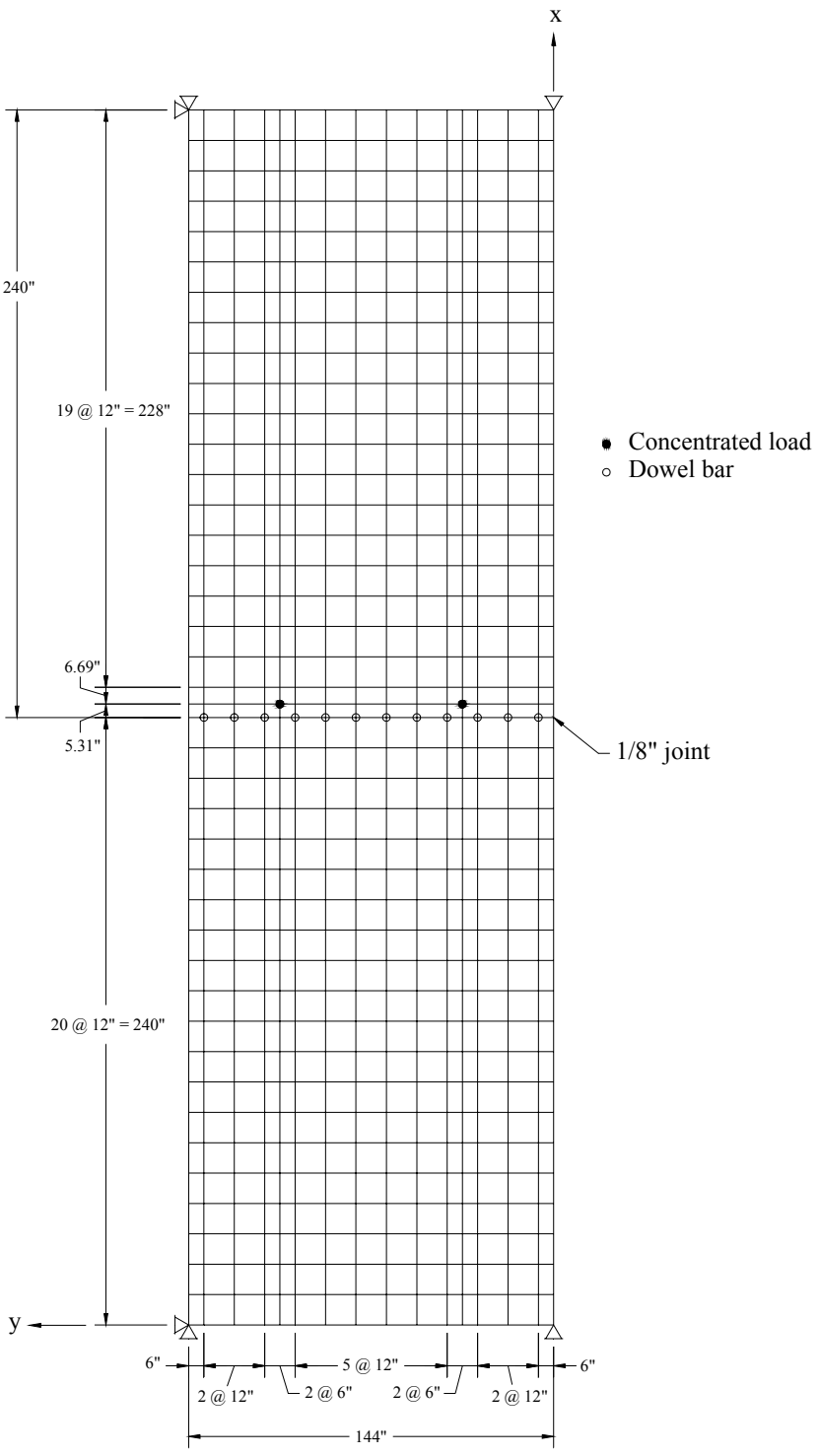

Figure 3.6 JPCP mesh

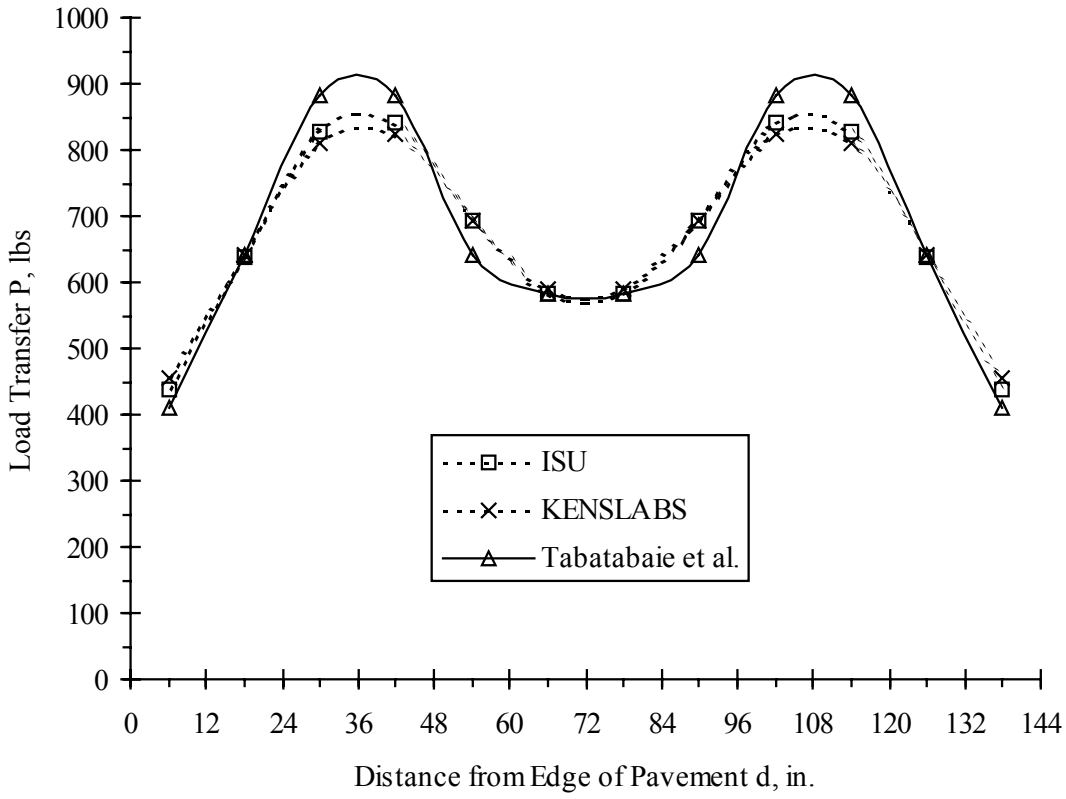

Figure 3.7 Load transfer comparison

Table 3.1 Relative deflection between adjacent pavement slabs

Solution	Relative Deflection Δ, in.
ISU	0.0015
KENSLABS	0.0015
Theoretical	0.0016

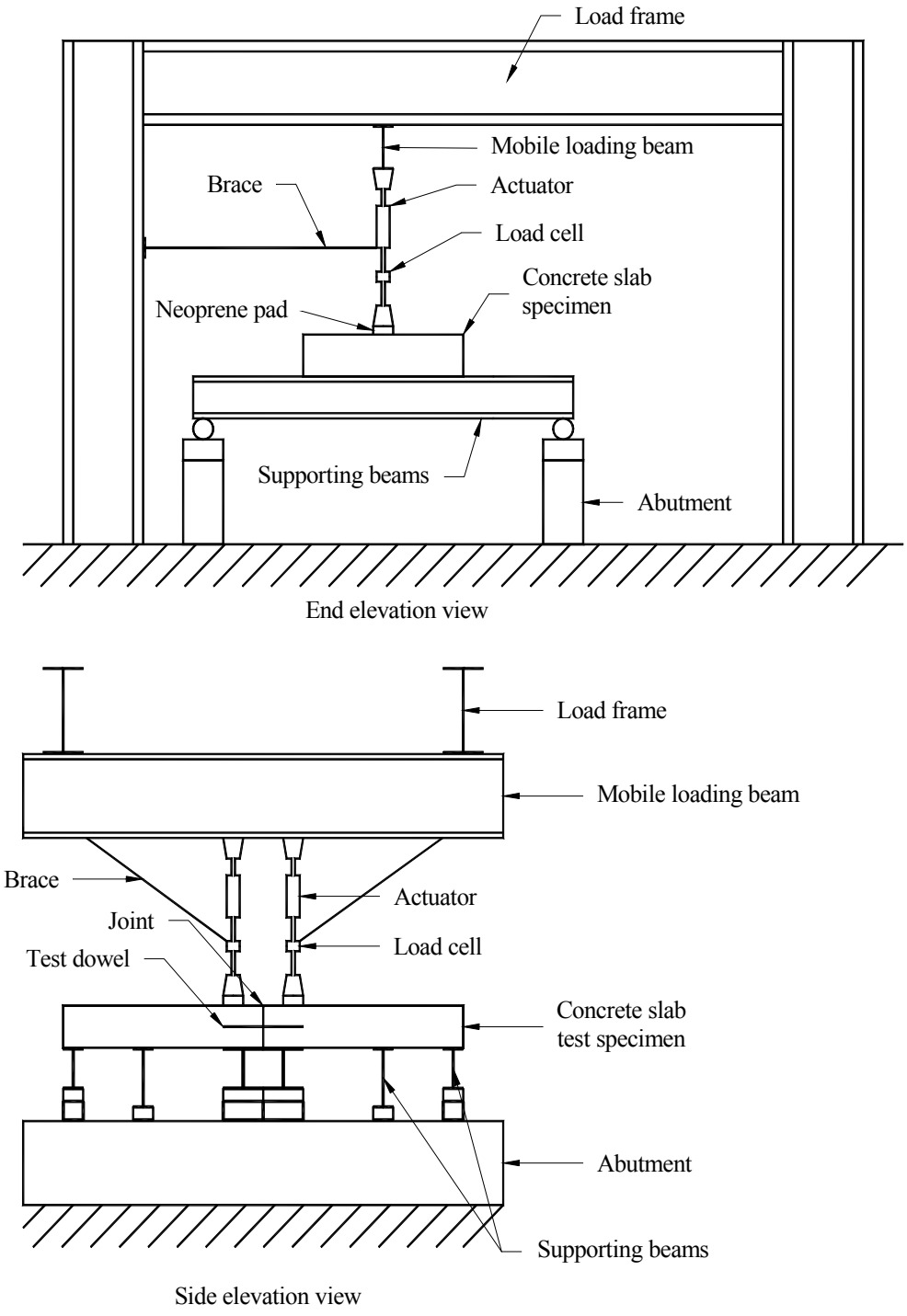

Figure 3.8 Laboratory test setup

3.2.2.2 Concrete Slab

The concrete slab placed on top of the steel beams was modeled using element Solid 73. This is a three dimensional element containing eight nodes having six degrees of freedom per node. The six degrees of freedom at each node consist of translations in the x, y, and z directions and rotations about the x, y, and z axes. The geometry, node locations, and coordinate system for this element are shown in Figure 3.9. The input data for the element consists of eight nodes and the material properties [21].

3.2.2.3 Slab-Beam Interface

During the construction of the laboratory specimens, a sheet of polyurethane was placed over the top of the steel beams to prevent a bond from developing between the concrete and steel. Since the concrete slab was not tied to the steel beams, the possibility that the concrete slab would lift off the outside beam during loading existed. The slab could also slide on the beams if the frictional resistance provided by the polyurethane is exceeded. To accurately model this interface, an element was needed that could consider these two situations. The element library within ANSYS contains an element entitled Contac 52 that was designed for this purpose.

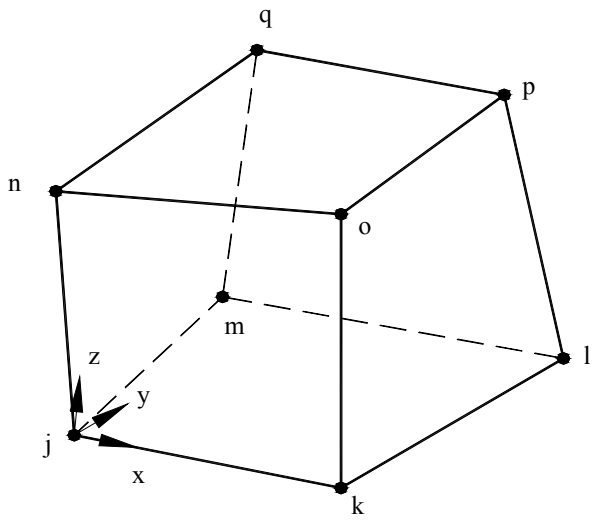

Figure 3.9 Solid 73

The contact element, Contac 52, was used to model the interface between the concrete slab and the steel beams. This element connects two nodes having three degrees of freedom per node. Translations in the x, y, and z directions constitute the three degrees of freedom at each node. The geometry, node locations, and coordinate system for this element are shown in Figure 3.10. Input data for the element includes two nodes, a shear and contact stiffness, a value for the coefficient of friction, and any initial gap or interference that exists between the surfaces [21].

3.2.2.4 Dowel Bars

The dowel bars were modeled using the Dowel 1 element developed in Section 3.1.2.3.

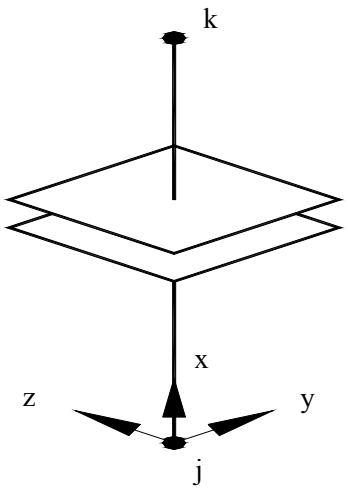

Figure 3.10 Contac 52

3.2.2.5 Mesh Density

The mesh selected for the laboratory model is shown in Figure 3.11. This mesh was the finest mesh that could be obtained without exceeding the limits of the software. Although a sensitivity study is usually conducted to determine the appropriate mesh density, preliminary analysis revealed that such a study was not necessary. Figures 3.12 and 3.13 show that the relative deflection between adjacent pavement slabs and the bearing stress in the concrete are relatively insensitive to the value of the modulus of subgrade reaction. Therefore, a precise value for the modulus of subgrade reaction is not required for the calculations of Section 5.2.2 and the mesh shown in Figure 3.11 was judged to be adequate for the determination of the modulus of subgrade reaction for the steel beams.

3.2.3 Subgrade Determination

To determine the modulus of subgrade reaction for the steel support beams, deflections from the laboratory model were compared to those obtained from several

finite element runs of the JPCP model described in Section 3.1. For each of the finite element runs of the JPCP model, a different value was inputted for the elastic foundation stiffness. Based on these comparisons, the modulus of subgrade reaction for the steel support beams is approximately equal to 160 pci. The authors note that this value is only used in the calculations of Section 5.2.2. The reported value for the modulus of subgrade reaction will be based on experimental data.

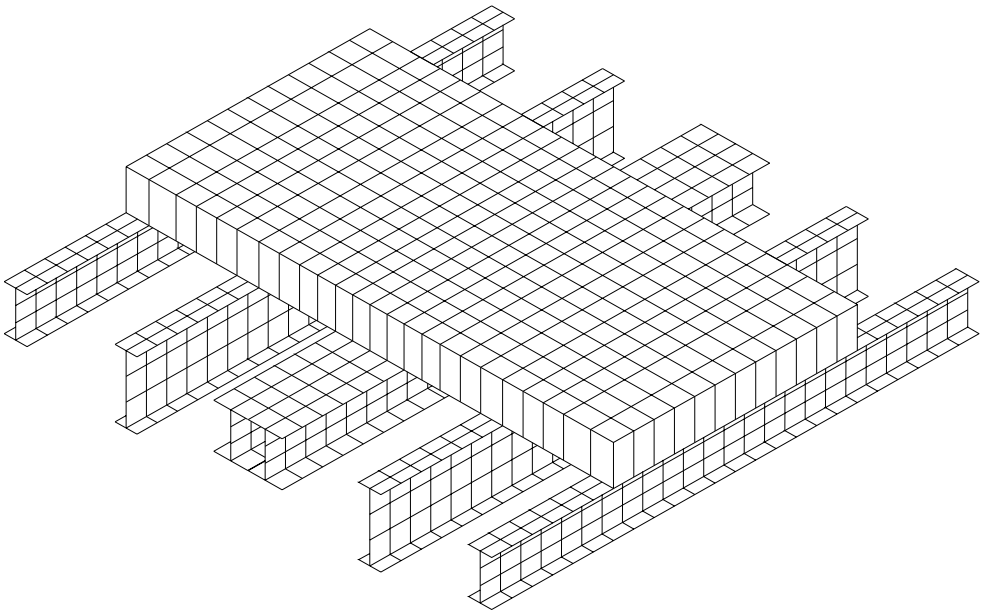

Figure 3.11 Laboratory model mesh

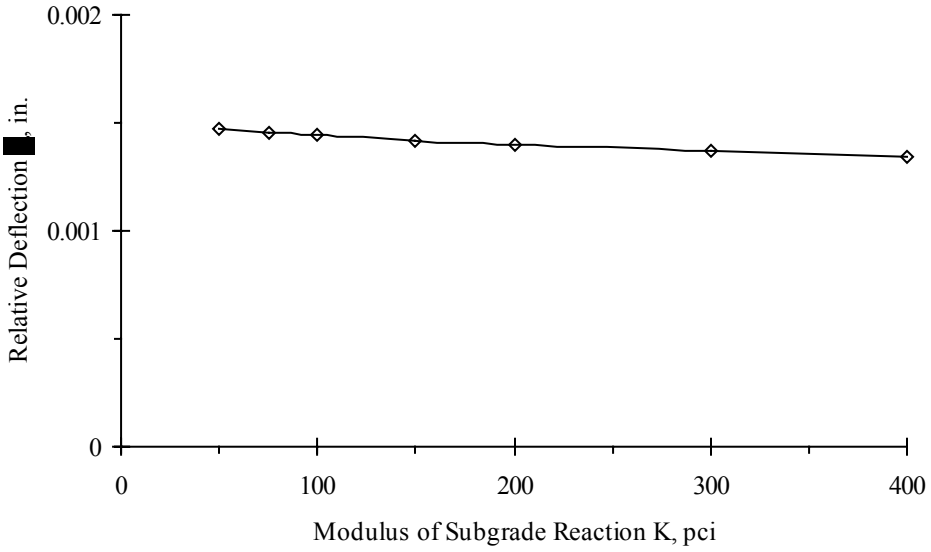

Figure 3.12 Relative deflection versus modulus of subgrade reaction

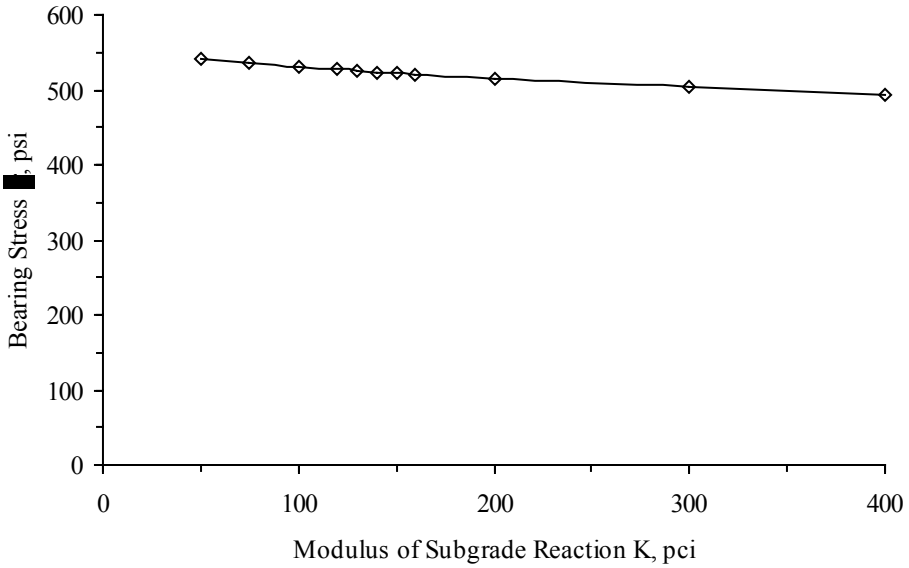

Figure 3.13 Bearing stress versus modulus of subgrade reaction

4.0 TESTING PROCEDURE

4.1 Phase I - Unaged Testing

4.1.1 Introduction

Experimental investigation was performed on aluminum, copper, epoxy coated steel, plain steel, stainless steel, and GFRP dowel bars. Unlike the steel, aluminum, and copper dowel materials, the GFRP dowels do not have previously established material properties. Therefore, the GFRP material properties must be determined through testing. The following section explains how the material properties were determined. Sections 4.1.3 and 4.1.4 will explain what test methods were investigated and which test methods were used to determine the load-deflection characteristics for all of the dowel-concrete systems tested in this research.

4.1.2 GFRP Dowel Property Testing

4.1.2.1 Introduction

In the design and analysis of pavement joints, both the flexural and shear properties of the dowel bar are needed. GFRP materials are anisotropic; therefore, the testing of GFRP materials is unlike the testing of metals because each material property that makes up the GFRP is different.

4.1.2.2 Proportions of GFRP Components

If composite material theory is to be used to determine the material properties, the proportions of the GFRP materials needs to be known. These proportions, when substituted into the proper equations, will give approximate values for the properties needed to carry out the design and analysis of dowel bars. Testing was done to determine

the proportions of E-glass and isophthalic polyester resin contained in the GFRP dowel bars used in this research.

Individual samples were taken from each of the GFRP dowel bars studied in this research. The sample was then taken and subjected to a high degree of heat that burned the resin and left the glass fibers. The procedure followed the ASTM D2584-68 [24] standard testing method. The end result of this test gives the weight fractions of the glass and the resin. The volume fractions were then calculated from their respective weight fractions. The results are shown below in Table 4.1

Table 4.1 Weight and volume fractions of GFRP dowel bars

Specimen	Weight Fraction	Volume Fraction
1.5”ϕ glass	0.6997	0.5179
1.5”ϕ resin	0.3003	0.4821
1.875”ϕ glass	0.7378	0.5746
1.875”ϕ resin	0.2622	0.4254

In order for the volume fractions of the GFRP dowel bars to be calculated, the specific gravity of the dowel bar was needed. The procedure used to calculate the specific gravity was the ASTM D792-91 [24] standard testing method. Table 4.2 shows the results for this test. Equations 4.1 and 4.2 show how to calculate the volume fractions for each dowel bar type using these results and the weight fractions.

Table 4.2 Specific gravity of GFRP dowel bars

Specimen	Specific Gravity
1.5”ϕ GFRP	1.880
1.875”ϕ GFRP	1.978

$$v_f = w_f \cdot \frac{SG_D}{SG_f} \cdot 100 \tag{4.1}$$

$$v_r = 1 - v_f \tag{4.2}$$

where:

v_f = volume fraction of fibers
v_r = volume fraction of resin
w_f = weight fraction of fibers
SG_D = specific gravity of dowel
SG_f = specific gravity of fibers

The calculations of the volume fractions were performed assuming that the specific gravity of E-glass, SG_f, was equal to 2.54, according to Auborg [25]. The specific gravity of the resin, SG_r, was also needed for the next section and was assumed equal to 1.25, according Ashland Chemicals [26].

4.1.2.3 Composite Material Theory

Tsai and Hahn [27] developed theoretical equations for the properties needed for the analysis and design of dowel bars. The composite properties of a GFRP dowel bar are determined considering the individual properties of both the glass and resin components. The volume fractions along with the individual material characteristics are the main parameters needed in the following theoretical equations taken from Tsai and Hahn [27]. The results from these theoretical equations are shown in Table 4.3.

$$E_x = v_f E_f + v_r E_r \tag{4.3}$$

$$\nu_{xy} = v_f \nu_f + v_r \nu_r \tag{4.4}$$

$$G_r = \frac{E_r}{2(1+\nu_r)} \tag{4.5}$$

$$G_f = \frac{E_f}{2(1+\nu_f)} \tag{4.6}$$

$$\frac{1}{E_y} = \frac{\left(\frac{v_f}{E_f} + \frac{\eta_y v_r}{E_r}\right)}{\left(v_f + \eta_y v_r\right)} \tag{4.7}$$

$$\frac{1}{G_{xy}} = \frac{\left(\frac{v_f}{G_f} + \frac{\eta_G v_r}{G_r}\right)}{\left(v_f + \eta_G v_r\right)} \tag{4.8}$$

$$\eta_y = \frac{1}{2\left(1 + \frac{E_r}{E_f}\right)} \tag{4.9}$$

$$\eta_G = \frac{\left(3 - 4v_r + \frac{G_r}{G_f}\right)}{4\left(1 - v_r\right)} \tag{4.10}$$

where:

E_x = longitudinal modulus of elasticity, psi (referred to as E for remaining text)
E_f = modulus of elasticity of fibers, psi
E_r = modulus of elasticity of resin, psi
ν_{xy} = transverse poisson's ratio
ν_f = poisson's ratio of fibers
ν_r = poisson's ratio of resin
G_r = shear modulus of resin, psi
G_f = shear modulus of fibers, psi
E_y = transverse modulus of elasticity, psi
G_{xy} = transverse shear modulus, psi
η_y = stress partitioning parameter for transverse modulus of elasticity
η_G = stress partitioning parameter for transverse shear modulus

Table 4.3 Theoretical properties of GFRP dowel bars

Specimen	E_x, psi	ν_{xy}	E_y, psi	G_{xy}, psi
1.5"ϕ GFRP	5.64E+06	0.259	1.47E+06	4.99E+05
1.875"ϕ GFRP	6.20E+06	0.255	1.67E+06	5.67E+05

4.1.2.4 Flexural Testing

4.1.2.4.1 Introduction

Experimental testing was conducted to determine the flexural properties of the GFRP dowel bar. In order to determine the flexural properties of dowels by testing, the

load and deflection must be measured at various levels in order to determine a relationship. The following sections will describe the flexural tests conducted.

4.1.2.4.2 Reduced-Size Dowel Specimens

Unlike steel and other similar materials, the flexural behavior of the GFRP dowel bars are influenced more by the shear properties. The analysis of data from the flexural testing of a full-size GFRP dowel will have higher shear deformation effects when compared to reduced-size dowels. However, the full-size test will be discussed in the next section.

Since the full-size GFRP dowels have a significant shear deformation during flexural testing, a reduced-size specimen was introduced by the ASTM D4476 [24] test method. The cross section is a semi-circular shape. The purpose of this semi-circular cross section is to reduce the effects of shear deformation. Therefore, the dowel should only experience flexural deformations. Another reason this test was introduced is that during the full-size specimen test premature compression on the top of the dowel caused by shear has been noted directly under the loading point during three-point flexural tests.

The ASTM D4476 [24] standard test method is used to test reduced-size GFRP dowel bars. Figure 4.1 shows the testing setup. The load-deflection data from this test was used to determine the bending modulus, E. Table 4.4 lists the results of the tests.

Table 4.4 Bending modulus values for GFRP dowel bars

Specimen	Bending Modulus, E, psi
1.5”ϕ GFRP	4.93E+06
1.875”ϕ GFRP	6.51E+06

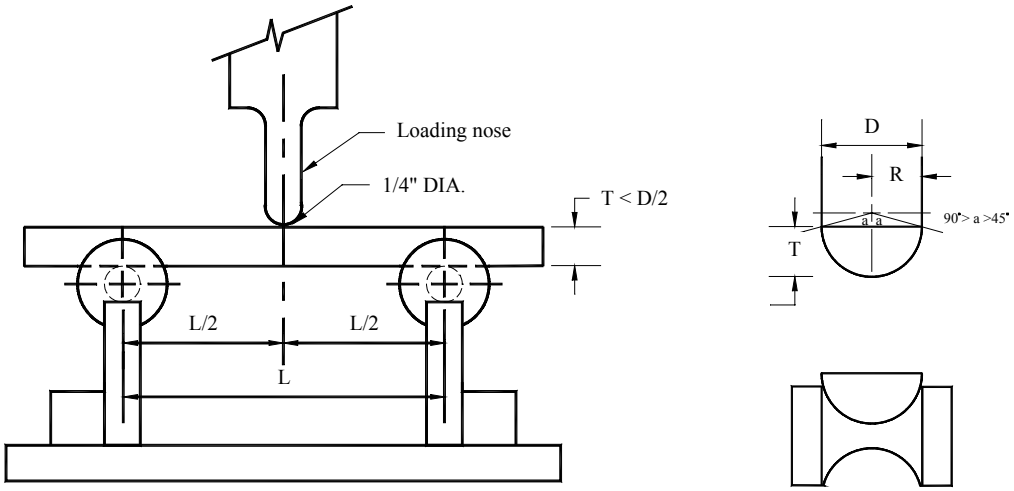

Figure 4.1 ASTM D4476 [24] test setup

4.1.2.4.3 Full-Size Dowel Specimens

The flexural test method can not determine the shear properties, such as the transverse shear modulus, G_{xy}. In order to determine G_{xy}, separate and independent testing must be performed. The easiest way to determine a value for the transverse shear modulus is to back calculate it from its respective load and deflection. According to Ugural [28], for a three-point test configuration for round bars, the deflection is calculated by Equation 4.11.

$$\Delta = \frac{P \cdot L^3}{48 \cdot E \cdot I} + \frac{5 \cdot P \cdot L}{18 \cdot G_{xy} \cdot A} \tag{4.11}$$

where:

A = cross sectional area of dowel bar, in.^{2}, and
other terms are previously defined.

The ASTM D4475 [24] standard test method was used to test full-size GFRP dowel bars. The testing setup is shown in Figure 4.2. The testing procedure was followed as stated. However, the actual test standard was to be used to determine the apparent horizontal shear strength. The load-deflection data as well as the bending modulus, determined from the reduced-size specimen tests, was used to determine the transverse shear modulus, G_{xy}. When solving Equation 4.11 for the transverse shear modulus, Equation 4.12 is generated. The results of this analysis are listed in Table 4.5.

$$G_{xy} = \frac{1}{\frac{18 \cdot A}{5 \cdot P \cdot L}\left(\Delta - \frac{PL^3}{48 \cdot E \cdot I}\right)} \tag{4.12}$$

Table 4.5 Shear modulus values for GFRP dowel bars

Specimen	Shear Modulus, G_{xy}, psi
1.5”ϕ GFRP	3.09E+05
1.875”ϕ GFRP	3.15E+05

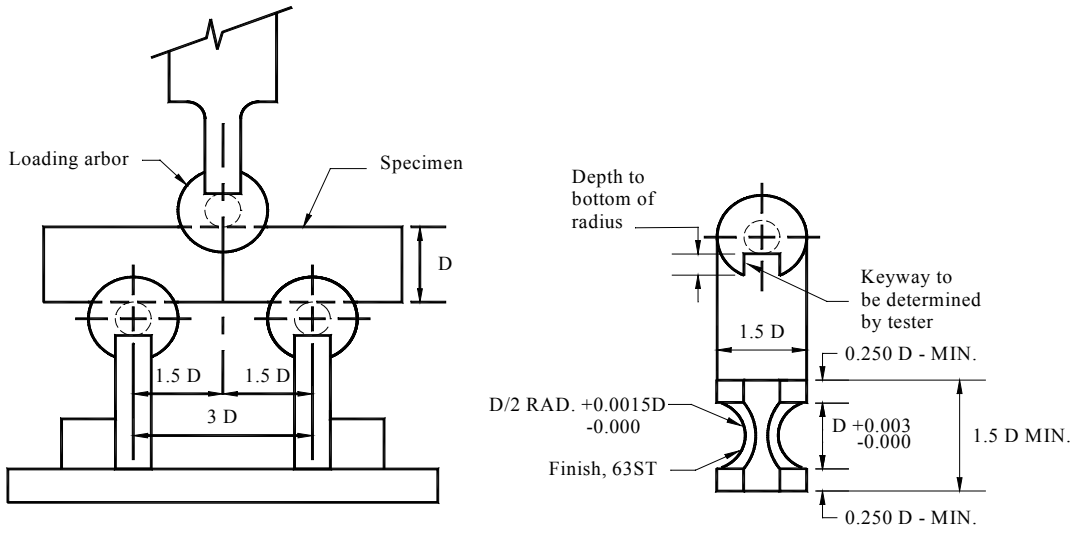

Figure 4.2 ASTM D4475 [24] test setup

4.1.3 Unaged Elemental Static Direct Shear Test Method

4.1.3.1 Introduction

Elemental direct shear tests provide a way to monitor the shear properties of the dowel-concrete system. In order to determine the shear properties of dowels by testing, the load and deflection must be measured at various levels in order to determine a relationship. There are a few ways to test the dowel-concrete system. The dowel-concrete system testing method needs to simulate the loading that a pavement dowel would see in the field. The following sections will describe shear-testing methods considered for the research project.

4.1.3.2 Iosipescu Shear Test Method

According the Walrath and Adams [29], the Iosipescu test achieves a state of pure shear loading at the centerline of the specimen because of the specimen's geometry. Figure 4.3 shows the original Iosipescu test developed by Adams and Walrath. Figure 4.4 shows the Iosipescu shear test specimen. To use the Iosipescu shear test method, a test frame was used that had been previously constructed for ISU research (Porter, Lorenz, et. al. [14]) and was based on smaller Iosipescu test frames developed by Adams. The test frame for testing Iosipescu specimens is shown in Figure 4.5. The dowel-concrete system is held tight by the tension rods to minimize bending and rotation. One end of the specimen is fixed and the other end is movable. This set up allows the load to be transferred as would be seen in the field resulting in direct shear of the dowel. The gap shown in Figure 4.4 allows the load to be transferred from one side to the other without having aggregate interlock or interface friction absorb some of the load.

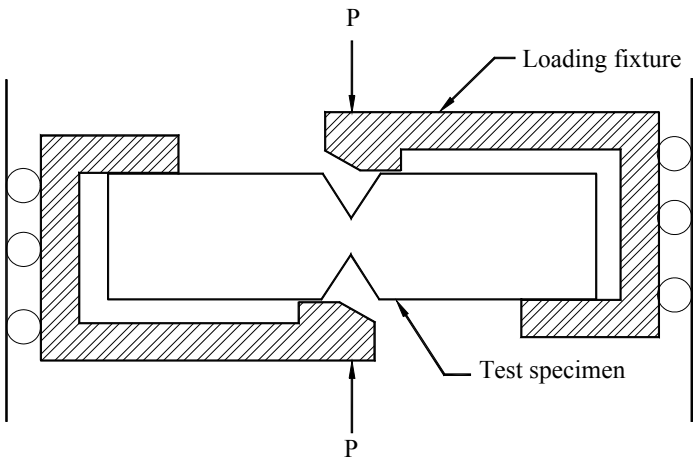

Figure 4.3 Iosipescu test designed by Adams and Walrath

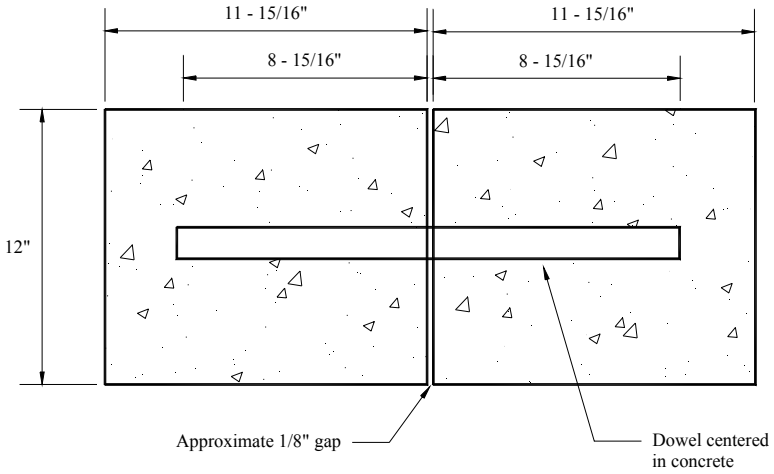

Side View

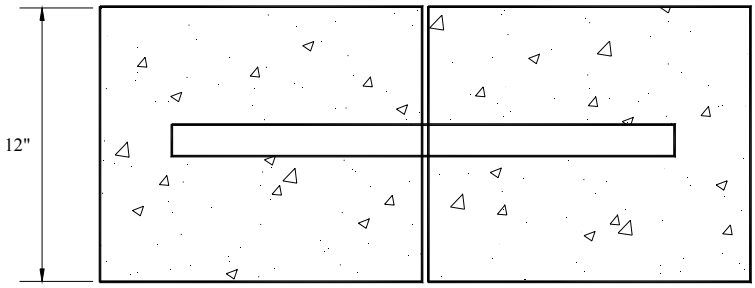

Top View

Figure 4.4 Iosipescu shear test specimen

The Iosipescu specimen can lead to the modulus of dowel support, K_o, by measuring the differential deflection, Δ, between the two concrete blocks as shown in Figure 4.6. The differential deflection is two times the deflection at the face of the concrete plus the shear deflection of the dowel, δ. The differential deflection is the equivalent of Equation 2.14, which is repeated here for convenience.

$$\Delta = 2y_o + \delta \tag{2.14}$$

The modulus of dowel support is directly related and can easily be determined once the deflection at the face is known. Determination of the modulus of dowel support is explained in Section 4.2.1. The modulus of dowel support is also very important in determining the bearing pressure seen by the concrete at the face.

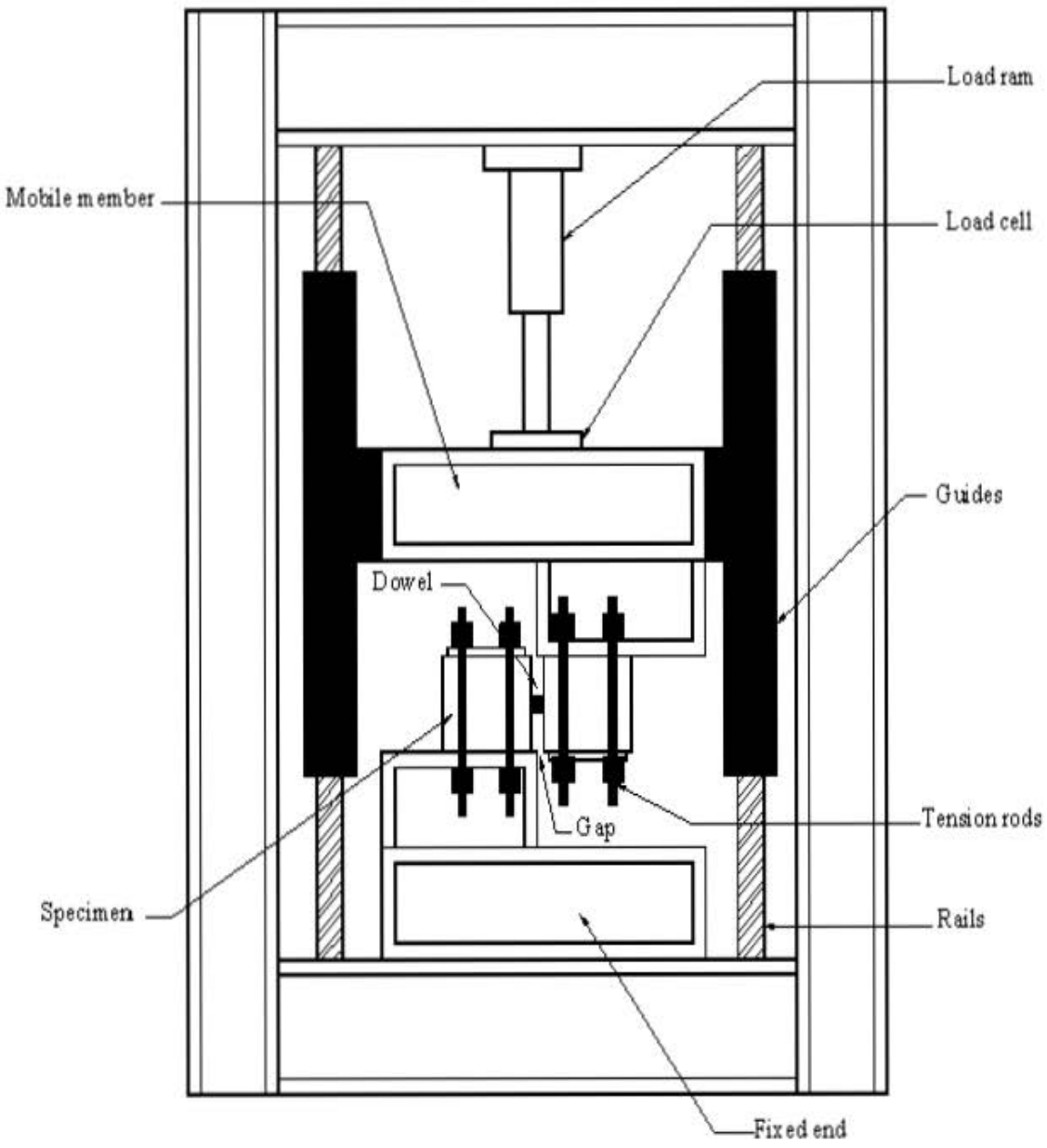

Figure 4.5 ISU Iosipescu testing frame [14]

4.1.3.3 AASHTO Shear Test Method

The AASHTO shear testing procedure applies loading to the dowel bars in a very similar manner as the Iosipescu shear test method. The only difference is the specimen and testing set up. The shear test method used for this research was based on the AASHTO T253-76 [5] standard test method. There are two dowels encased in concrete, which simulates two 12-inch high contraction joints. The test specimen is shown in Figure 4.7. The AASHTO test applies a uniform load as shown in Figure 4.8 to the middle concrete block. The deflected shape of the AASHTO specimen is also shown in Figure 4.8. Each dowel encased within the concrete block deflects the same as the specimen shown in Figure 4.6. For tests conducted at Iowa State University (ISU), the AASHTO setup was modified slightly. In the modified setup the joints were changed to a 1/8-inch gap to reflect actual field conditions. The width was also changed from 12 inches to 10 inches.

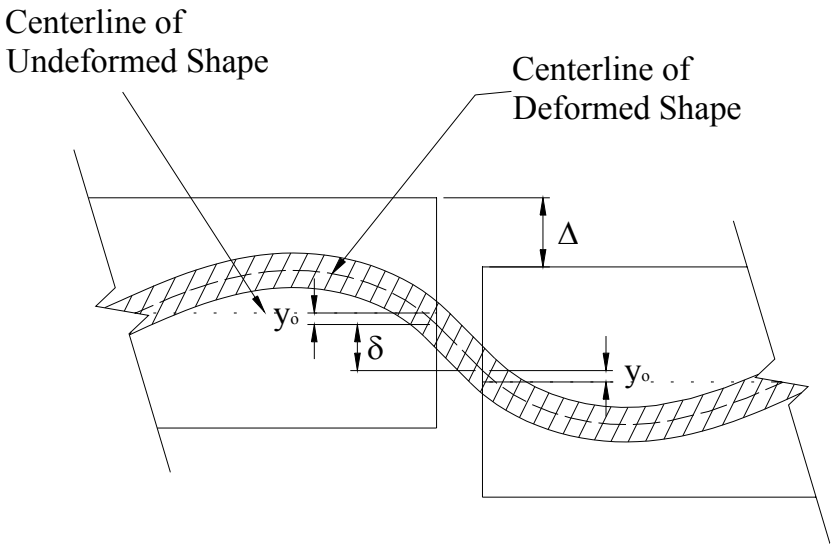

Figure 4.6 Differential deflection at the joint

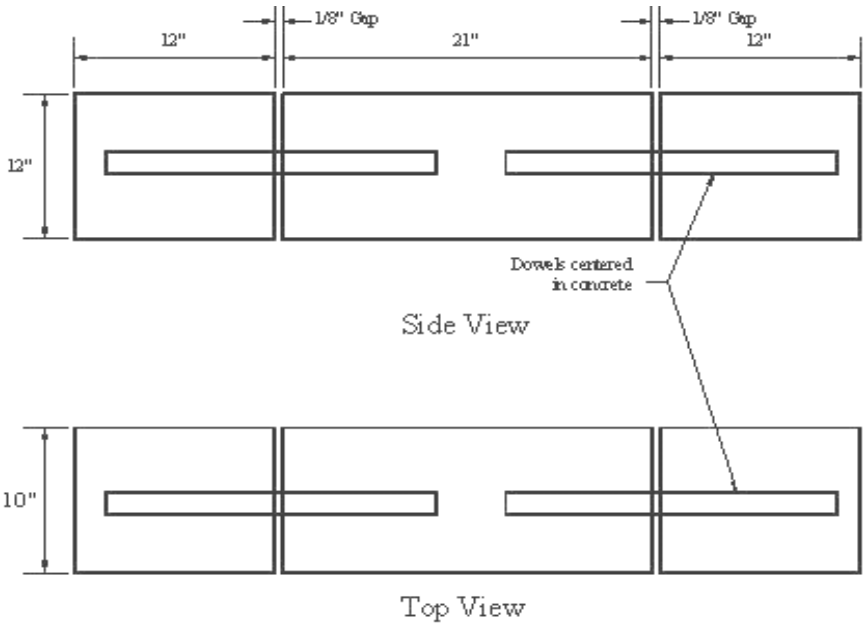

Figure 4.7 Modified AASHTO T253 test specimen [5]

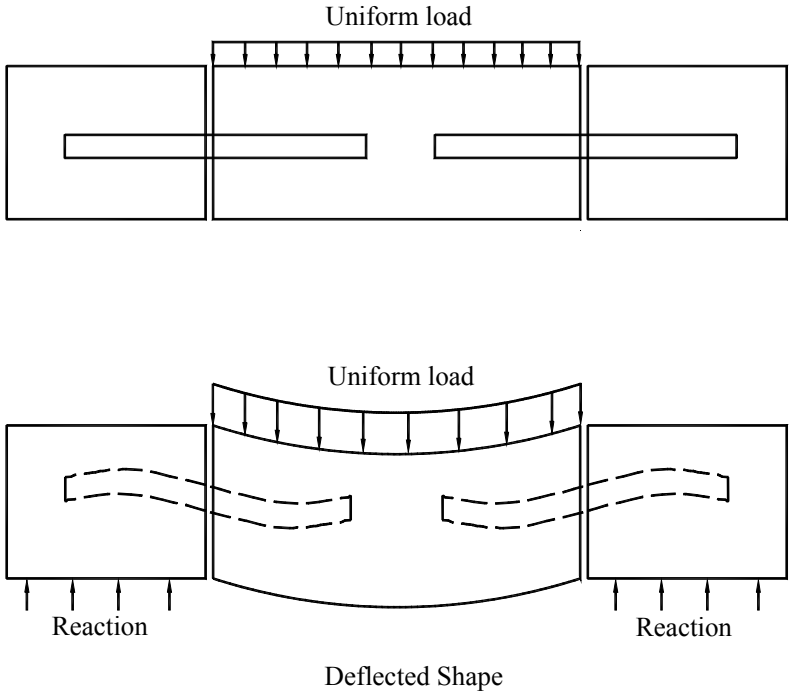

Figure 4.8 Uniform load applied to AASHTO specimen [5]

From the AASHTO specimen, the load-deflection characteristics need to be known as in the Iosipescu specimens to calculate the modulus of dowel support, K_o. Equation 2.14 is still used to calculate the differential deflection as in an Iosipescu specimen. The use of the AASHTO specimen is warranted as long as the moment distribution is the same as that of the Iosipescu specimen. The next section attempts to verify whether or not the AASHTO shear test is a valid method in determining the modulus of dowel support.

4.1.3.4 Selection of Shear Test Method

The modified AASHTO shear test method was the one chosen to test for the modulus of dowel support in this research. The reason that the Iosipescu shear test was not chosen was due to problems experienced in past tests done by the authors. The two

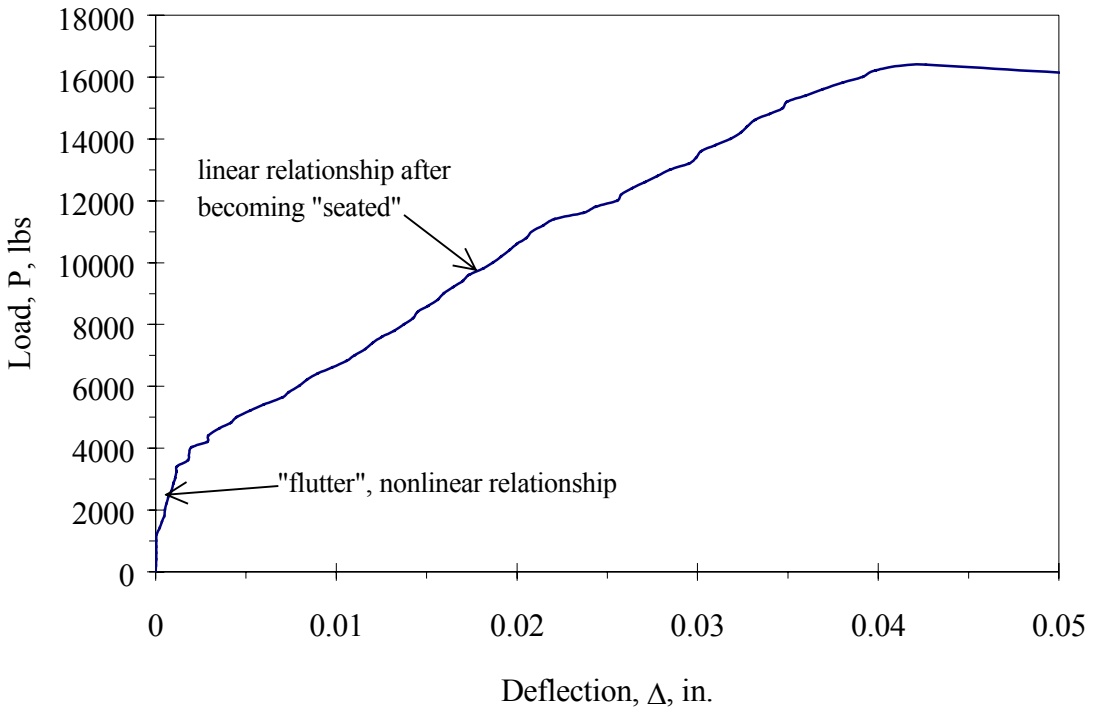

Figure 4.9 Iosipescu shear test indicating rotational problems until seated

blocks rotated slightly relative to each other and caused a nonlinear load-deflection relation. The load-deflection became linear after the blocks were "seated" in the testing frame. A typical load versus deflection for an Iosipescu specimen is shown in Figure 4.9. When sample AASHTO specimens were tested, a linear relationship was experienced between the load and deflection. In order for the AASHTO specimen shear test to be validated, an inflection point had to occur in the joint opening.

Strain gages were attached to the dowel bars encased in the concrete to see whether the dowel behaved the same as an Iosipescu specimen, i.e. moment equal to zero at the center of the joint opening. The configuration of strain gages is shown in Figure 4.10. The average values of the moments at each side of the joint opening were determined from the strain gage data. Using the annotation in Figure 2.4, the average value for M_1 was 174 pound-inches and M_2 had an average value of 18 pound-inches.

These average values just mentioned indicate that the moments do not agree with the theoretical assumptions of having an inflection point exactly in the middle. This

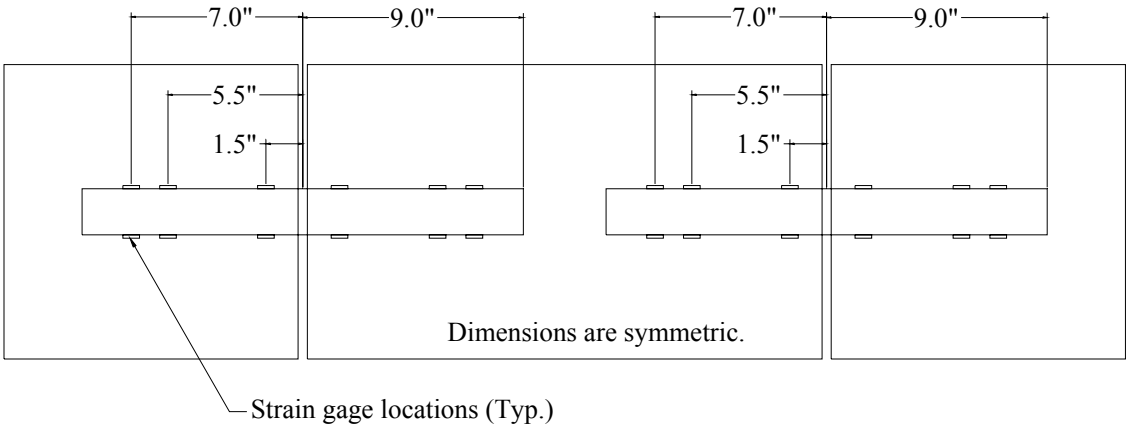

Figure 4.10 Strain gage layout on AASHTO specimens as shown in Figure 4.7

moment distribution indicates that the side of the joint, which has the higher moment, has the higher deflection at the face of the joint, y_o. However, the unequal moments are assumed to be acceptable since the modulus of dowel support is being determined using an average y_o value and the unequal moments will not be a factor affecting the modulus of dowel support value. Therefore, the AASHTO specimens are an acceptable representation of the action experienced by the highway pavement joints in the field.

4.1.3.5 Materials and Specimens

Since, the purpose of this research was to see how the modulus of dowel support, K_o, varies with dowel diameter and different dowel materials. The concrete strength was also varied to see if this had any effect on the modulus of dowel support. The specimens used were made like the AASHTO specimen shown in Figure 4.7. Epoxy-coated steel dowel bars are the typical dowel bars used in highway pavements. Therefore, the dowel materials chosen should somehow relate back to the standard dowels. This relation was accomplished by using aluminum and copper dowel bars both having a diameter of 1.5 inches and a diameter that would give the same modulus of rigidity, EI, as that of the standard dowel bar. Two different sizes of GFRP dowel were also used. Table 4.6 shows the different sizes and material properties. The properties for the steel, aluminum, and copper shown in Table 4.6 were obtained from Ugural's [28] textbook.

The concrete strengths were to represent the strength that a pavement would typically experience. The target concrete mix strength was 6000 psi for each set of dowel bars shown in Table 4.6. Once the concrete reached the desired strength, the specimens were tested.

Table 4.6 Dowel material and sizes used in static testing

Material	Diameter, in.	E, (10^6) psi	EI, (10^6) lb-in^2
Epoxy-coated Steel	1.5	29	7.206
Stainless Steel	1.5	28	6.958
Plain Steel[a]	1.5	29	7.206
Aluminum[b]	1.5	10	2.485
	1.957		7.200
Copper[b]	1.5	17	4.225
	1.714		7.202
GFRP	1.5	4.93	1.225
GFRP[b]	1.75	6.20[c]	2.854
GFRP	1.875	6.51	3.950

[a] Plain Steel indicates an epoxy coated dowel bar with the coating removed.
[b] These dowel bars were only tested in unaged specimens.
[c] Properties were taken from work done by Porter et al. [11] and [13].

4.1.3.6 Testing Setup

In order to get accurate results from an experiment, the proper testing setup is needed. The testing frame needs to be able to withstand the maximum load expected in the testing process. Figure 4.11 shows the testing frame used to test the AASHTO specimens. The specimens themselves should have the proper instrumentation needed to obtain usable results. Figure 4.11 also shows the instrumentation used throughout the specimen testing.

4.1.3.7 Testing Procedure

The load-deflection testing procedure was slightly modified from the procedure listed in the AASHTO T253 [5] standard test. The joint width used for this research was 1/8 inch instead of the recommended 3/8-inch width. The concrete was allowed to cure until the concrete cylinders broke at the desired strength. Then, the specimens were

tested. All of the specimens were loaded at the rate of 2,000 pounds per minute. The specimens were loaded until failure.

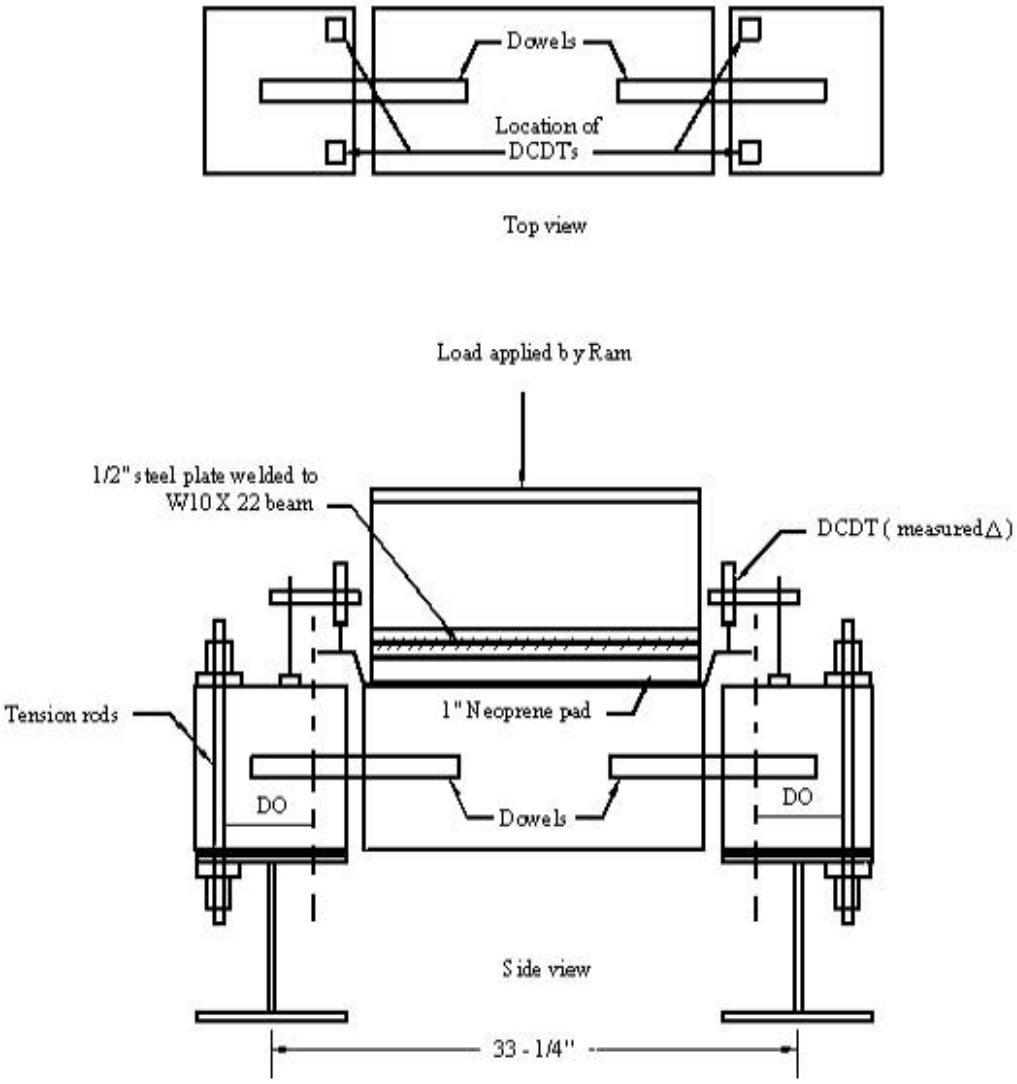

Figure 4.11 AASHTO testing setup [5]

4.1.4 Unaged Elemental Fatigue Test Method

4.1.4.1 Introduction

Elemental fatigue tests provide a fast and efficient means of examining the fatigue behavior of a dowel bar in a short period of time. This section describes the elemental fatigue testing program developed at Iowa State University.

4.1.4.2 Modified AASHTO Fatigue Test Method

As outlined in Section 4.1.3.3 a modified AASHTO test was used for a portion of the direct shear testing. This test was slightly modified and a special test frame was constructed for use in the elemental fatigue testing. The only modification made to the previously discussed AAHSTO method was a change in the loading. In the static shear test a uniform load was applied to the center block, as shown in Figure 4.11. However, in the fatigue testing the uniform load was changed to point loads positioned near the joints. This change was made so that clamps could be attached to the center block and the actuator could press down on the specimen as well as apply an upward force. The positioning of the two clamps near the ends of the center block was also done to decrease the deflection in the center of the block and force the inflection point towards the center of the joint. This reversal of load was used to subject the dowel bars to a stress reversal, as experienced when the wheel load passes over the joint. A test setup of this procedure is shown in Figures 4.12 and 4.13.

4.1.4.3 Loading

The loading actuators shown in Figure 4.12 applied a load of 3300 lbs to the specimen. This is the equivalent of 1650 lbs on each dowel. This load is closely related to what the critical dowel would experience on a 12-inch slab with the dowel bars spaced

at 12 inches. A deflection versus load diagram was taken before any fatiguing of the specimen had occurred. The specimen was then tested for 1 million cycles at a rate of approximately 4 cycles per second. After the specimen had seen one million cycles, a

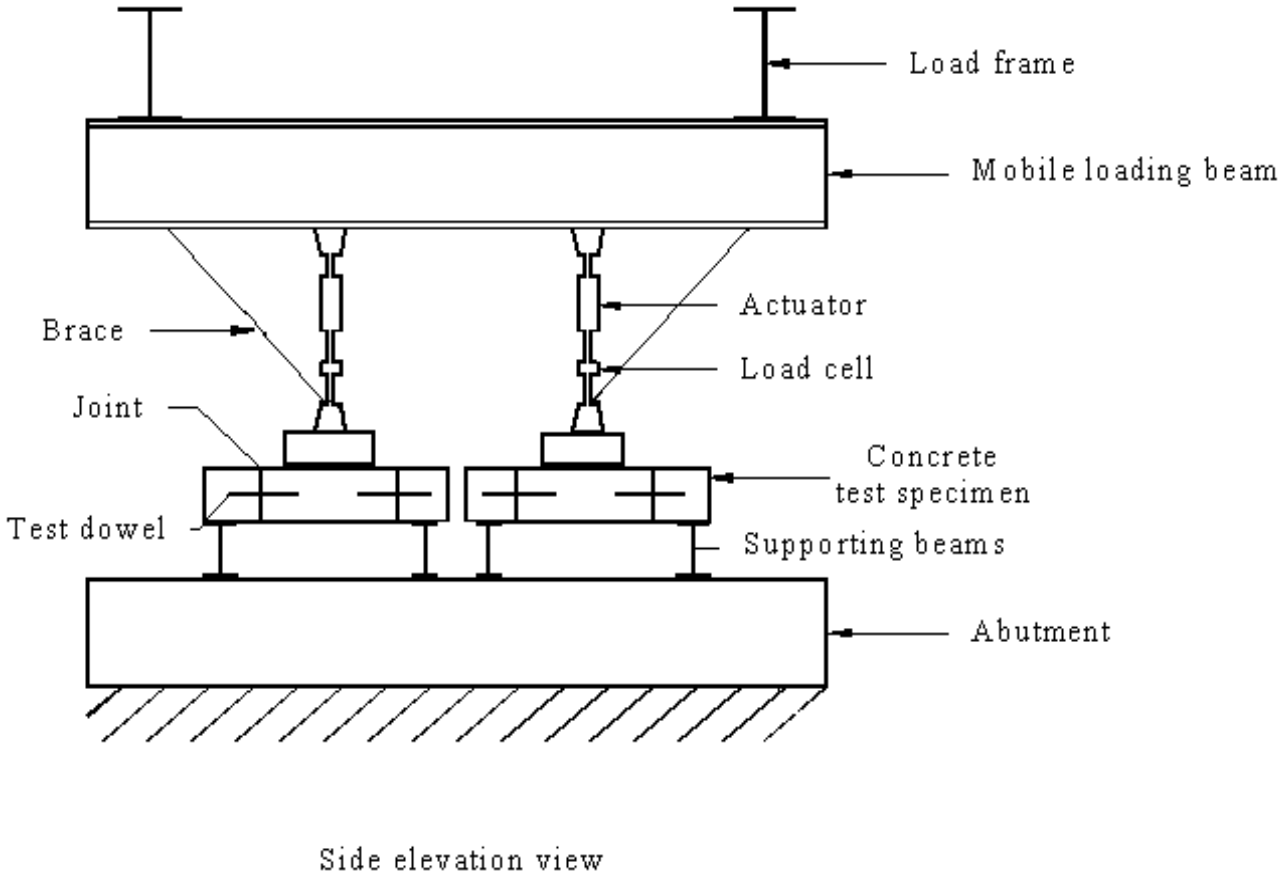

Figure 4.12 Testing frame for modified AASHTO fatigue test

second deflection versus load diagram was developed. The two deflection versus load diagrams were used to calculate the modulus of dowel support for the dowel bar before and after fatiguing. These values where then used to check the effects of fatigue on the dowel bars.

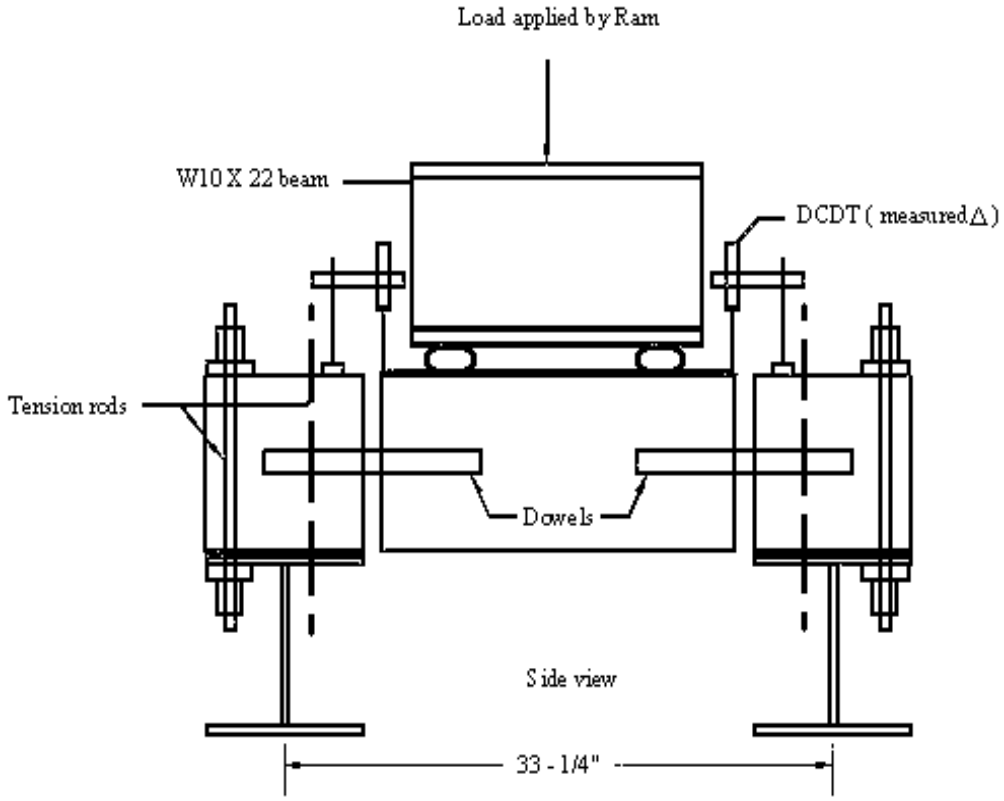

Figure 4.13 Loading of fatigue specimen

4.1.4.4 Materials

The dowel bars tested in the elemental fatigue tests consisted of bars that were made out of varying shapes and materials. Three types of dowel bars tested in the fatigue test were also tested in the static test. There were also two additional, alternately shaped dowel bars tested, an elliptical and a shaved dowel bar. The dimensions of these alternately shaped dowel bars can be seen in Figure 4.14. Table 4.7 shows the different shapes and materials that were used in the elemental fatigue testing.

Table 4.7 Dowel material and sizes used in fatigue testing

Material	Diameter, in.	E, (10^6) psi	EI, (10^6) lb-in^2
Epoxy-coated Steel	1.5	29	7.206
Stainless Steel	1.5	28	6.958
Elliptical GFRP[a]	Figure 4.14	8.66	2.210
Shaved GFRP[a b]	Figure 4.14	6.51	1.619
GFRP	1.5	4.93	1.255
GFRP	1.875	6.51	3.950

[a] These dowel bars were only tested in unaged specimens.
[b] The Shaved GFRP dowel bars were cut from the 1.875"ϕ Dowel bars.

4.1.5 Unaged Pullout Test Method

4.1.5.1 Introduction

As pavements go through various seasons, they are subjected to many adverse weather conditions. Since the weather conditions change throughout the seasons, especially the temperature, the concrete expands and contracts. If the concrete is going to expand and contract, the dowel bars must allow the concrete to move.

4.1.5.2 Objective

The objective for this part of the research is to subject the dowel bars to a pure axial load and monitor how the dowel bars slide within the concrete once they have completley lost bond with the concrete. These pullout tests should be able to tell whether or not the stainless steel and GFRP dowel bars react in a comparable manner to that of the standard epoxy coated steel dowel bars.

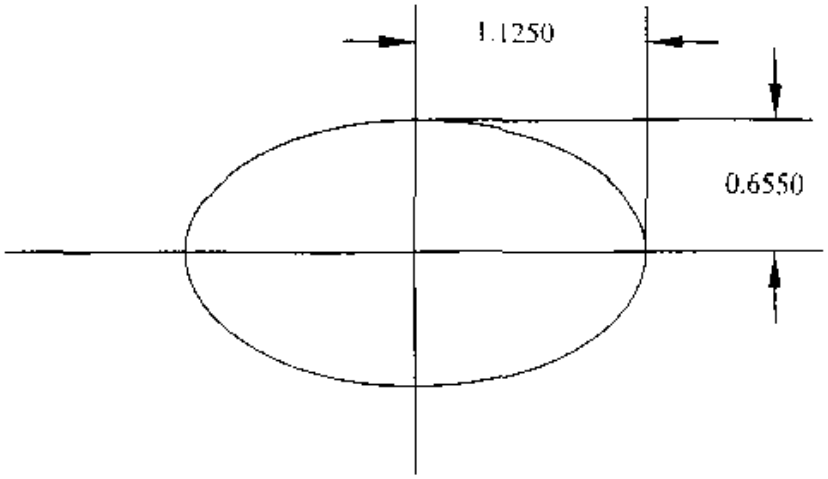

Alternate Shape #1 : Ellipse

Equation of the Ellipse: $\frac{x^2}{1.125^2} + \frac{y^2}{0.655^2} = 1$

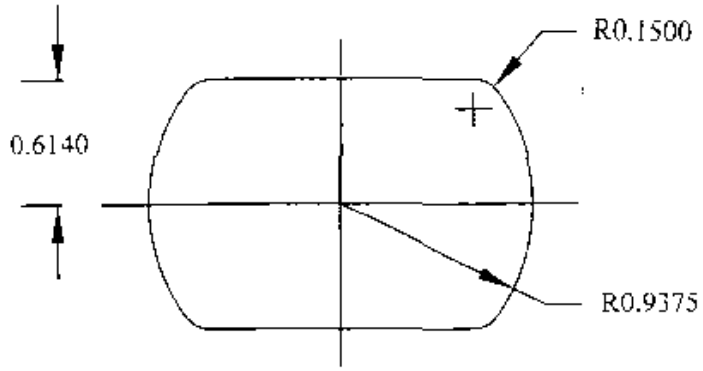

Alternate Shape #2 : Originally a 1.875 inch diameter dowel bar with the top and bottom halves shaved. The corners have a fillet with a radius of 0.15 inches.

Figure 4.14 Alternately shaped dowel bars

4.1.5.3 Scope

The scope for this part of the research includes the construction of 12 specimens. There are four different types of dowel bars to be tested. The different types of dowel bars include:

- standard epoxy coated,
- stainless steel,
- 1.5”ϕ GFRP, and
- 1.875”ϕ GFRP.

4.1.5.4 Materials and Specimens

The pullout specimens where fabricated to the dimensions shown in Figure 4.15. The dowel bars where cast into a 12-x 12- x 12-inch block of concrete. For the stainless steel and epoxy coated steel dowel bars, a sufficient length of #5 reinforcment was welded to the end of the dowel bar to allow for gripping. For the GFRP dowel bars, an 8-inch hole was drilled into the dowel bar to allow a #4 reinforcment to be placed in the end of the dowel. A sufficient length of #4 reinforcment was then glued in using a high strength epoxy.

4.1.5.5 Testing Procedure

The pullout tests were performed using a universal-testing machine. The concrete portion of the pullout specimens was held firmly in placve by the lower head of the testing machine while the upper head gripped the rebar with a clamping device. A tensile load was applied to the specimen with a loading rate of 0.030 inches per minute. The load was applied until at least ½-in of dowel pullout was achieved. However, a loading was contuniued until 1 inch of the dowel pullout had been achieved. The last half-inch

was done to see whether or not the load contunied to increase after the intial ½-inch pullout. Pullout was measured by mounting a Direct Current Displacment Transducer (DCDT) to the dowel bar as shown in Figure 4.15.

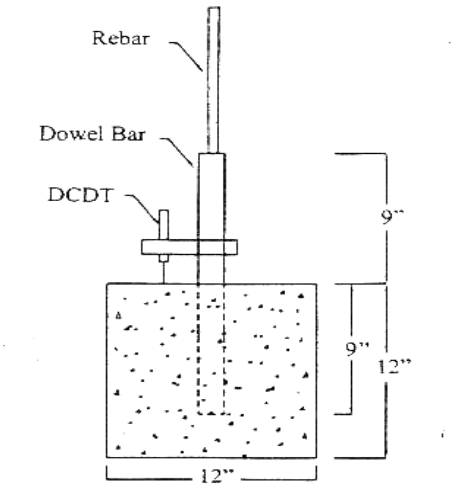

Figure 4.15 Pullout Specimen

4.2 Phase II – Aged Testing

4.2.1 Aged Elemental Static Direct Shear Test Method

Specimens were constructed indentically to the unaged specimens. After allowing the specimens to cure for 28 days, they were placed in a 131.3ºF solution of NaOH and $Ca(OH)_2$ with a pH of 12.0-12.5 for 99 days. This aging is equivilent to 18247 days or approximately 50 years of real time aging. The specimens were tested as described in Section 4.1.3. A listing of the dowel bars tested can be found in Table 4.6.

4.2.2 Aged Elemental Fatigue Test Method

Specimens were constructed identically to the unaged specimens. The specimens were aged as outlined in Section 4.2.1. These elements were tested as described in Section 4.1.4. A listing of the dowel bars tested can be found in Table 4.7.

4.2.3 Aged Pullout Test Method

Specimens were constructed similarly to the unaged specimens. The only difference is that the rebar was not attached until after the specimens were done aging. The specimens were aged as outlined in Section 4.2.1. The specimens were tested as described in Section 4.1.5.

4.3 Phase III – Full-Scale Laboroatory Testing

4.3.1 Introduction

The purpose of this experimental investigation was to evaluate the performance of two different GFRP dowel systems. A laboratory test setup previously developed at ISU that simulates actual pavement loading conditions was employed to achieve this goal. Experimental results from this investigation were compared to those obtained from theoretical and numerical analyses. Test results and comparisons provided additional insight to the performance of GFRP dowels and aided in the development of design recommendations for GFRP dowels.

4.3.2 Materials and Specimens

Two full-scale pavement slabs were constructed to the following dimensions: 12 inches thick, 6 feet wide, and 12 feet long. One specimen contained 1.5-inch diameter

GFRP dowels spaced at 12 inches, referred to as Slab 1, while the other specimen, referred to as Slab 2, contained the same diameter GFRP dowels but spaced at an equivalent spacing of 6 inches, as will be explained in Section 5.2.2.2. Both specimens were cast in place on top of steel supporting beams and contained an 1/8-inch formed transverse joint at midlength. A joint opening of 1/8-inch was determined to represent actual field conditions during the majority of a pavement's life as a result of shrinkage and temperature contraction. Dowel bars were positioned at middepth and centered in the middle of the joint in both specimens.

A concrete mix designated C3-WR-C20 by the Iowa Department of Transportation (IDOT) was used in constructing the specimens. Testing did not begin until the concrete had cured for at least 28 days. This provided an ample amount of time for the concrete strength to stabilize before testing, thus, eliminating the influence of strength gain on the results. The average compressive strength of the concrete was determined by testing 3 standard 6- x 12-inch cylinders. The modulus of rupture or flexural strength of the concrete was determined by breaking 2 standard 6- x 6-inch beams. The compressive and flexural strength of each specimen at the time testing began is shown in Table 4.8.

Table 4.8 Compressive and flexural strengths of specimens

Specimen	Compressive Strength f'_c, psi		Modulus of Rupture MOR, psi	
	North	South	North	South
Slab 1	7484	6357	520	510
Slab 2	6891	5671	570	505

Due to construction difficulties in forming the transverse joint, each specimen had to be cast in two separate pours. The staging of the construction was such that the north half of the specimen was poured on one day while the south half of the specimen was poured on the following day. Since the concrete used in constructing both halves of the specimen did not come from the same batch, cylinders and beams were made for each half of the specimen. When necessary in the discussion of the experimental investigation this north or south notation will be used. A complete discussion on the construction of the specimen is given in Section 5.3.

The 1.5-inch diameter GFRP dowels used in this study consisted of E-glass fibers encased in an isophthalic polyester resin. Volume fractions for the two components of the 1.5-inch diameter GFRP dowels are shown in Table 4.9. The material properties for the 1.5-inch diameter dowels were given in Table 4.6.

Table 4.9 Volume fractions for 1.5-inch diameter GFRP dowels

Component	Volume Fraction
Glass	0.5179
Resin	0.4821

4.3.3 Test Setup

4.3.3.1 Subgrade Simulation

Previous investigators at ISU decided to simulate a subgrade through the use of steel beams in their laboratory test setup. Steel beams provide a subgrade support that does not change as testing progresses and requires the minimum amount of maintenance. In the case of an actual soil subgrade, considerable effort is put forth in preparing the subgrade to a specified value for the modulus of subgrade reaction only for this value to

change throughout the course of testing due to additional compaction of the soil from repetitive loading. The steel beams selected and their positions are shown in Figure 4.16. This particular arrangement of beams resulted in a simulated subgrade having a modulus of subgrade reaction equal to 160 pci, as determined in Section 3.2.3. A detailed explanation of the original design of the subgrade was presented in Section 3.2.1.

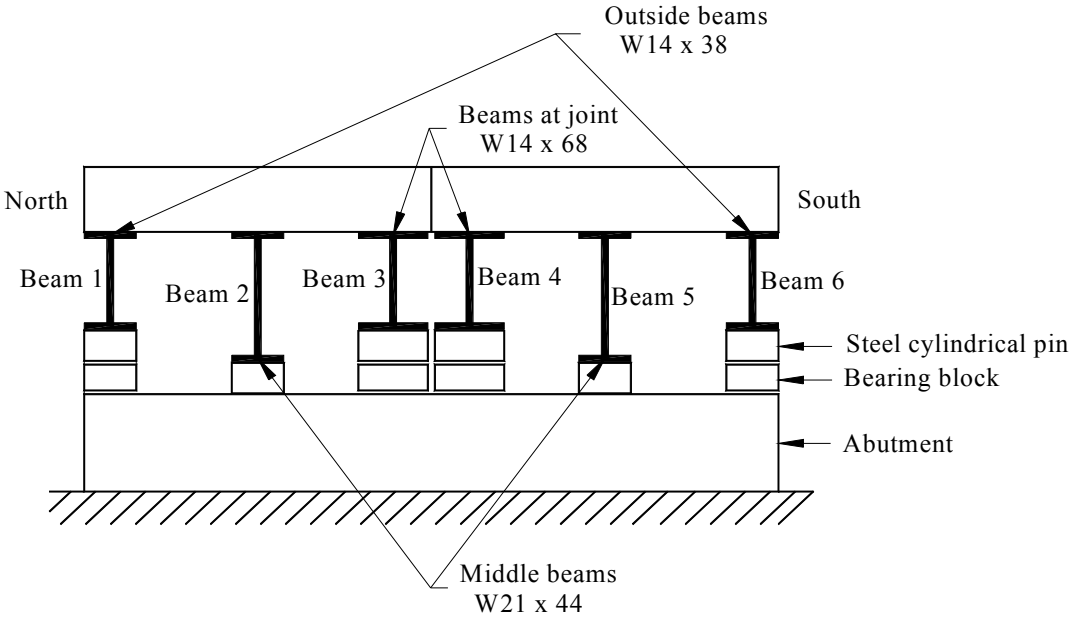

Figure 4.16 Steel supporting beams

A considerable difference in depth existed between the two W21x44 beams and the four W14 series beams. To make up the height difference between the two different series of beams, the four W14 series beams were placed on bearing blocks as shown in Figure 4.17. To prevent a bearing failure in the concrete abutment, the two W21x44

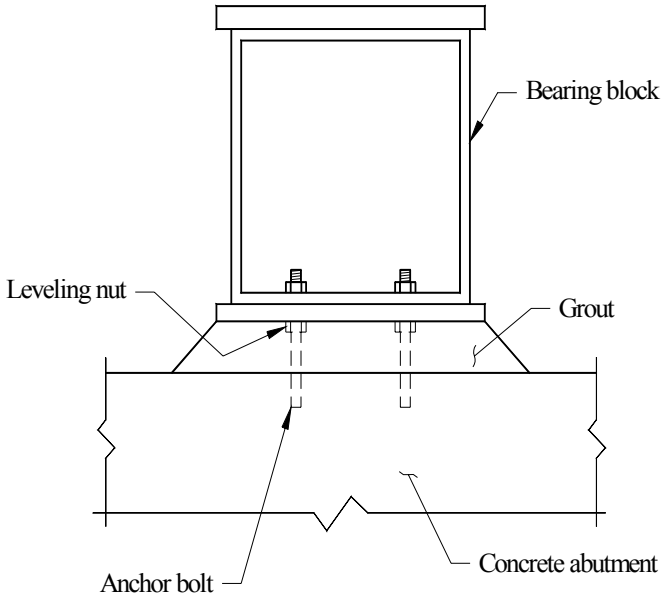

Figure 4.17 Bearing block

beams rested on bearing plates. These bearing blocks and plates could be adjusted up or down through the use of leveling nuts, which were attached to anchor bolts placed in the abutments, to obtain a level surface across the top of the supporting beams. The elevation required for the top of a bearing block or plate was back calculated from the known elevation for the top of the beam and its corresponding depth. The bearing blocks and plates were placed on top of the leveling nuts and adjusted until the top of the block or plate was level and at the proper elevation. Once all the bearing blocks and plates were at their proper elevations, they were bolted down and non-shrink grout was injected in the space between the top of the abutment and the bottom of each block and plate.

Steel cylindrical pins were placed on top of all the bearing blocks and plates to serve as roller supports for the beams. A stable, simply supported condition was formed by welding the pin to the top of the block or plate at one end of the beam.

4.3.3.2 Test Slabs

A unique construction technique requiring the casting of a slab in two halves over two consecutive days was used to form both specimens. Construction difficulties experienced in previous research in forming a transverse joint at midlength of a specimen justified this technique. On the first day, formwork for one half of the slab was assembled and concrete for this half poured. On the following day, formwork for the other half of the slab was assembled in the morning and concrete poured that afternoon.

Wood formwork was placed between the beams to form the bottom of the slab while steel forms were used to form the sides and ends of the slab. A 1/8-inch thick sheet of polyvinyl chloride (PVC), supported laterally by a 2- x 12-inch board, was used to form the face of the joint on the first half of the slab constructed. Holes were drilled in the board and PVC at the locations of the dowel bars. Once the holes were drilled, the board and PVC were ripped lengthwise to allow for the removal of the board and PVC after the first half of the slab was poured. The dimensions of the PVC sheet were such that the top half of the sheet stuck above the formwork and the bottom half protruded below the center supporting beams. This additional width provided something to grab on to and pull when trying to remove the top and bottom halves of the PVC sheet.

After the wood formwork and steel forms were in place and the board and PVC fabricated, the formwork used to form the face of the joint was assembled. The bottom portion of the PVC was slid between the two center beams and clamped into position.

The top portion of the PVC was then positioned and clamped. Once both portions of the PVC were in position, the 2- x 12-inch board was bolted to the ends of the side forms, sandwiching the PVC between the ends of the side forms and the 2- x 12-inch board. After the board was in place, dowels were inserted through the predrilled holes and positioned. Angle iron was screwed to the outside of the board to prevent the top and bottom half of the board from separating. Bracing was then attached to the angle iron closest to the center of the board and welded to one of the center beams to prevent the board from bowing, thus ensuring that a straight joint was formed. To prevent adhesion to the concrete, a thin layer of grease was applied to the PVC. Figures 4.18 and 4.19 show the formwork used to pour the first half of Slab 2.

Before placing the concrete, a sheet of polyurethane was placed over the top of the steel beams and wood formwork. This prevented a bond from developing between the concrete and steel. Neoprene was used in past studies at ISU for this purpose; however, neoprene has a tendency to lose its elastic properties after prolonged exposure to compressive stresses. Since the affect of the degradation of the elastic properties of the neoprene on the value of the modulus of subgrade reaction for the steel supporting beams was unknown, the authors selected to use polyurethane for the purpose of separating the slab from the beam.

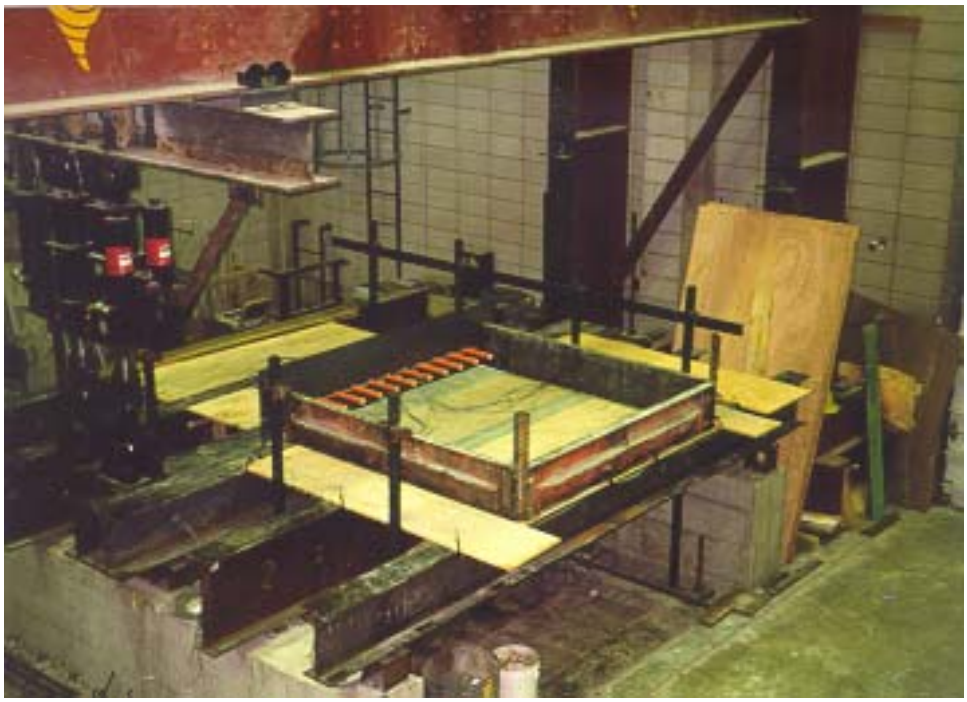

Figure 4.18 Formwork for north half of Slab 2

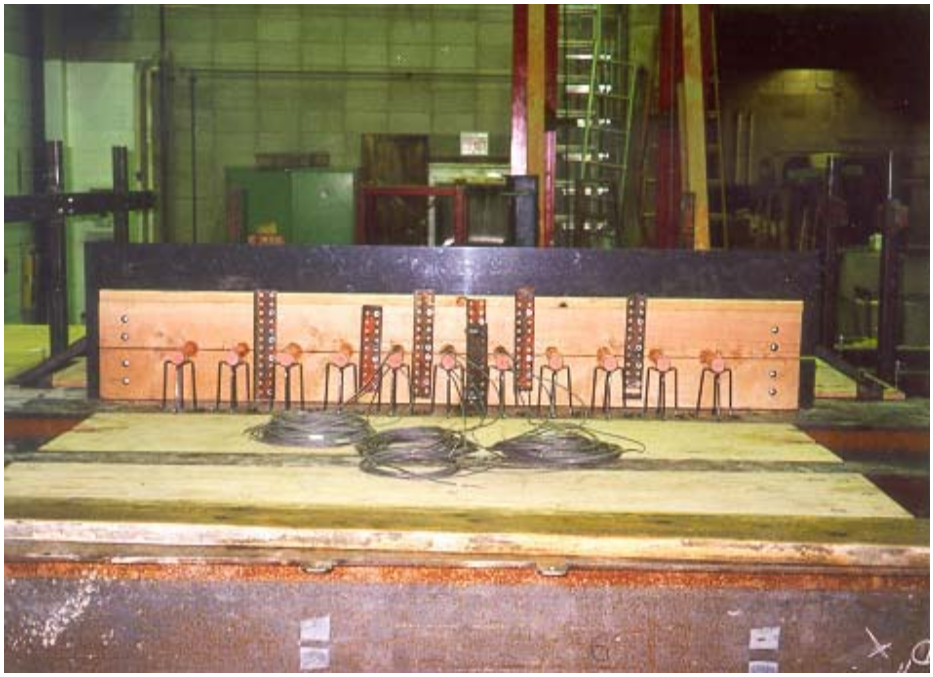

Figure 4.19 Formwork used to form a straight joint for Slab 2

The day after concrete was poured for the first half of the slab, the 2- x 12-inch board used to support the PVC was removed and formwork for the other half of the slab was assembled. The ends of the side forms for the second half of the slab were butted up against the PVC and bolted to the ends of the side forms used in casting the first half of the slab. A thin layer of grease was also applied to the surface of the PVC that was against the 2- x 12-inch board during the first pour. Formwork for the second half of Slab 1 is shown in Figure 4.20.

Figure 4.20 Formwork for second half of Slab 1

After the concrete had cured for approximately seven days, the PVC sheeting and formwork were removed. The top half of the PVC was removed by pulling on this half from the top of the slab. The bottom half of the PVC was removed by crawling under the

laboratory setup and pulling down on the PVC. The PVC was removed from between the two halves of the specimen with little effort. The authors attribute the easy removal of the PVC to the thin layer of grease applied to the surfaces of the PVC.

4.3.3.3 Loading System

Cyclic testing was accomplished through the use of a MTS, closed-loop, servo-controlled, testing system. In order to simulate the loading of the joint by a truck tire, a sinusoidal-shaped load function was selected for both actuators with the two functions 180 degrees out of phase. For each function, the load ranged from a maximum of 9000 pounds to a minimum of 300 pounds. The frequency of the load application was set at 5 hertz. The two load functions used during cyclic testing are shown in Figure 4.21.

The measure of joint performance as given by AASHTO in Section 2.1.1 assumes the data used in calculating this measure was obtained from 9000 pound wheel load applications. Since Brown and Bartholomew [2] and ACPA [3] remained silent on this point, a maximum load of 9000 pounds was selected. A maximum load of 9000 pounds was also used in previous testing conducted at ISU. A minimum load of 300 pounds ensured that the specimen would not “walk out” from under the actuators.

Cyclic load was applied to the specimens through the use of two hydraulic actuators positioned on each side of the joint along the centerline of the specimen. The center of each actuator was approximately 7.25 inches from the center of the joint. Imminent contact between components on the two actuators prevented the actuators from being placed any closer to the joint. A 10.61-inch square load plate was attached to the bottom of both actuators. The shape and dimensions of the load plate were selected to represent the equivalent contact area for a set of dual tires inflated to a pressure of 80 psi

and carrying a load of 9000 pounds, as determined by ACPA's equation for tire contact area [6]. A 3/4-inch thick neoprene pad was placed between the load plate and the top of the concrete slab to avoid local crushing of the concrete and to evenly distribute the applied load.

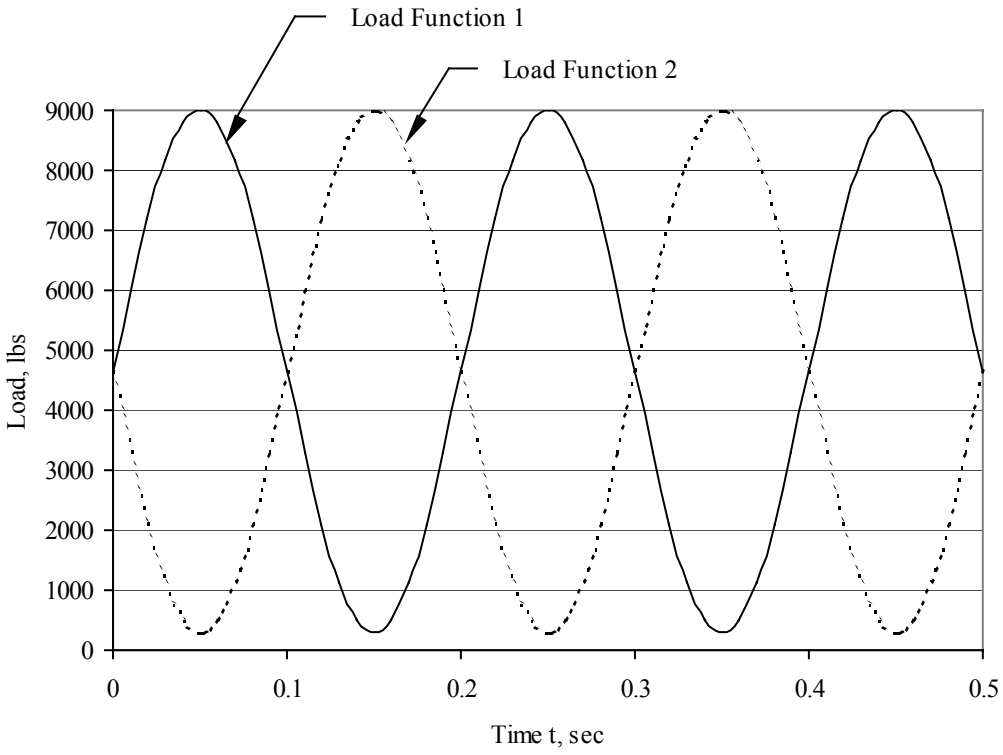

Figure 4.21 Load functions

The actuators were supported by a moveable beam that was attached to a steel load frame, as can be seen in Figure 3.8. The steel frame was in turn fixed to the tie-down floor of the testing laboratory. To prevent the movement of the actuators during cyclic testing, the actuators were braced horizontally to the steel frame and longitudinally to the moveable beam. The moveable beam permitted the actuators to be rolled out of

position without having to dismantle the actuators for the construction of the second test specimen.

4.3.4 Instrumentation

Slab deflections, applied load, and load transfer needed to be measured and recorded throughout the experimental investigation in order to determine the performance of the doweled joints. Instrumentation used to collect this type of data consisted of direct current displacement transducers (DCDTs), load cells, and strain gages. Data from the instrumentation was only collected during static-load testing of the specimens, which was conducted between intervals of cyclic loading. A data acquisition system was used to collect the data from static-load tests for further analysis.

4.3.4.1 Slab Deflections

Vertical displacements were of particular interest in analyzing the behavior and performance of each slab. DCDTs were placed on top of the slabs and mounted to an external frame in order to monitor the vertical displacements of each slab. To prevent the frame from vibrating during testing, the frame was built around the specimens and did not touch any part of the test setup. The stability of the frame was ensured by fixing it to the tie-down floor. Figure 4.22 demonstrates the use of this frame during testing.

A total of 18 DCDTs were used during the testing of Slab 1. A layout for the DCDT instrumentation for Slab 1 is given in Figure 4.23. To obtain a deflection profile for both sides of the transverse joint, DCDTs were placed along both sides of the joint at the location of every dowel bar. In addition, a DCDT was placed on each side of the joint at the centerline of the specimen. Data from these two DCDTs was used to evaluate the

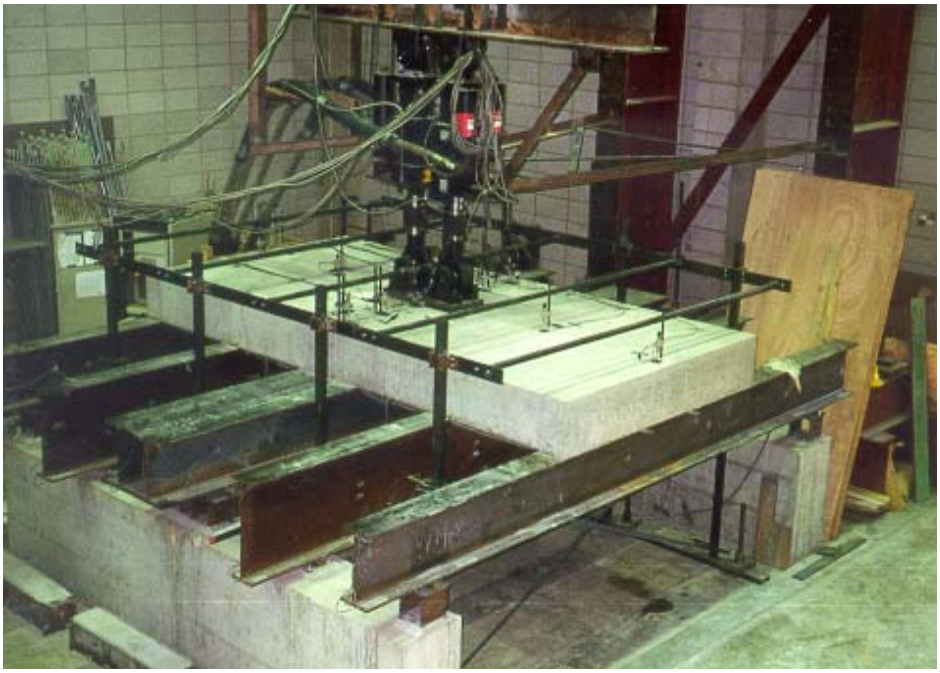

Figure 4.22 DCDT instrumentation frame

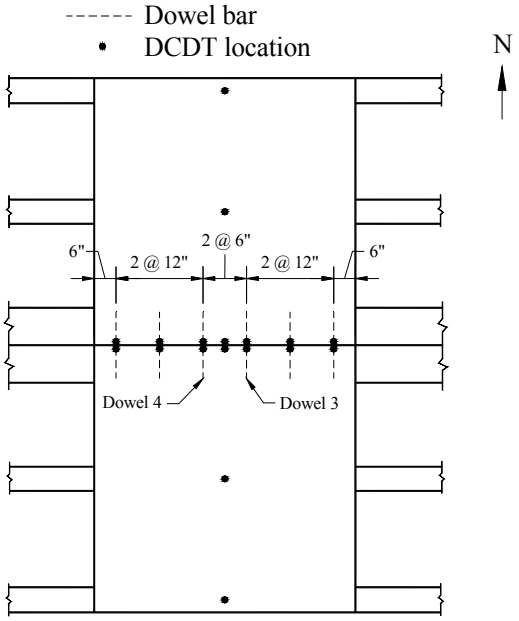

Figure 4.23 DCDT instrumentation layout for Slab 1

performance of the joint. The stems of these 14 DCDTs were approximately 3/4-inch from the centerline of the joint. DCDTs were also placed at the points of intersection of the centerline of the specimen with the centerlines of the middle and outside beams on both sides of the joint. Deflection measurements from the DCDTs along the centerline of the slab were used to create a deflection profile for the centerline of the slab. Deflection profiles were used to verify the modulus of subgrade reaction for the supporting beams and that the behavior of the laboratory test setup was comparable to actual field conditions.

Since Slab 1 contained fewer dowels and a majority of the DCDT instrumentation for this slab was for verification purposes, the instrumentation layout for Slab 2 differed from Slab 1. The layout for the DCDT instrumentation for Slab 2 is given in Figure 4.24. Fourteen DCDTs were placed along both sides of the joint at the location of every dowel bar except at the location of the two outside dowels on each side of the centerline of the specimen. DCDTs were not placed at these locations because the comparison of results between Slab 1 and finite element analyses showed deflection measurements taken from the outside of the slab were invalid. The stems of these fourteen DCDTs were approximately 3/4-inch from the center of the joint.

In both slabs, the stems of the DCDTs rested on rectangular PVC plates. The use of these PVC plates guaranteed a flat surface for the stems to bear against. All PVC plates were cut from the leftover PVC sheeting used in forming the joint and were epoxied down to the top of the slab.

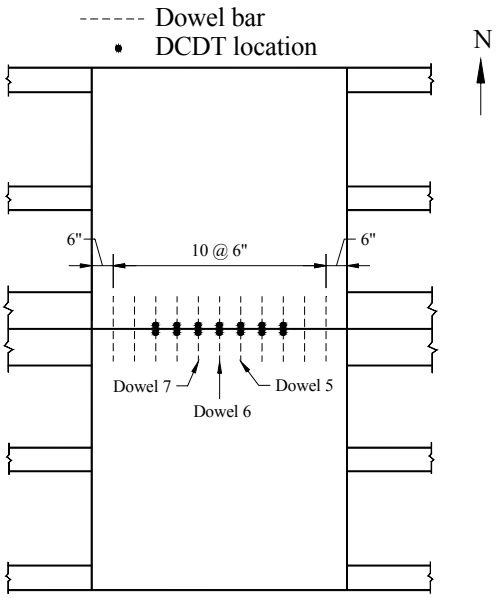

Figure 4.24 DCDT instrumentation layout for Slab 2

4.3.4.2 Load

Load cells were used to measure the load applied by each actuator. These load cells were integral with the actuators and were located between the piston and base of the actuators. Each load cell was calibrated before testing of the specimens began. Calibration of each load cell was accomplished by placing a load cell that was known to be calibrated correctly between the load plate attached to the bottom of each actuator and the top of the concrete slab. Load was applied to the correctly calibrated load cell by each actuator and the load cells integral with the actuators were adjusted to read the same load as recorded by the correctly calibrated load cell.

4.3.4.3 Load Transfer

Load transfer across the joint was monitored through strain gages attached to the supporting beams and dowel bars. Load tests were performed to develop force-strain

relationships for each beam and dowel bar instrumented. These relationships were used to determine the magnitude of force distributed to each beam and dowel bar. Knowing the distribution of the applied load amongst the elements of the test setup, the load transfer across the joint could be determined.

To determine the relationship between strain and the load distributed to each beam, strain gages were placed at two locations along the length of the supporting beams, as shown in Figure 4.25. At each location, a total of four strain gages were attached to the flanges of the beams. One gage was glued to the underside of both the top and bottom flange on each side of the web, as shown in Figure 4.25. Four gages were placed at each location as a precaution against damage; therefore, up to three gages could be ruined without totally negating the collection of strain data at a location. Of course, a better measure of strain would be provided if data was collected from all four gages. Strain gages were not placed on the two outside beams since the finite element analysis of the laboratory setup showed that none of the applied load was distributed to these two beams.

For the dowel bars, the moment along the length of the dowel was of particular interest. Knowing the moment at two locations on either side of the centerline of the dowel would enable the determination of the constants C and D in Equation 2.5 (constants A and B are equal to zero for the case of a dowel bar of semi-infinite length). Knowing the constants C and D, the load transferred through the dowel could be obtained by successive differentiation of Equation 2.5. Therefore, strain gages were placed on both sides of the centerline of the dowel at two locations as illustrated in Figure 4.26. At each location two strain gages were placed diametrically opposite each

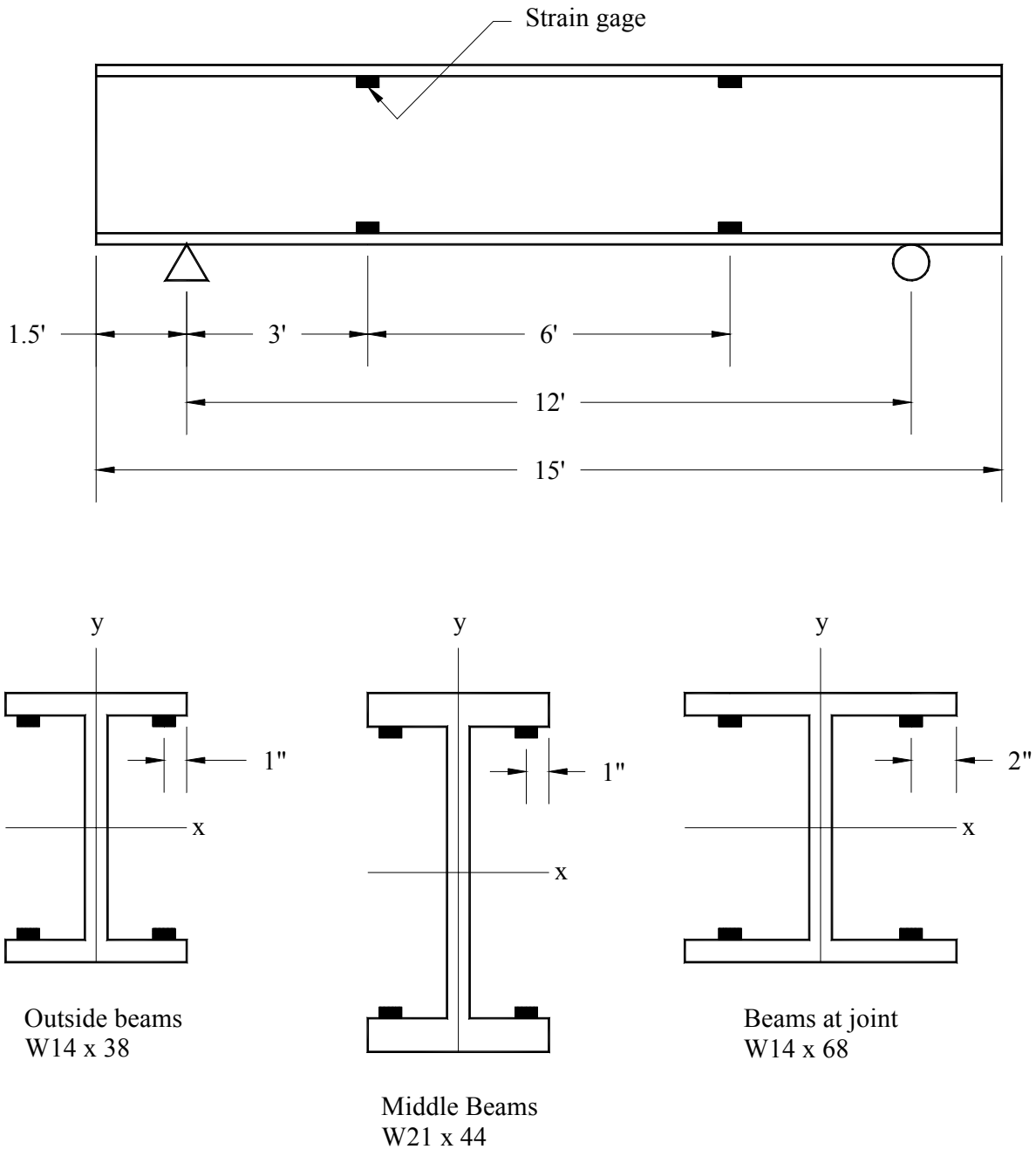

Note: All strain gages are placed symmetrically about the x and y axes

Figure 4.25 Location of strain gages on steel supporting beams

other. A more complete description of the determination of the load transferred through each dowel from measured strains is given in Section 5.5.5.

Since a majority of the applied load is transferred across the joint through the dowels located closet to the point of application of the load, only the dowels located closet to the centerline of the specimen had strain gages placed on them. For Slab 1, only the two dowels 6 inches east and west of the centerline of the slab possessed strain gages. For Slab 2, only the dowel at the centerline of the slab and the two dowels 6 inches east and west of the centerline of the slab contained strain gages.

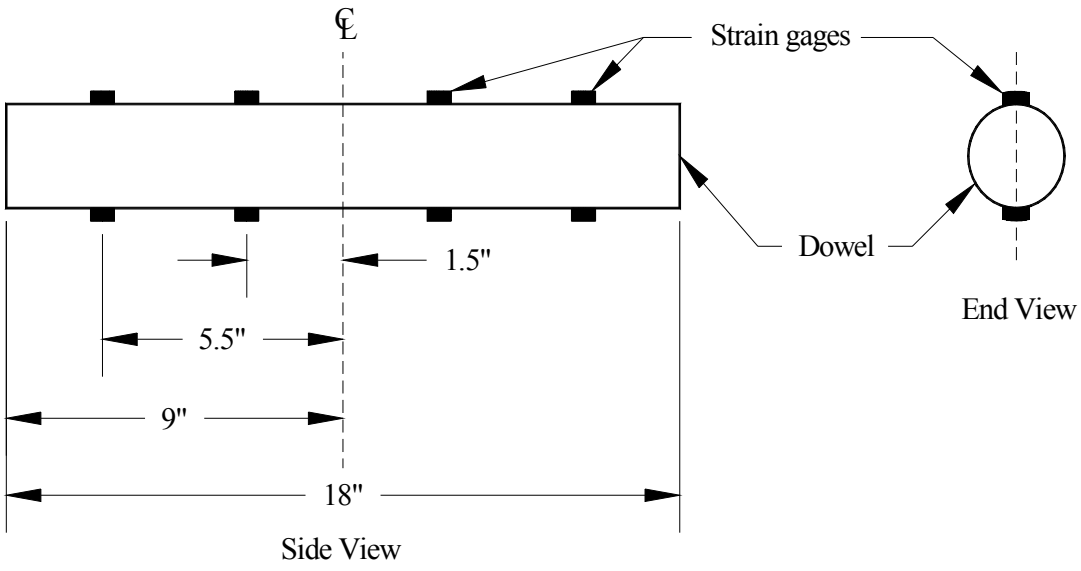

Note: Location of strain gages is symmetric about C.L.

Figure 4.26 Location of strain gages on GFRP dowels

4.3.5 Test Procedure

4.3.5.1 Load Tests

Before the supporting beams were set in place on the abutments or the dowel bars encased in the slab, load tests were performed on each beam and dowel bar that contained strain gages. A relationship between the applied load and corresponding strain could have been determined theoretically; however, misalignment of the strain gages and variation in material properties and section dimensions introduces errors into the relationship. Therefore, load tests were performed to experimentally determine the force-strain relationship desired.

During load testing of the support beams, each beam was subject to three-point bending. The span between supports for the beams was 12 feet, which was equal to the span of the beams in the test setup. A single hydraulic actuator was used to apply a concentrated load to the midspan of each beam. The load was applied in 250 pound increments using force control on the MTS, closed-loop, servo-controlled, testing system. A minimum of two tests was conducted on each beam. The first test was employed to allow the beam to settle on its supports. Additional tests were performed until there was a consistency in test data between two successive tests. Results from the last test on each beam were used to develop a load-strain relationship for that beam.

Dowel bars were load tested under three-point bending, with load applied by a 400,000 pound capacity, universal testing machine. The number of tests carried out on each dowel bar was as explained above for the support beams.

4.3.5.2 Static and Cyclic Loading

Both static and cyclic loads were applied to the test specimens; however, data was only collected during application of the static load. A total of 5,000,000 applications of cyclic load was applied to Slab 1, whereas, Slab 2 was subjected to a total of 5,682,000 applications of cyclic load. This Cyclic load was applied to each specimen through the use of two hydraulic actuators as explained in Section 4.3.3.3. Static loading of a specimen only took place after a certain number of load cycles had been applied to the specimen. For Slab 1, static loading occurred at the end of the following number of load cycles (in thousands): 0; 25; 50; 75; 100; 150; 200; 300; 400; 500; 750; 1,000; 1,500; 2,000; 3,000; 4,000; and 5,000. Static loading for Slab 2 took place at the same number of load cycles as for Slab 1 except that a static test was performed at the end of 5,682 cycles instead of 5,000, which was the result of a malfunction in the automatic shutoff on the MTS testing system.

During static loading of the test specimens, force control was used to apply a maximum load of 9,000 pounds in 500 pound intervals. Data was collected from the instrumentation at each interval of load. Two static tests were performed after the specified number of load cycles had been applied to the specimen. The purpose of the first test was to seat the components of the test setup while the purpose of the second test was to collect data for analysis. For each static test, load was first applied to the north half of the slab and then to the south half of the slab.

5.0 RESULTS

5.1 GFRP Material Properties

As discussed previously in Section 4.1.2, the experimental results for the geometric properties of the GFRP bars are listed in Tables 4.1, 4.2, 4.4, and 4.5. These tables are repeated below for convenience.

Table 4.1 Weight and volume fractions of GFRP dowel bars

Specimen	Weight Fraction	Volume Fraction
1.5”ϕ glass	0.6997	0.5179
1.5”ϕ resin	0.3003	0.4821
1.875”ϕ glass	0.7378	0.5746
1.875”ϕ resin	0.2622	0.4254

Table 4.2 Specific gravity of GFRP dowel bars

Specimen	Specific Gravity
1.5”ϕ GFRP	1.880
1.875”ϕ GFRP	1.978

Table 4.4 Bending modulus values for GFRP dowel bars

Specimen	Bending Modulus, E, psi
1.5”ϕ GFRP	4.93E+06
1.875”ϕ GFRP	6.51E+06

Table 4.5 Shear modulus values for GFRP dowel bars

Specimen	Shear Modulus, G_{xy}, psi
1.5”ϕ GFRP	3.09E+05
1.875”ϕ GFRP	3.15E+05

The properties calculated using the theoretical equation are given in Table 4.3 and is repeated here for convenience.

Table 4.3 Theoretical properties of GFRP dowel bars

Specimen	E_x, psi	ν_{xy}	E_y, psi	G_{xy}, psi
1.5”ϕ GFRP	5.64E+06	0.259	1.47E+06	4.99E+05
1.875”ϕ GFRP	6.20E+06	0.255	1.67E+06	5.67E+05

As can be seen in the tables, the theoretical equation was not accurate in determining the geometric properties when compared to the properties determined using the ASTM standard tests [24]. Table 5.1 compares the theoretical results of the bending and shear modulus to the results received from the ASTM standard tests. Table 5.1 shows the percent error of the bending modulus and the shear modulus when using the experimental results as the standard.

Table 5.1 Percent error of the theoretical GFRP properties

Specimen	% Error, E	% Error, G
1.5”ϕ GFRP	14.4	61.5
1.875”ϕ GFRP	-5.8	80.0

In both GFRP dowel bar types the theoretical results for the shear modulus were severely over-estimated. Only the 1.875”ϕ GFRP bending modulus was under-estimated and that result also had the smallest error. In both of these bars the theoretical results did not agree with the experimental results. The values determined from the experimental ASTM standard tests were the values used throughout the project.

5.2 Elemental Direct Shear Test Results

5.2.1 Modulus of Dowel Support

From the actual deflection versus load diagrams that were created during testing, linear regression was used to determine a load-deflection equation for each specimen. Using this relationship, a relative deflection was obtained for a dowel load of 2,000 pounds. A 2,000 pound load represents the maximum load that a dowel in a typical pavement would be expected to experience. The deflection at the face of the joint, y_o, was determined by rewriting Equation 2.14 to arrive at Equation 5.1. The equation for shear deflection, δ, is shown in Equation 5.2 and was obtained from Young [30].

$$y_0 = \frac{\Delta - \delta}{2} \tag{5.1}$$

$$\delta = \frac{10 \cdot P \cdot z}{9 \cdot G_{xy} \cdot A} \tag{5.2}$$

Table 5.2 gives the average total relative deflection, average shear deflection, and average deflection at the face of the joint for each type of dowel bar using an Iosipescu shear test. Table 5.3 is a listing of the average total relative deflection, average shear deflection, and average deflection at the face of the joint using the modified AASHTO direct shear test. The values in both tables were calculated for a 2000 pound load and are for unaged specimens.

Table 5.4 shows the average total relative deflection, average shear deflection, and average deflection at the face of the joint for each type of dowel bar using an Iosipescu shear test for the aged specimens. The values were calculated for a 2,000 pound load. This information corresponds to the unaged Iosipescu test results that are given in Table 5.2. There were no aged specimens tested using the modified AASHTO static test method.

Table 5.2 Iosipescu Test – **Unaged** - Average relative deflection, shear deflection, and deflection at face of joint.

Dowel Bar	**Average Δ, in.***	**Average δ, in.***	**Average y_o, in.***
1.5”ϕ Epoxy Coated	0.003211	0.000014	0.001599
1.5”ϕ Stainless Steel	0.003600	0.000015	0.001793
1.5”ϕ Plain Steel	0.002699	0.000014	0.001343
1.5”ϕ GFRP	0.006137	0.000679	0.003035
1.75”ϕ GFRP[a]	0.007637	0.000242	0.003698

[a] Properties were taken from work done by Porter et al. [14].
*Note: The deflections cannot be measured this accurately, but are needed to display the effects of shear deflection.

Table 5.3 Modified AASHTO Test – **Unaged** - Average relative deflection, shear deflection, and deflection at face of joint.

Dowel Bar	**Average Δ, in.***	**Average δ, in.***	**Average y_o, in.***
1.5”ϕ Epoxy Coated	0.005426	0.000014	0.002706
1.5”ϕ Aluminum	0.009710	0.000041	0.004835
1.957”ϕ Aluminum	0.007901	0.000024	0.003938
1.5”ϕ Copper	0.006512	0.000024	0.003244
1.714”ϕ Copper	0.005415	0.000018	0.002698
1.5”ϕ GFRP	0.010810	0.000679	0.005065
1.875”ϕ GFRP	0.007472	0.000319	0.003576

*Note: The deflections cannot be measured this accurately, but are needed to display the effects of shear deflection.

Table 5.4 Iosipescu Test – **Aged** - Average relative deflection, shear deflection, and deflection at face of joint.

Dowel Bar	**Average Δ, in.***	**Average δ, in.***	**Average y_o, in.***
1.5”ϕ Epoxy Coated	0.003415	0.000014	0.001701
1.5”ϕ Stainless Steel	0.002978	0.000015	0.001482
1.5”ϕ Plain Steel	0.002729	0.000014	0.001358
1.5”ϕ GFRP	0.005863	0.000679	0.002592
1.875”ϕ GFRP	0.006606	0.000319	0.003144

*Note: The deflections cannot be measured this accurately, but are needed to display the effects of shear deflection.

With the deflections calculated, the next step is to calculate K_o. This calculation is done by imputing the bar properties and numerous values of K_o into Equation 2.9. Equation 2.9 is repeated here for convenience.

$$y_o = \frac{P}{4\beta^3 EI}(2 + \beta z) \tag{2.9}$$

where,

$$\beta = \sqrt[4]{\frac{K_o b}{4EI}} = \text{relative stiffness of the dowel bar encased in concrete } (in^{-1})$$

By imputing various values of K_o into Equation 2.9, a K_o versus y_o graph can be created. Since Equation 2.9 is dependant on the bar shape and material properties, a K_o versus y_o graph must be created for each dowel bar of a different shape and/or material. Shown in Figure 5.1 is a sample K_o versus y_o graph for a 1.5"ϕ round epoxy coated steel dowel bar calculated at a 2000 pound load. However, since there was a linear relationship between the load and the deflection, the results for the modulus of dowel support does not depend on the load.

Using the modulus of dowel support and the deflection at the face of the joint the concrete bearing stress can be calculated. Again, this equation is repeated here for convenience.

$$\sigma_o = K_o y_o = \frac{K_o P}{4\beta^3 EI}(2 + \beta z) \tag{2.15}$$

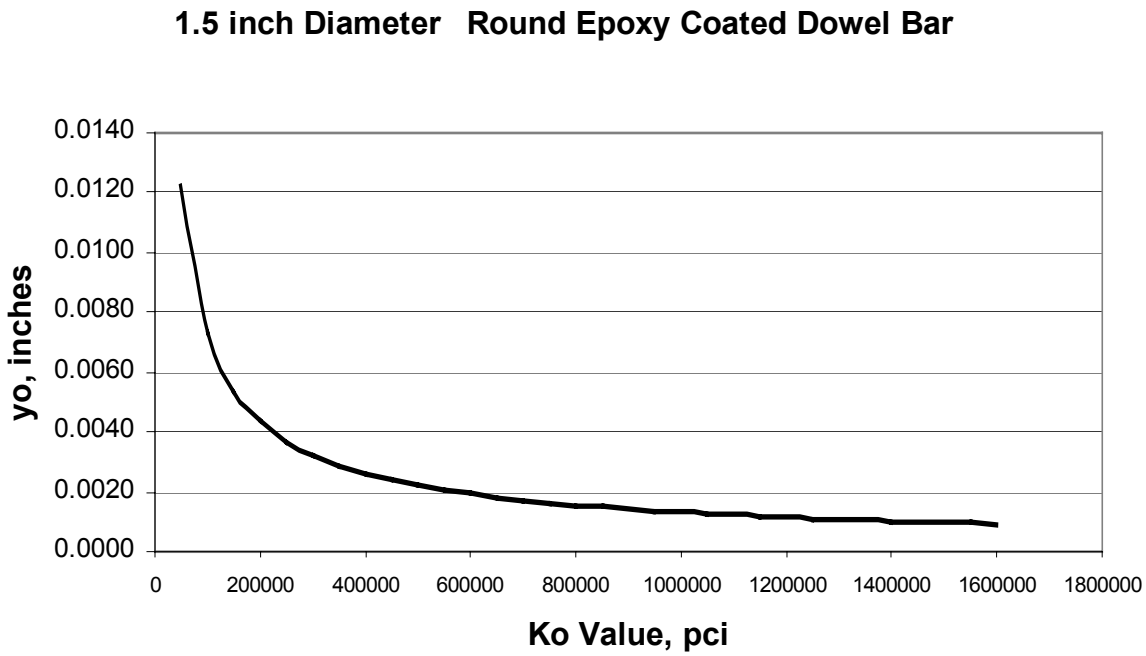

Figure 5.1 K_o versus y_o for the 1.5"ϕ round epoxy coated steel dowel bar at a 2000 lb load

Table 5.5 is a listing of each unaged specimen type and the associated average modulus of dowel support and average concrete bearing stress. Table 5.6 shows the aged specimens values for average modulus of dowel support and bearing stress. Again, this has been calculated for a load of 2000 pounds. The results in Table 5.6 are from the Iosipescu test method since no aged specimens were tested using the modified AASHTO method.

Table 5.5 Unaged - Average modulus of dowel support and bearing stress values

Dowel Bar	Average K_o , pci	Average σ_o, psi
Iosipescu		
1.5”ϕ Epoxy Coated	772,330	1235
1.5”ϕ Stainless Steel	665,170	1193
1.5”ϕ Plain Steel	976,750	1312
1.5”ϕ GFRP	690,500	2096
1.75”ϕ GFRP	300,000	1109
Modified AASHTO		
1.5”ϕ Epoxy Coated	410,267	1110
1.5”ϕ Aluminum	251,133	1214
1.957”ϕ Aluminum	176,500	695
1.5”ϕ Copper	503,100	1632
1.714”ϕ Copper	387,233	1045
1.5”ϕ GFRP	326,700	1655
1.875”ϕ GFRP	256,233	916

Table 5.6 Iosipescu Test - Aged - Average modulus of dowel support and bearing stress values

Dowel Bar	Average K_o , pci	Average σ_o, psi
1.5”ϕ Epoxy Coated	772,400	1314
1.5”ϕ Stainless Steel	861,930	1277
1.5”ϕ Plain Steel	1,059,400	1439
1.5”ϕ GFRP	706,100	1830
1.875”ϕ GFRP	320,700	1009

As can be seen in Table 5.5, the values given for the modulus of dowel support vary greatly between the Iosipescu and the modified AASHTO tests. Even with the large variation in the modulus of dowel support the bearing stresses determined are relatively close when comparing both tests. Since the bearing stress is the primary concern in this research, the authors felt that all of the values where appropriate to be used collectively in this report. However, due to the large difference in the modulus of dowel support, the

values of both methods should only be used to show trends in the behavior of the dowel bars and the values from one test should not be compared directly to the other test.

When comparing Tables 5.5 and 5.6 a trend can be seen with the dowel bars. With an aged specimen containing a steel dowel bar the modulus of dowel support increases, as does the bearing stress, when compared to the unaged specimen. However, the opposite may be true with the GFRP dowel bars. As can be seen in the above tables, the 1.5"ϕ GFRP dowel bar is the only GFRP dowel bar that was done by the Iosipescu as an aged and unaged specimen. The aged 1.5"ϕ GFRP dowel bar has a lower modulus of dowel support and bearing stress when compared to the unaged specimens. However, this difference is very small when one considers how a small change in deflection can have a large affect on the results for the values for the modulus of dowel support. With the results above there is not enough information to make a prediction on the behavior of the GFRP dowel bars when aged.

5.2.2 Dowel Bar Spacing

5.2.2.1 Introduction

A theoretical investigation was conducted to determine various combinations of GFRP dowel diameter and spacing that when installed in a concrete highway pavement would perform as well or better in transferring load than the epoxy-coated steel dowel bars currently used. Results from the investigation were used to select the diameter and spacing of the GFRP dowels utilized in the second laboratory test specimen described in Section 4.3.2.

5.2.2.2 GFRP Dowel Design

Standard practice for doweled joints is to space epoxy-coated steel dowels at 12 inches on center. The recommended diameter for the steel dowels depends on the governing agency and the thickness of the pavement as shown in Table 5.7. Since GFRP has different properties than steel, the validity of applying this standard to GFRP dowels is questionable.

Table 5.7 Recommended steel dowel bar diameter (in.)

Pavement Thickness h, in.	Agency	
	AASHTO[a]	ACPA[b]
14	1.75	1.5
12	1.5	1.5
10	1.25	1.5
8	1	1.25
6	0.75	1.25

[a] Source: Reference [5]
[b] Source: Reference [4]

To investigate whether the current design standard applies to GFRP dowels, two GFRP dowel systems were designed for laboratory testing. The first GFRP dowel system was based on the current design standard and consisted of 1.5-inch diameter GFRP dowels spaced at 12 inches on center. This GFRP dowel system was incorporated into the first laboratory test specimen described in Section 4.3.2.

The diameter and spacing for the second GFRP dowel system was selected such that both the bearing stress in the concrete and relative displacement of the slab at the location of the applied wheel load were approximately equal to or less than that resulting from the use of steel dowels. The authors assumed that if both the bearing stress and relative displacement for the GFRP dowel system were approximately equal to or less than that for the recommended steel dowel system, then both dowel systems would be

equally effective in transferring load across a joint. The magnitude of the bearing stress and relative displacement is an excellent indication of the effectiveness of a joint in transferring load. If the bearing stress in the concrete around the dowel is high, repetitive loading of the doweled joint will result in the formation of a void directly above and below the dowel. When a load is applied to the pavement, the dowels become active in transferring load only after the loaded edge has displaced an amount equal to the size of the void. This increased displacement results in the loss of load transfer across the joint. Large relative displacements indicate that most of the applied wheel load is being absorbed by the subgrade instead of being transferred across the joint by the dowels. Large relative displacements are also accompanied by large flexural stresses, which are detrimental to the pavement. Therefore, if the magnitude of both the bearing stress and relative displacement at the location of the applied wheel load is approximately equal to or less than that for the recommended steel dowels, then the load transfer across the joint as well as the flexural stresses in the pavement should be identical for both steel and GFRP dowel systems.

Diameters of 1.5, 1.75, and 1.875 inches were considered for the GFRP dowels of the second laboratory test specimen. Properties for the three different diameters of GFRP dowels along with those for an epoxy-coated steel dowel can be found back in Table 4.6. Relative displacements and bearing stresses were calculated for these dowels using Equations 2.14 and 2.15. The results of these calculations are presented in Tables 5.8 and 5.9 for spacings of 12, 10, 8, 6, and 4 inches. Since the values for βL were greater than 2 for all of the bars, Equation 2.9 was used to determine y_o. The value for the load

transferred by a fictious dowel located directly beneath the wheel load, P_c, was determined from Equation 2.12.

The criterion mentioned in the paragraph before last was used to determine possible combinations of diameter and spacing for the GFRP dowels of the second laboratory test specimen. As shown in Tables 5.8 and 5.9, the correct diameter and spacing for the GFRP dowels is that which results in a relative displacement and bearing stress of approximately 0.0018 inches and 1365 psi, respectively. Table 5.10 shows the various combinations of GFRP dowel bar diameter and spacing that satisfy the aforesaid conditions. The most economical GFRP dowel system consists of the 1.5-inch diameter dowels spaced at 6 inches on center; therefore, this combination of diameter and spacing was selected for the second laboratory test specimen. This dowel design was verified with the JPCP model developed in Section 3.1.

Table 5.8 Relative displacements (in.)

Dowel Bar Material	Dowel Bar Diameter b, in.	Dowel Bar Spacing, in.				
		12	10	8	6	4
Steel	1.5	0.0018	----	----	----	----
GFRP	1.5	0.0034	0.0029	0.0022	0.0017	0.0011
GFRP	1.75	0.0042	0.0035	0.0027	0.0021	0.0014
GFRP	1.875	0.0060	0.0051	0.0040	0.0030	0.0020

Table 5.9 Bearing stresses (psi)

Dowel Bar Material	Dowel Bar Diameter b, in.	Dowel Bar Spacing, in.				
		12	10	8	6	4
Steel	1.5	1365	----	----	----	----
GFRP	1.5	2348	2002	1547	1174	787
GFRP	1.75	1260	1050	810	630	420
GFRP	1.875	906	770	604	453	302

Table 5.10 GFRP dowel bar diameter and spacing combinations

Dowel Bar Diameter b, in.	Dowel Bar Spacing, in.
1.5	6
1.75	6
1.875	4

5.3 Elemental Fatigue Test Results

5.3.1 Introduction

The purpose of the elemental fatigue testing was to determine if there is a significant decline in the modulus of dowel support for the different dowel bars tested. The trends seen with these results are to be used to determine if one dowel bar may be more resistant to oblonging of the concrete adjacent to the dowel bar.

5.3.2 Modulus of Dowel Support

The method that was used to calculate the modulus of dowel support and the bearing stress for the static shear test was also used to calculate those values for the fatigue testing, see Section 5.2. The average relative deflection, shear deflection and the averaged deflection at the face of the joint can be seen in Tables 5.11 thru 5.14. Tables 5.11 and 5.12 show the results before any cycling of the specimens had occurred for unaged and aged specimens, respectively. While Tables 5.13 and 5.14 contain the results

after 1 million cycles had been applied to the specimens for unaged and aged specimens, respectively. These tables were calculated for a load of 2000 pounds.

Table 5.11 Fatigue Testing – **Unaged, 0 Cycles** - Average relative deflection, shear deflection, and deflection at face of joint.

Dowel Bar	**Average Δ, in.***	**Average δ, in.***	**Average y_o, in.***
1.5"ϕ Stainless Steel	0.001357	0.000015	0.000671
Elliptical GFRP	0.002729	0.000529	0.001100
Shaved GFRP	0.002778	0.000415	0.001181
1.5"ϕ GFRP	0.005542	0.000681	0.002431
1.875"ϕ GFRP	0.004424	0.000319	0.002052

*Note: The deflections cannot be measured this accurately, but are needed to display the effects of shear deflection.

Table 5.12 Fatigue Testing – **Aged, 0 Cycles** - Average relative deflection, shear deflection, and deflection at face of joint.

Dowel Bar	**Average Δ, in.***	**Average δ, in.***	**Average y_o, in.***
1.5"ϕ Epoxy Coated	0.001889	0.000014	0.000937
1.5"ϕ Stainless Steel	0.002230	0.000015	0.001108
1.5"ϕ GFRP	0.003734	0.000681	0.001527
1.875"ϕ GFRP	0.004881	0.000319	0.002281

*Note: The deflections cannot be measured this accurately, but are needed to display the effects of shear deflection.

Table 5.13 Fatigue Testing – **Unaged, 1 Million Cycles** - Average relative deflection, shear deflection, and deflection at face of joint.

Dowel Bar	**Average Δ, in.***	**Average δ, in.***	**Average y_o, in.***
1.5"ϕ Stainless Steel	0.001218	0.000015	0.000602
Elliptical GFRP	0.002357	0.000529	0.000914
Shaved GFRP	0.002791	0.000415	0.001188
1.5"ϕ GFRP	0.005277	0.000681	0.002298
1.875"ϕ GFRP	0.004515	0.000319	0.002098

*Note: The deflections cannot be measured this accurately, but are needed to display the effects of shear deflection.

Table 5.14 Fatigue Testing – **Aged, 1 Million Cycles** - Average relative deflection, shear deflection, and deflection at face of joint.

Dowel Bar	**Average Δ, in.***	**Average δ, in.***	**Average y_o, in.***
1.5”ϕ Epoxy Coated	0.003644	0.000014	0.001815
1.5”ϕ Stainless Steel	0.002503	0.000015	0.001244
1.5”ϕ GFRP	0.004404	0.000681	0.001861
1.875”ϕ GFRP	0.006761	0.000319	0.003221

*Note: The deflections cannot be measured this accurately, but are needed to display the effects of shear deflection.

The modulus of dowel support and bearing stress that were calculated can be seen in Tables 5.15 thru 5.18. Tables 5.15 and 5.16 are the results for the dowel bars at 0 cycles and Tables 5.17 and 5.18 are the results for the dowel bars at 1 million cycles. Tables 5.15 and 5.17 are the results for unaged specimen while the other two tables show the results for aged specimens.

Table 5.15 **Unaged, 0 Cycles** - Average modulus of dowel support and bearing stress values

Dowel Bar	**Average K_o , pci**	**Average σ_o, psi**
1.5”ϕ Stainless Steel	2,429,740	1,673
Elliptical GFRP	1,282,372	1,410
Shaved GFRP	1,557,594	1,840
1.5”ϕ GFRP	807,378	1,963
1.875”ϕ GFRP	538,623	1,106

Table 5.16 **Aged, 0 Cycles** - Average modulus of dowel support and bearing stress values

Dowel Bar	**Average K_o , pci**	**Average σ_o, psi**
1.5”ϕ Epoxy Coated	1,570,173	1,472
1.5”ϕ Stainless Steel	1,271,193	1,408
1.5”ϕ GFRP	815,294	1,245
1.875”ϕ GFRP	467,336	1,066

Table 5.17 **Unaged, 1 Million Cycles** - Average modulus of dowel support and bearing stress values

Dowel Bar	Average K_o , pci	Average σ_o, psi
1.5”ϕ Stainless Steel	2,885,501	1,737
Elliptical GFRP	1,647,085	1,505
Shaved GFRP	1,545,786	1,837
1.5”ϕ GFRP	870,874	2,002
1.875”ϕ GFRP	523,052	1,097

Table 5.18 **Aged, 1 Million Cycles** - Average modulus of dowel support and bearing stress values

Dowel Bar	Average K_o , pci	Average σ_o, psi
1.5”ϕ Epoxy Coated	646,154	1,173
1.5”ϕ Stainless Steel	1,086,978	1,353
1.5”ϕ GFRP	624,517	1,163
1.875”ϕ GFRP	293,688	946

When comparing the unaged specimens from zero cycles to that at one million cycles a slight trend is apparent. The values for the modulus of dowel support and the bearing stress stay very near the same value. There is a slight trend in that after a million cycles the values tend to decrease slightly. A similar trend can also be seen when comparing the aged specimen across a million cycles. Not all of the specimens bearing stresses decrease and even a few of them show a slight increase. This trend can again be attributed to the asymptotic nature of the K_o versus y_o graph. At some point in the K_o versus y_o graph a small decrease in deflection at the face of the joint would relate to a large jump in the resulting value for the modulus of dowel support. Likewise, there is also a point on the K_o versus y_o graph where a large deflection would be required to get a small increase in the modulus of dowel support. With the K_o versus y_o graph being so dependent on deflection, small differences in the value of the modulus of dowel support

can essentially be taken as being equal when comparing the same dowel bar. No correlation of aged to unaged specimens can be made using the data observed from the fatigue testing, as will be discussed in a later section.

5.4 Pullout Test Results

5.4.1 Introduction

As the temperature outside varies, the concrete will expand and contract. Since dowels bars are embedded in the concrete, the dowel bars have to allow the concrete around them to move. The purpose of the testing contained in the section is to determine how the stainless and GRFP dowel bars behave under an axial force compared to that of the epoxy coated dowel bar.

5.4.2 Test Results

The testing procedure was outlined in Section 4.1.5. The load at which ½ inch dowel bar pullout occurred on the unaged specimens can be seen in Table 5.19.

Table 5.19 **Unaged** - Load at which ½ inch pullout occurred

Dowel Bar	Load, lbs
1.5”ϕ Epoxy Coated	N.G.
1.5”ϕ Stainless Steel	1250
1.5”ϕ GFRP	700
1.875”ϕ GFRP	1120

Table 5.20 lists the results of the load at which one-half inch dowel bar pullout occurred on the aged specimens.

Table 5.20 **Aged** - Load at which ½ inch pullout occurred

Dowel Bar	Load, lbs
1.5"ϕ Epoxy Coated	11,490
1.5"ϕ Stainless Steel	940
1.5"ϕ GFRP	1430
1.875"ϕ GFRP	1660*

*Note: Concrete strength was approximately 1,100 psi more than other specimens.

As can be seen in the above tables, the epoxy coated dowel bars adhere to the concrete better than the stainless steel or the GFRP dowel bars. The epoxy coated dowel bars required on the order of about 10 times more force to return the same amount of movement. Based on the results listed above, the authors have no concerns with the movement of the concrete with stainless steel or GFRP dowel bars.

5.5 Full-Scale Laboratory Results

5.5.1 Introduction

As discussed in Section 4.3.5.2, a total of two static full-scale tests were conducted at the end of each interval of cyclic loading. Only data collected at the maximum load of 9000 pounds from the second static test was analyzed to determine the performance of the doweled joint. Performance variables were calculated from the collected data at each of the specified number of load cycles. The performance of the joint under repetitive loading was displayed through rectilinear plots produced for each performance variable. To determine the relationship between the performance variable and the number of applied load cycles, a graphical analysis was performed.

5.5.2 Deflection Data

Deflection measurements from the two DCDTs located at the centerline of each specimen on either side of the joint were substituted into Equations 2.2 and 2.3 to determine the joint effectiveness and load transfer efficiency for Slabs 1 and 2. Figures 5.2 and 5.3 show plots of the calculated joint effectiveness and load transfer efficiency versus the number of applied load cycles for Slabs 1 and 2. At zero cycles the joint effectiveness and load transfer efficiency were 84.4 and 73.1 percent, respectively, for Slab 1 and 89.7 and 81.3 percent, respectively, for Slab 2. However, as shown by the graphs, the performance of each joint degraded as the number of load cycles increased. This degradation occurred at a high rate initially, however, as the number of load cycles increased the rate of degradation decreased. At the end of 5 million cycles the joint effectiveness and load transfer efficiency were reduced to 80.6 and 67.5 percent, respectively, for Slab 1 and 84.8 and 73.7 percent, respectively, for Slab 2, as determined from the empirical equation for each graph.

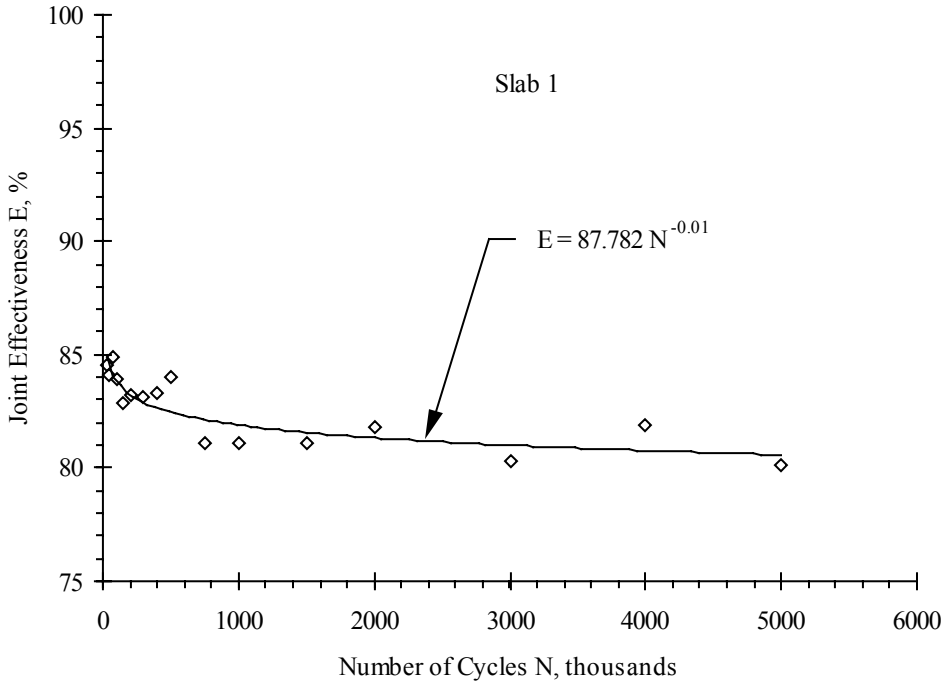

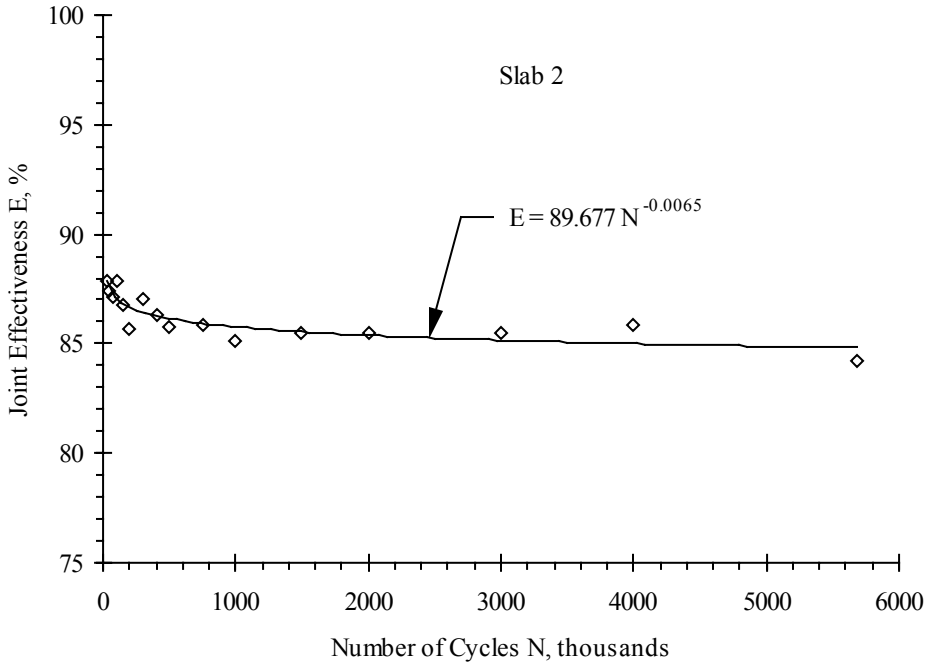

Figure 5.2 Joint effectiveness versus number of cycles for Slabs 1 and 2

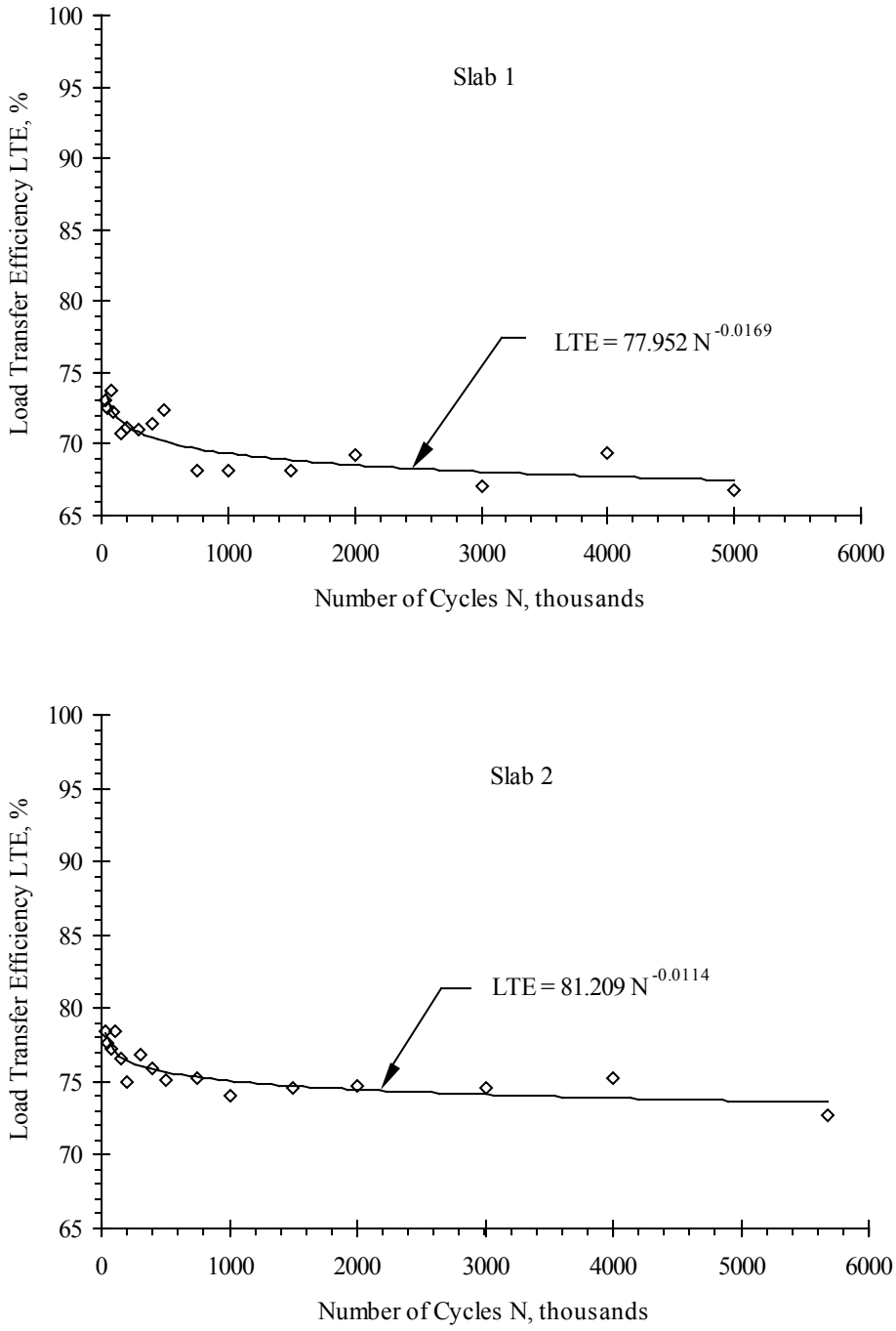

Figure 5.3 Load transfer efficiency versus number of cycles for Slabs 1 and 2

As an additional measure of performance, the relative displacements along the joint were calculated for each slab. In determining the relative displacement at a particular point along the joint, the deflection measured by the DCDT on one side of the joint was subtracted from that obtained from the corresponding DCDT on the other side of the joint. Plots of relative displacement at the centerline and 6 inches east and west of the centerline versus number of load cycles for each slab are shown in Figures 5.4 and 5.5.

After reviewing Figure 5.4, the authors determined that the relative displacements at a higher number of load cycles were not accurately represented by the given trendline. This trendline was heavily weighted by the smaller relative displacements at the lower number of load cycles. Since the relative displacements at a higher number of load cycles were of particular interest, a new trendline, as shown in Figure 5.6, was developed for Slab 1 using the following load cycles (in thousands): 25, 1000, 2000, 3000, 4000, and 5,000.

As shown by Figures 5.5 and 5.6, the relative displacement increases with increasing load cycles. For Slabs 1 and 2, the initial relative displacement at centerline was 0.0041 and 0.0029 inches, respectively. The relative displacement at zero cycles 6 inches east and west of centerline was 0.0024 and 0.0025 inches, respectively, for Slab 1 and 0.0014 and 0.0021 inches, respectively, for Slab 2. After 5 million applications of cyclic load, the relative displacement at centerline increased to 0.0047 and 0.0032 inches, respectively, for Slabs 1 and 2, as determined from the corresponding empirical equation

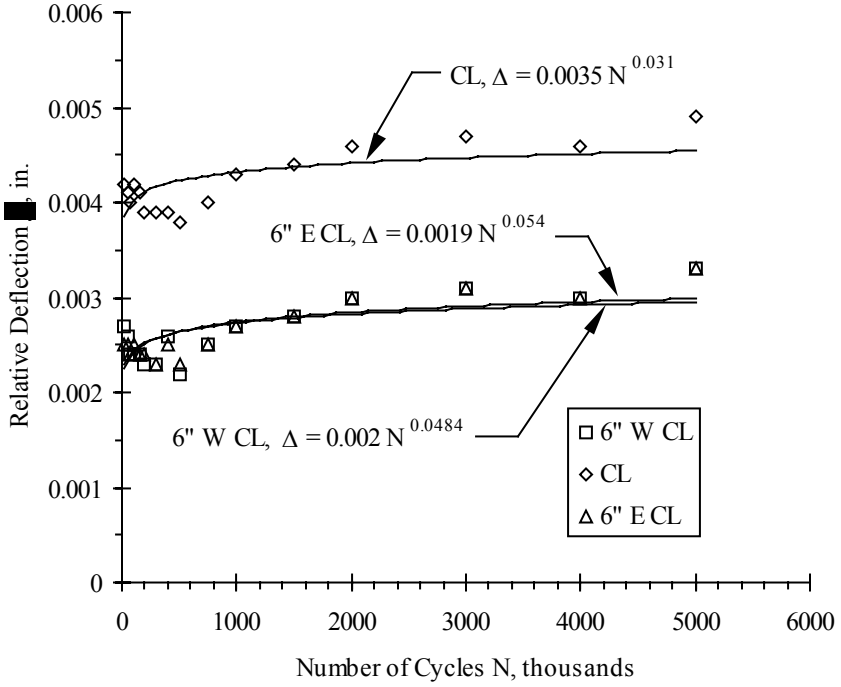

Figure 5.4 Relative deflection versus number of cycles for Slab 1

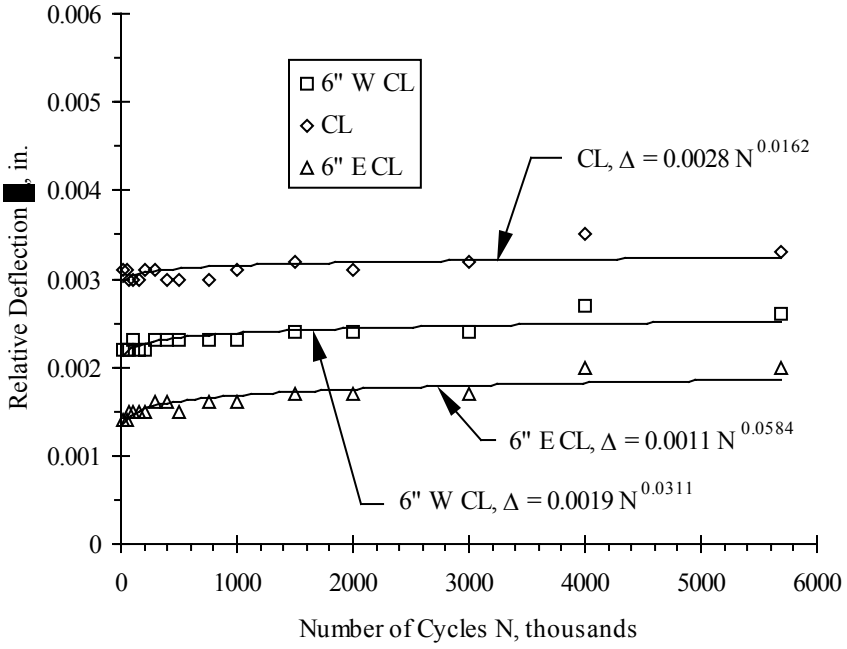

Figure 5.5 Relative deflection versus number of cycles for Slab 2

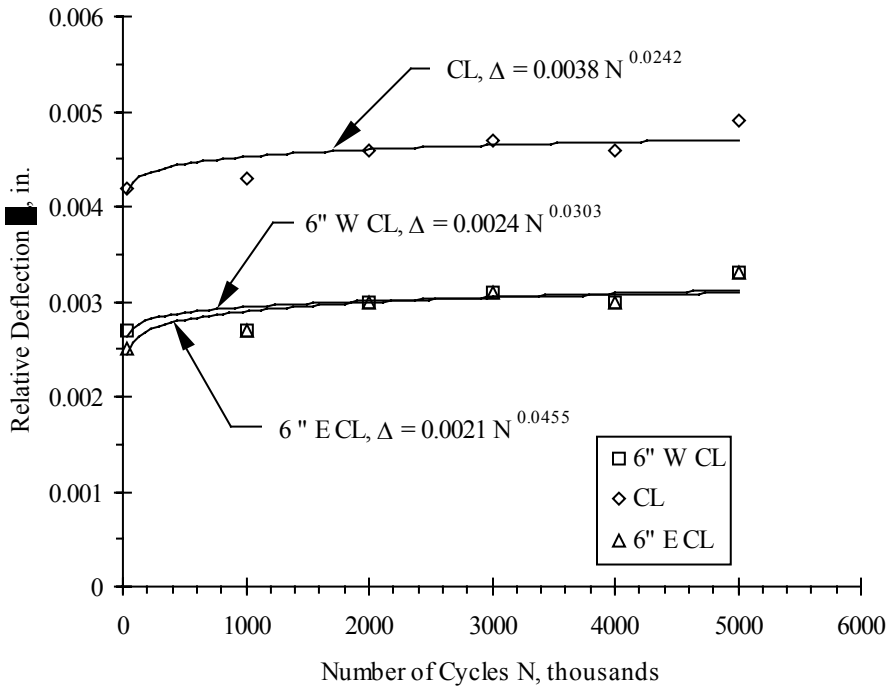

Figure 5.6 Revised relative deflection versus number of cycles plot for Slab 1

for each graph. At 6 inches east and west of centerline, the relative displacement increased to 0.0031 inches (for both sides), respectively, for Slab 1 and 0.0018 and 0.0025 inches, respectively, for Slab 2, as determined from the empirical equation for each graph.

The trendline feature in Microsoft Excel was used to calculate the constants in the empirical equations shown in the graphs. A prior knowledge of the type of trendline that most closely approximated the data was a prerequisite for the trendline feature in Microsoft Excel. In trying to determine the type of equation that best approximated the data, the authors assumed that the data could be approximated by one of three types of functions: linear, exponential, or power law. The data was plotted on three different types of graphs: a rectilinear (Cartesian) graph, a semi-log graph, and a log-log graph. When the data plotted as a straight line on a rectilinear graph, the empirical equation that

best approximated the data was assumed to be linear. However, if the data plotted as a straight line on a semi-log graph, an exponential function was assumed to be the best fit. If the data did not plot as a straight line on a rectilinear or semi-log graph but plotted as a straight line on a log-log graph, a power law equation was assumed to represent the data. Knowing the type of equation the data approximated, Excel's trendline feature could be used to determine the constants for the equation. Rectilinear, semi-log, and log-log plots of the data for joint effectiveness, load transfer efficiency, and relative displacements are displayed in Appendix A. From the graphs in Appendix A, the data tends to plot as a straight line on both semi-log and log-log graphs. After plotting both exponential and power law trendlines, the power law was determined to best fit the data. The authors note that the power law is often used to represent cyclic data.

5.5.3 Beam Strain Gage Data

Data from the load tests was used to develop a load-strain relationship for each beam. Assuming the load distributed to each beam during static testing could be represented as a uniform load, a direct relationship existed between the applied load during load testing and the load distributed to the beam during static testing. Therefore, the applied load versus strain was plotted for each beam and a linear regression was used to develop the load-strain relationship. The resulting plots are displayed in Appendix B. Refer to Figure 4.16 for the location of each beam within the test setup.

Equation 2.1 was used to determine the transferred load efficiency for each slab. The applied wheel load, P_w, in Equation 2.1 was taken as the sum of the loads on all beams, whereas, the transferred load was taken as the sum of the loads on the beams under the unloaded side of the slab. To determine the magnitude of the load distributed

to each beam at the maximum applied load of 9,000 pounds, an average of the eight strains recorded from the eight gages was taken. This average was then inserted into the relationship developed for that particular beam to give the magnitude of the distributed load.

Plots of the transferred load efficiency versus the number of applied load cycles for both slabs are displayed in Figure 5.7. The transferred load efficiency for both slabs is relatively constant at 42 percent for Slab 1 and 42.2 percent for Slab 2, as determined from the respective empirical equation. The empirical equation for each graph was determined as explained in Section 5.5.2. Rectilinear, semi-log, and log-log plots of the data used in determining the type of trendline can be found in Appendix A.

5.5.4 Dowel Strain Gage Data

Data collected from load tests performed on each dowel bar was used to develop a relationship between the strain at a particular point and the corresponding moment for each bar. The moment in the dowel at each strain gage location was determined from the known dimensions of the test setup employed for load testing. Plots of the moment in the dowel at each strain gage location versus the corresponding strain were produced and regression analyses were performed to establish the moment-strain relationships. The resulting plots are displayed in Appendix B. Refer to Figures 4.23 and 4.24 for the location of the dowels within Slab 1 and Slab 2.

The load transferred through a dowel was determined from Equation 5.3.

$$P = EI\frac{d^3y}{dx^3} \tag{5.3}$$

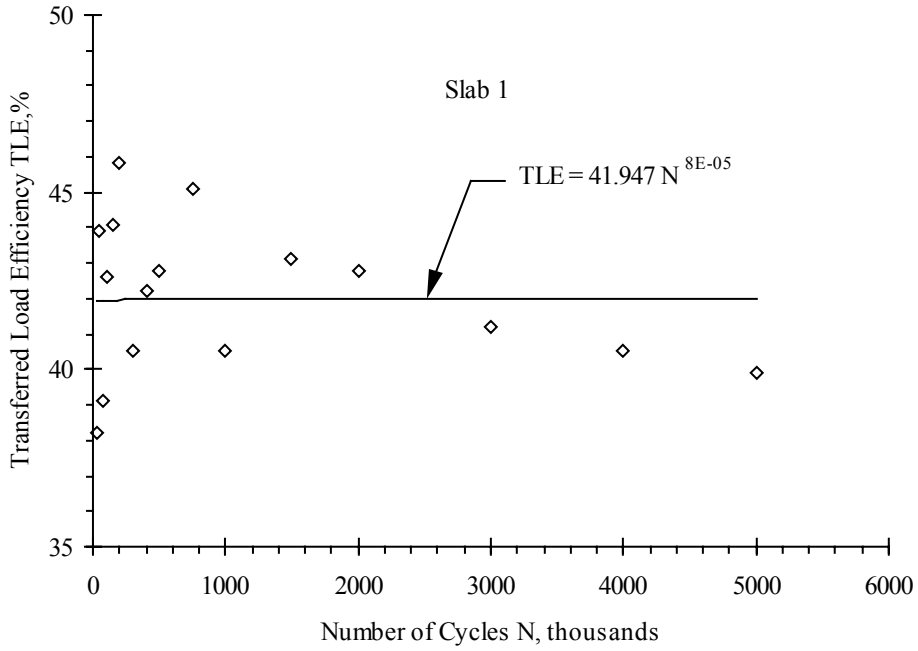

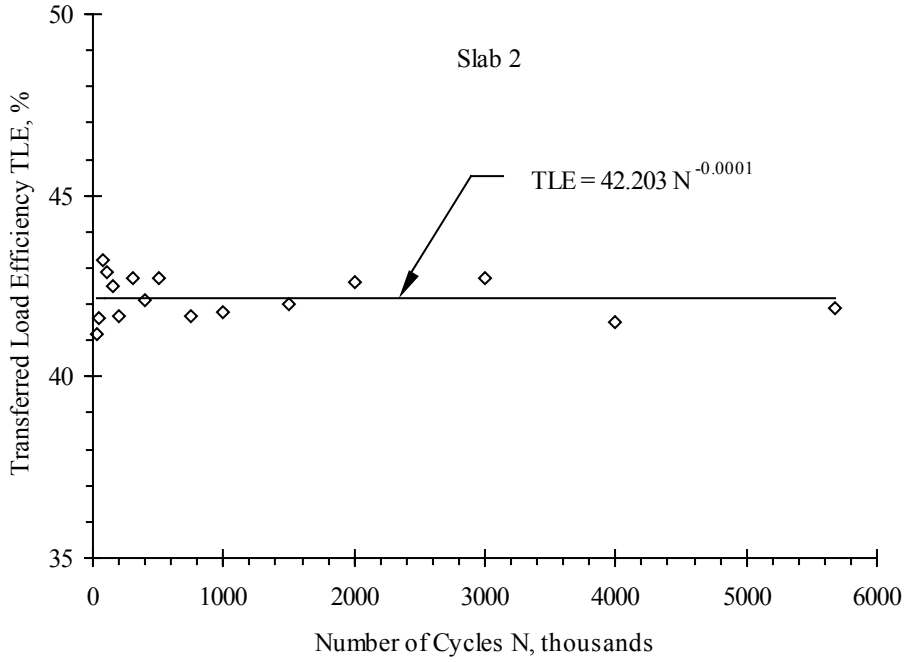

Figure 5.7 Transferred load efficiency versus number of cycles for Slabs 1 and 2

Assuming the case of a dowel bar of semi-infinite length (constants A and B are equal to zero) and differentiating Equation 2.6 three times with respect to x and then setting x equal to zero gives Equation 5.4.

$$\frac{d^3y}{dx^3} = 2C\beta^3 + 2D\beta^3 \tag{5.4}$$

This equation shows that the constants C and D must be known before the load transferred through the dowel can be computed.

The constants C and D can be solved if the moments at two locations along the dowel are known. Designating the deflection of the dowel bar as positive downward, the moment in the dowel bar at any given location is given by Equation 5.5.

$$M = -EI\frac{d^2y}{dx^2} \tag{5.5}$$

For a dowel bar of semi-infinite length, the second derivative of Equation 2.5 is as follows:

$$\frac{d^2y}{dx^2} = 2Ce^{-\beta x}\beta^2 \sin \beta x - 2De^{-\beta x}\beta^2 \cos \beta x \tag{5.6}$$

Substituting the moment at 1.5 and 5.5 inches from the center of the dowel and the expression for d^2y/dx^2 into Equation 5.5 gives Equations 5.7 and 5.8, respectively, which were solved simultaneously to give the constants C and D.

$$M_{1.5} = EI\,(-2Ce^{-1.5\beta}\beta^2 \sin 1.5\beta + 2De^{-1.5\beta}\beta^2 \cos 1.5\beta) \tag{5.7}$$

$$M_{5.5} = EI\,(-2Ce^{-5.5\beta}\beta^2 \sin 5.5\beta + 2De^{-5.5\beta}\beta^2 \cos 5.5\beta) \tag{5.8}$$

Taking an average of the two strains at each location and substituting this value into the moment-strain relationship developed for that dowel produced the moment at these two locations.

In analyzing the strain data to determine the load transferred through each dowel, the authors noticed that the magnitude of this load was extremely sensitive to the value of strain in the gage located 5.5 inches from the center of the dowel. In fact, a change of 1 microstrain produced a change of 100 pounds in the computed magnitude of the load. Considering that the noise in the strain gages accounted for between 0 and 3 microstrains, the results from the analysis of this data were deamed unreliable and are not displayed.

6.0 COMPARISON AND RELATION OF RESULTS

6.1 GFRP Material Properties

As was briefly discussed in Section 5.1.1, the theoretical equations tended to overestimate the material properties and the authors suggest that they not be used to determine the GFRP properties. When the properties of a GFRP dowel bar are needed, the ASTM standard tests should be conducted to determine the properties. The ASTM tests were based upon simple principles and were relatively simple to conduct.

The only problem associated with mandating the ASTM tests is the costs that could be incurred before testing a dowel bar of each new shape or size. These tests are increasingly more important as research is headed in the direction of alternatively shaped dowel bars. This additional cost of testing alternatively shaped dowel bars is due to the need for the machining of equipment to fit the shape of dowel bars.

6.2 Elemental Direct Shear Tests

6.2.1 Dowel Size Relationship

The results of these tests were listed in Tables 5.5 and 5.6 and have been repeated here for convenience. The initial shear test procedure used at ISU was the Iosipescu test. Due to challenges experienced with this procedure in the past, as previously discussed in Section 4.1.3.4, the modified AASHTO test was adopted and used on this project so that a few dowel bars could be compared for accuracy between the two test methods.

Table 5.5 Unaged - Average modulus of dowel support and bearing stress values

Dowel Bar	Average K_o , pci	Average σ_o, psi
Iosipescu		
1.5”ϕ Epoxy Coated	772,330	1235
1.5”ϕ Stainless Steel	665,170	1193
1.5”ϕ Plain Steel	976,750	1312
1.5”ϕ GFRP	690,500	2096
1.75”ϕ GFRP	300,000	1109
Modified AASHTO		
1.5”ϕ Epoxy Coated	410,267	1110
1.5”ϕ Aluminum	251,133	1214
1.957”ϕ Aluminum	176,500	695
1.5”ϕ Copper	503,100	1632
1.714”ϕ Copper	387,233	1045
1.5”ϕ GFRP	326,700	1655
1.875”ϕ GFRP	256,233	916

Table 5.6 Iosipescu Test - Aged - Average modulus of dowel support and bearing stress values

Dowel Bar	Average K_o, pci	Average σ_o, psi
1.5”ϕ Epoxy Coated	772,400	1314
1.5”ϕ Stainless	861,930	1277
1.5”ϕ Plain Steel	1,059,400	1439
1.5”ϕ GFRP	706,100	1830
1.875”ϕ GFRP	320,700	1009

As can be seen in Table 5.5, the moduli of dowel support determined by the two test procedures differ by a significant amount. For this reason a direct comparison should not be made between the two test methods. However, both methods can be used to indicate trends in the behavior of the dowel bars.

In both test methods the 1.5”ϕ GFRP dowel bars have the highest average bearing stress. There is a trend in the bearing stress as the size of the dowel bars increase. For dowel bars of the same material, a decrease in bearing stress with an increase in dowel bar size is intuitively expected. Since a larger dowel bar would have a larger bearing surface against the concrete the stress on the outer face should decrease. An argument could be made that the relationship is due to the increased stiffness of the larger dowel bar and not the larger bearing width. However, the modified AASHTO method indicates that the 1.957”ϕ aluminum dowel bars have the lowest bearing stress of the dowel bars tested using that method. This is also the largest dowel bar that was tested. Recall that the 1.957”ϕ aluminum and the 1.714”ϕ copper were selected because they have the same stiffness, EI, as a 1.5”ϕ epoxy coated steel dowel bar. The relationship of these three bars in Table 5.1 again indicates that an increase in dowel bar diameter causes a decrease in the bearing stress on the concrete. In this case however, the stiffness of the dowel bar is a constant and the larger dowel bar still indicates the lowest bearing stress. Thus, the bearing stress on the concrete relies more on the bearing width of the dowel bar and less on the stiffness of the dowel bar. Although the stiffness of the dowel bar is still important since it will relate directly to the amount of relative deflection seen at the joint.

6.2.2 Aged versus Unaged

There appears to be a trend with the modulus of dowel support between the aged and unaged specimens. With the aged specimens the modulus of dowel support increases slightly with each dowel bar when compared to that of the unaged specimens. This behavior could be due to the fact that the aged specimens have a higher concrete strength. The aged specimens had a concrete strength of approximately 7162 psi while the unaged

specimens had a concrete strength of only 5770 psi. The modulus of dowel support is basically a value relating the behavior of the dowel bar to the concrete of which it is embedded. Therefore, the modulus of dowel support is dependant on the modulus of elasticity of the concrete. As concrete strength increases so does the value of the concrete's modulus of elasticity. Therefore, the trend seen in Table 5.5 and 5.6 follows the definition of the modulus of dowel support since the aged specimens have a higher concrete strength. With this larger modulus of dowel support, a slightly larger bearing stress is also observed for the specimens containing steel dowel bars.

The modulus of dowel support for the GFRP dowel bars that were tested with the Iosipescu method, as aged and unaged specimens, also followed this trend. More specimens should be checked to ensure that this material does indeed follow the trend discussed above. This additional testing would also allow researchers the chance to verify the behavior of the bearing stress with the aged specimens. With the limited GFRP results available, apparently the 1.5"ϕ GFRP dowel bars have a decreasing bearing stress when aged, the opposite of the steel dowel bars. More research is needed to verify that the GFRP dowel bar bearing stress behavior is accurate.

6.3 Elemental Fatigue Tests

6.3.1 Fatigue Results

The purpose of the fatigue testing was to determine the modulus of dowel support and the concrete bearing stress before cycling and then again after the specimens had been subjected to cycling. The elemental fatigue specimens were subjected to 1 million cycles in this project. The results of these tests before and after cycling were listed in Tables 5.15 thru 5.18 and have been repeated here for convenience.

Table 5.15 **Unaged, 0 Cycles** - Average modulus of dowel support and bearing stress values

Dowel Bar	**Average K_o , pci**	**Average σ_o, psi**
1.5”ϕ Stainless	2,429,740	1,673
Elliptical GFRP	1,282,372	1,410
Shaved GFRP	1,557,594	1,840
1.5”ϕ GFRP	807,378	1,963
1.875”ϕ GFRP	538,623	1,106

Table 5.16 **Aged, 0 Cycles** - Average modulus of dowel support and bearing stress values

Dowel Bar	**Average K_o , pci**	**Average σ_o, psi**
1.5”ϕ Epoxy Coated	1,570,173	1,472
1.5”ϕ Stainless	1,271,193	1,408
1.5”ϕ GFRP	815,294	1,245
1.875”ϕ GFRP	467,336	1,066

Table 5.17 **Unaged, 1 Million Cycles** - Average modulus of dowel support and bearing stress values

Dowel Bar	Average K_o , pci	Average σ_o, psi
1.5”ϕ Stainless	2,885,501	1,737
Elliptical GFRP	1,647,085	1,505
Shaved GFRP	1,545,786	1,837
1.5”ϕ GFRP	870,874	2,002
1.875”ϕ GFRP	523,052	1,097

Table 5.18 **Aged, 1 Million Cycles** - Average modulus of dowel support and bearing stress values

Dowel Bar	Average K_o , pci	Average σ_o, psi
1.5”ϕ Epoxy Coated	646,154	1,173
1.5”ϕ Stainless	1,086,978	1,353
1.5”ϕ GFRP	624,517	1,163
1.875”ϕ GFRP	293,688	946

There is a trend in the data indicating that as the slab cycles the modulus of dowel support decreases. The decrease in the modulus of dowel support indicates that the deflection at the face of the joint is increasing. As can be seen in Equation 2.19, a decrease in the modulus of dowel support would cause an increase in the deflection at the face of the joint. The increase in deflection at the face of the joint is due to the beginning of the formation of a void. As the load cycles applied to the specimen continued, the size of the void around the concrete increased so the value for the modulus of dowel support decreased.

6.3.2 Aged versus Unaged

In the elemental fatigue specimens the results indicated that the modulus of dowel support declined with the aged specimens. This decline with the aged specimens is opposite of the trend that was seen with the elemental direct shear specimens. The same type of dowel bars in the elemental fatigue tests showed a higher variance than which was seen in the elemental direct shear tests. The elemental fatigue test also used a different testing method than the elemental static test. After the tests were conducted there were a few small problems found with the elemental fatigue test. For these reasons the authors feel that the proper correlation was seen with the elemental direct shear specimens. The problems that were discovered with the elemental shear test will be discussed in greater detail in the next chapter.

6.4 Pullout Tests

The pullout tests on all the dowel bars worked correctly on the aged specimens. Unfortunately, due to a problem during testing, the unaged epoxy coated steel dowel specimens data was not available. Without the results from the epoxy coated steel dowel bars the pullout test conclusions are made more difficult. Since there was a testing problem with the unaged epoxy coated dowel bars the conclusions will be made by comparing only the results from the aged specimens.

The results from the pullout aged specimens show that the stainless steel and both GFRP dowel bars are dramatically lower in the axial force required to achieve ½-inch of pullout compared to the epoxy coated dowel bars. The stainless steel and both GFRP

dowel bars are all grouped around 1,000 pounds for pullout while the epoxy coated dowel bars required approximately 10 times that force.

This pullout testing was performed to determine when the stainless steel and GFRP dowel bars would allow movement of the concrete for expansion and contraction compared to that of the epoxy coated steel dowel bars. A higher force required for pullout of the dowel bars indicates a potential for higher internal forces in the concrete. The results of this data indicated that the stainless steel and GFRP dowel bars allow movement at a force well below the epoxy coated dowel bars. Thus, GFRP and stainless steel dowel bars are more beneficial to the concrete since the concrete would carry less internal force before slipping than that of the epoxy coated steel dowel bars.

6.5 Field Study

6.5.1 Background

In order to see if experimental results are close to actual field conditions, a field study including the same type of dowel bars must be completed. Current research has been conducted on a highway that includes 1.5" epoxy coated steel, 1.5" GFRP, and 1.875" GFRP dowel bars. The data collected from this project was then analyzed to compare the authors' experimental results to the field results.

6.5.2 Background Field Data Collection

The load-deflection characteristics of the pavement were measured by using a falling weight deflectometer (FWD). The FWD testing method is a nondestructive way to determine the load-deflection characteristics. The FWD applies a known load and

measures the relative deflection between the two slabs. ERES Consultants [31] completed the FWD tests for the field evaluation.

Deflection testing was performed in the westbound lanes of the US-65 bypass near Carlisle, Iowa. Both the driving and passing traffic lanes were tested. The load was dropped at a distance of two feet from the shoulder in the passing lane and at a distance of four feet from the shoulder in the driving lane. Figure 6.1 shows the load drop locations.

From this data, many relationships were calculated that were necessary in the analysis of dowel bars. The amount of deflection for its respective load is the most important factor needed in determining the modulus of dowel support, K_o. The subgrade modulus, k, is also important. This modulus is used to determine the radius of relative stiffness, ℓ_r, which determines how much the dowel experiences of the applied load. From the point of the applied load, there is a linearly decreasing amount of load that each dowel experiences. Therefore, depending on which dowel is being analyzed; the distance of the dowel from the applied loads has a considerable effect. The dowels that are at a distance greater than the radius of relative stiffness do not experience any load and are not effective in transferring the wheel load.

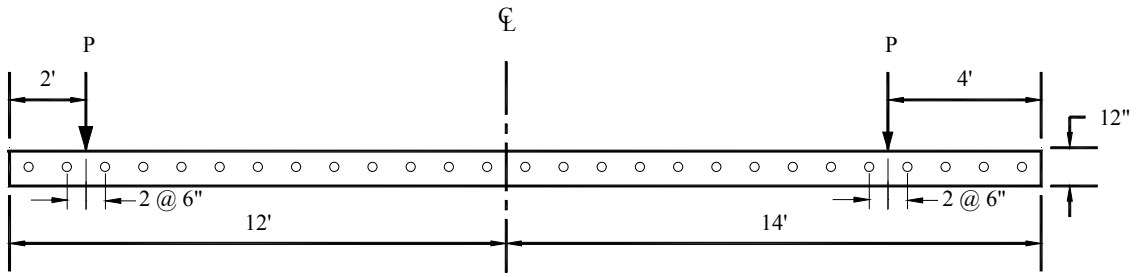

Figure 6.1 Falling weight deflectometer load application points

6.5.3 Analysis Background of Field Data

There were a total of 216 dowel bar tests that were analyzed. These 216 dowel bar tests consisted of 72 epoxy coated steel, 72 1.5" GFRP, and 72 1.875" GFRP specimens. For each type of dowel bar, the 72 tests consisted of dropping three different loads, four different times at six different joint locations. All of the dowels analyzed had a spacing of 12 inches. The average load, differential deflection, and subgrade modulus were determined for each type of dowel bar. Table 6.1 shows the average results for each type of dowel bar.

Table 6.1 Average load, subgrade modulus, and deflection of dowels

Dowel	Avg. Load, lb	Avg. k, lb/in^3	Avg. Deflection, in.
1.5"ϕ Epoxy Coated Steel	13,428	133	0.000649
1.5"ϕ GFRP	12,885	156	0.001388
1.875"ϕ GFRP	12,645	135	0.001451

The concrete mix design used for this project was the same nominal concrete mix design used in the experimental investigation that produced a concrete strength of 6300

psi. Therefore, the author assumed a concrete strength of 6300 psi. With this assumption, the results from the experimental data for a 6300-psi concrete mix were compared to the field results.

Dowel bars are designed for the loads that they are expected to experience during their lifetime. The actual wheel load is not what each dowel bar experiences. Yoder[1] stated that the most a transverse joint is expected to experience is 45 percent of the wheel load. The author used Yoder's assumption for the analysis of the dowels. From the 45 percent of the wheel load that each joint experiences, a dowel still is only subjected to a small fraction of this load. The reason for each dowel only experiencing a portion of the transferred wheel load is because only the dowels located within the radius of relative stiffness contribute in supporting the wheel load. The number of dowels that contribute support to the wheel load are referred to as the number of effective dowels.

The number of dowels located within the radius of relative stiffness must first be known in order to determine the number of effective dowels. Then, the fraction of load that each dowel experiences must be determined. The number of effective dowels is determined by adding all the dowels respective load fractions within the radius of relative stiffness. Dividing the load on each joint by the number of effective dowels determines the applied load that was used to compare the field values to the experimental values.

All of the above assumptions and the closeness of the dowel to the applied load were used to determine how much of the load that the dowel experiences. The dowel that was closest to the load was analyzed. As shown in Figure 6.1, the dowels in both the driving and passing lane are only 6 inches away from the load.

Using the average subgrade modulus, k, the radius of relative stiffness was calculated for each type of dowel. Then, using the ratio of a distance 6 inches less than the radius of relative stiffness to the radius of relative stiffness, the load that the dowel of interest experiences was calculated for all dowel types at all joint locations.

Using the factored loads and measured deflections at the joint locations, the modulus of dowel support, K_o, values were calculated. The method used to calculate the modulus of dowel support is thoroughly explained in Chapter 5. Table 6.2 shows the factored load, deflection, and modulus of dowel support calculated for each respective dowel bar type.

6.5.4 Field Study Results Compared to Selected Experimental Results

In comparing the field study results to the experimental results, the modulus of dowel support is significantly higher in the field results. The comparison of field results to the experimental results is not a good comparison to make because below the pavement slab in the field, the subbase and/or subgrade help support the pavement slab.

Table 6.2 Factored load, deflection, and modulus of dowel support

Dowel	Factored Load, lb	Deflection, Δ, in.*	Modulus of Dowel Support, lb/in^3
Driving Lane			
1.5”ϕ Epoxy Coated Steel	1,497	0.00051	5,984,000
1.5”ϕ GFRP	1,460	0.00098	5,437,000
1.875”ϕ GFRP	1,387	0.00110	2,082,000
Passing Lane			
1.5”ϕ Epoxy Coated Steel	1,220	0.00079	2,524,000
1.5”ϕ GFRP	1,231	0.00179	1,698,000
1.875”ϕ GFRP	1,177	0.00181	817,200

*Note: The deflections cannot be measured this accurately, but are needed to display the effects of shear deflection.

The subbase and/or subgrade significantly reduce the relative deflection between the two slabs when compared with the relative deflection an experimental specimen of the same load. Table 6.3 shows the load, deflection, modulus of dowel support, K_o, for both the experimental and field results for the respective dowel bars.

The results in Table 6.3 show the significantly higher modulus of dowel support for the field data. The analysis of dowels using pavement joints in the field leads to an inaccurate modulus of dowel support. The inaccuracy of these results is due to the small deflections measured at the field site. The reason for these small deflections was discussed earlier. Figure 5.1 showed the relationship between the modulus of dowel support, K_o, and the deflection at the face of the joint, y_o. This figure clearly shows why for a smaller deflection at the face, the higher the modulus of dowel support.

Table 6.3 Load, deflection, and K_o value for experimental and field data.

Dowel	Load, lb	Field Deflection, Δ, in.*	Experimental Deflection, Δ, in.*	Field K_o, lb/in^3	Experimental K_o, lb/in^3
Driving Lane					
1.5”ϕ Epoxy Coated Steel	1,497	0.00051	0.00338	5,984,000	410,267
1.5”ϕ GFRP	1,460	0.00098	0.00782	5,437,000	326,700
1.875”ϕ GFRP	1,387	0.00110	0.00451	2,082,000	256,233
Passing Lane					
1.5”ϕ Epoxy Coated Steel	1,220	0.00079	0.00276	2,524,000	410,267
1.5”ϕ GFRP	1,231	0.00179	0.00659	1,698,000	326,700
1.875”ϕ GFRP	1,177	0.00181	0.00383	817,200	256,233

*Note: The deflections cannot be measured this accurately, but are needed to display the effects of shear deflection.

6.5.5 Conclusions From the Results

The results from the field study are clearly not close to the experimental results because the deflections are significantly different. The difference in the results is simply due to the difference in relative deflections. Past researchers [9,16,17] typically adopted a value of either 1,000,000 lb/in^3 or 1,500,000 lb/in^3 for the modulus of dowel support. Also, the modulus of dowel support cannot be more than the modulus of elasticity of the concrete. The assumed 6300-psi concrete strength gives a modulus of elasticity approximately equal to 4,500,000 psi. If 4,500,000 lb/in^3 was the maximum modulus of dowel support allowable, the field results for the epoxy and 1.5" GFRP dowel bars are wrong. Therefore, the analysis of field data should be further investigated.

6.6 Full-Slab Tests

6.6.1 Experimental versus Computer Modeling

Experimental data collected from Slab 1 was compared to results obtained from several finite element runs of the JPCP model described in Section 3.1. The comparisons enabled the determination of the modulus of subgrade reaction for the steel supporting beams and verified that the laboratory specimens behaved similar to an actual concrete highway pavement.

The deflection measurements recorded by the DCDTs along the transverse joint of Slab 1 were plotted to form a deflection profile for the joint. In determining the value for the modulus of subgrade reaction that the steel supporting beams provided, this deflection profile was compared to several obtained from finite element runs of the JPCP model. For each finite element run, a different value was used for the stiffness of the Winkler foundation. From these comparisons the authors concluded that the steel supporting beams represented a soil having a modulus of subgrade reaction approximately equal to 145 pci, as shown by Figure 6.2. Values for the modulus of subgrade reaction used in the design of pavements typically fall between 100 and 150 pci [23].

Within 18 inches of either side of the centerline, the deflection profile for the loaded edge of Slab 1 is slightly concaved upward and matches that of the finite element model. Unlike the loaded edge, the deflection profile for the unloaded edge of Slab 1 is concaved downward. This shape could have resulted from localized bearing failures of the concrete at the outside edges of the slab. However, a visual inspection of the bottom of the slab when it was lifted off the beams did not reveal any evidence that a bearing failure of the concrete had taken place. The deflected shape of the unloaded edge could

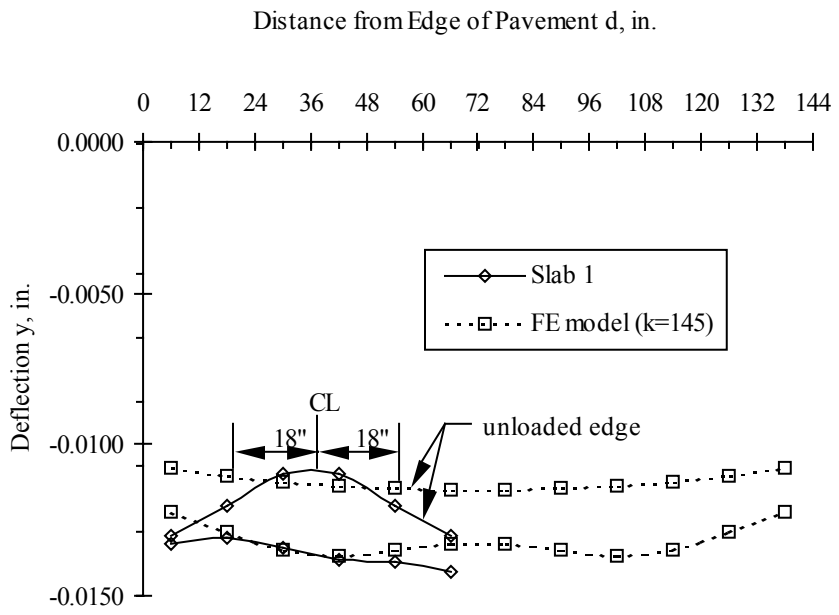

Figure 6.2 Determination of modulus of subgrade reaction

have also resulted from the placement of the instrumentation. Measurements from the center of the slab were critical in determining the performance of the joint; therefore, DCDTs with a higher resolution were placed towards the center of the slab. Since the higher resolution DCDTs were placed near the center of the slab, deflection measurements taken at the edges were not as precise as those recorded near the center of the slab. Because the deflected shapes of the loaded and unloaded edge deviate from those of the finite element model towards the outside of the slab,
the modulus of subgrade reaction determined for the laboratory setup is only valid for a 3-foot section of the specimen as illustrated in Figure 6.2.

In addition to the deflections along the joint, the rotations of the adjacent faces of the joint at the centerline of the slab were used to verify the behavior of the test specimen. The rotations of the joint faces for the JPCP model were obtained from the output of the

program. For Slab 1, assuming plane sections remain plane, the rotations of the faces of the joint are equivalent to the slopes of the two halves of the test specimen. The slopes were found through linear regression of the deflection data collected along the centerline of Slab 1. Centerline deflections along with the resulting linear trendline are displayed in Figure 6.3, which includes the centerline deflections for the JPCP model for comparison. As shown in the figure, the rotations of the adjacent faces of the joint, which are equivalent to the slopes of the two halves of the pavement, are equal to 0.0002 for both the loaded and unloaded side of the specimen. The rotations from the JPCP model were 0.00018 for the loaded side and 0.00017 for the unloaded side. Comparing the two rotations, an 11.1 and 17.6 percent difference, respectively, exists between the JPCP model and Slab 1 for the loaded and unloaded sides. Excluding the portions of the test specimen near the edges, the difference in deflections and rotations between the JPCP model and Slab 1 are small enough to conclude that the test specimen behave similarly to an actual pavement.

6.6.2 Slab 1 versus Slab 2

For comparison purposes, identical performance parameters for both slabs were plotted on one graph, as shown in Figures 6.4, 6.5, and 6.6. From viewing the figures, one can see that the trendlines for any given performance parameter are similar in shape for both slabs. Although the values for any given parameter are consistently lower for Slab 1 than for Slab 2, these values decrease at approximately the same rate for both slabs. Since the values of the performance parameters for Slab 1 are less than those for Slab 2, the authors concluded that the performance of Slab 2 was superior to that of Slab 1.

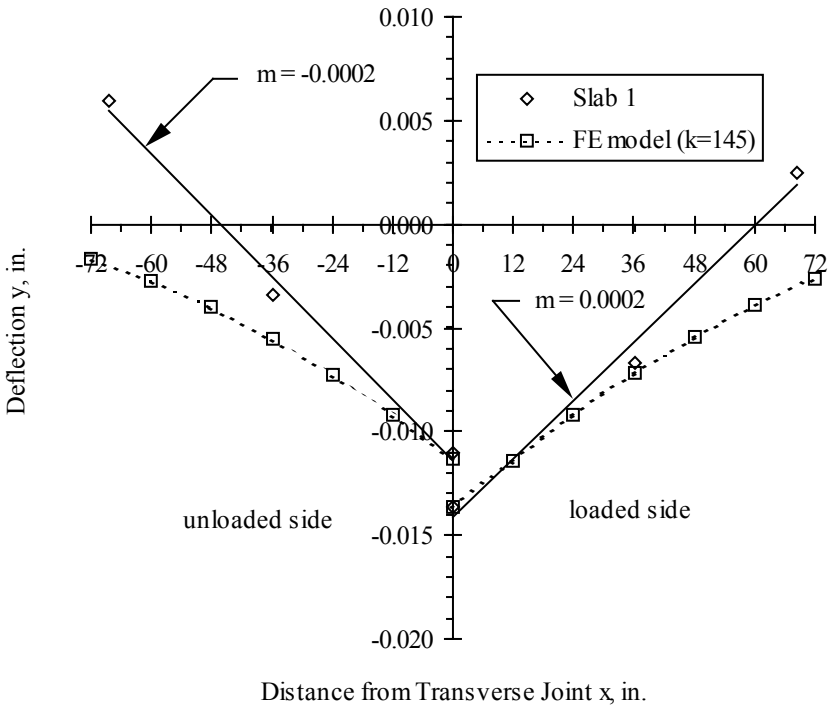

Figure 6.3 Centerline deflections for finite element model and Slab 1

The effectiveness of each joint in transferring medium to heavy wheel loads over the design life of the pavement, which is typically 40 years for interstate highways [23], was evaluated based on the joint effectiveness, load transfer efficiency, and transferred load efficiency of each slab. Over its design life, a pavement can accumulate on average as many as 100 million ESALs [*23*]. Therefore, the joint effectiveness, load transfer efficiency, and transferred load efficiency of each slab for 100 million cycles of load were required. These values were obtained through the use of the empirical equations derived in Sections 5.3.2 and 5.3.3. The results are tabulated in Table 6.4, which includes minimum values for acceptable performance.

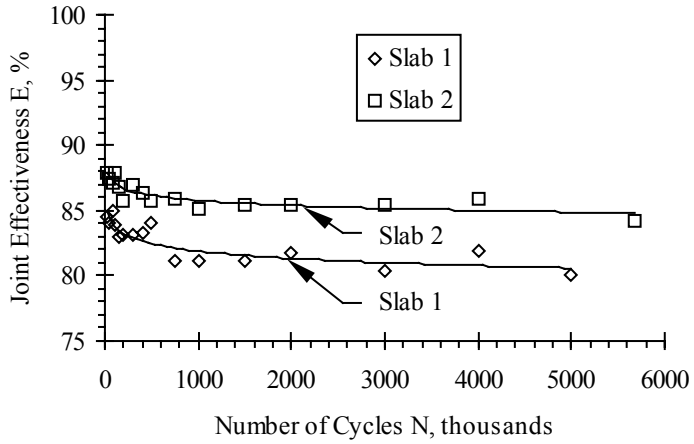

Figure 6.4 Joint effectiveness versus number of cycles comparison

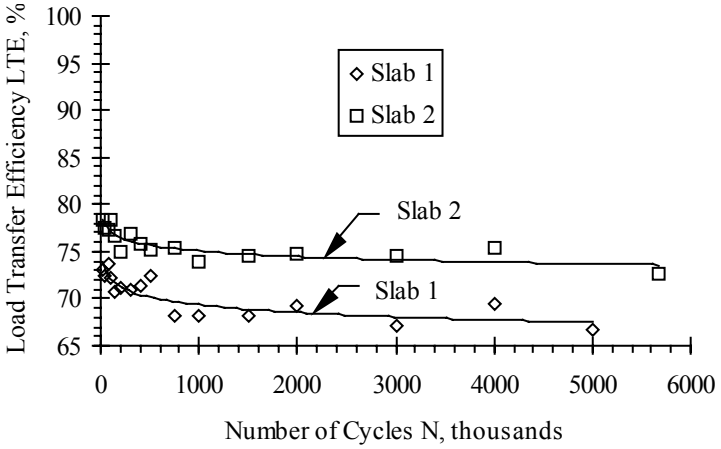

Figure 6.5 Load transfer efficiency versus number of cycles comparison

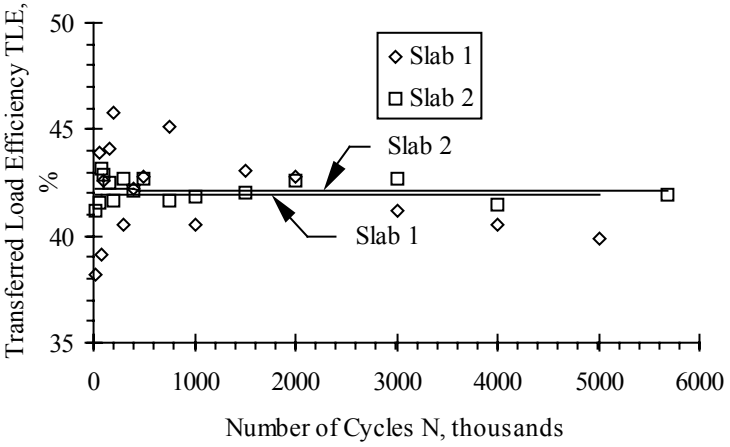

Figure 6.6 Transferred load efficiency versus number of cycles comparison

Table 6.4 Joint performance at an extrapolated 100 million cycles of load

Slab	E, %	E_{min},%	E/E_{min}	LTE,%	LTE_{min},%	LTE/LTE_{min}	TLE,%	TLE_{min},%	TLE/TLE_{min}
	(1)	(2)	(3)	(4)	(5)	(6)	(7)	(8)	(9)
1	78.2	75	1.04	64.2	70	0.92	42.0	35	1.20
2	83.2	75	1.11	71.2	70	1.02	42.0	35	1.21

If any value is less than the minimum, which is indicated by a value of less than one in column 3, 6, or 9 of Table 6.4, then the joint was assumed to be ineffective in transferring load. As indicated in Table 6.4, the dowel design for Slab 1, 1.5-inch diameter GFRP dowels spaced at 12 inches, is inadequate for medium to heavy truck loads based on load transfer efficiency. Setting the empirical equation given in Figure 5.3 for Slab 1 equal to seventy and solving for N, one finds that the load transfer efficiency falls below the minimum after only 582,000 cycles of load.

Although the calculated values of joint effectiveness and transferred load efficiency were above the minimum for Slab 1, the authors remind the reader that the magnitude of the applied load to be used in determining these two parameters was not specified, as was pointed out in Section 4.3.3.3. Therefore, the use of the load transfer efficiency parameter in judging the adequacy of the joint seems appropriate; whereas, the use of the joint effectiveness or transferred load efficiency variable is questionable.

For comparison purposes, the relative displacements for Slab 1 and Slab 2 were plotted on the same graph, as shown in Figure 6.7. The relative displacement 6 inches from the centerline of the joint represents the average of the relative displacements 6 inches east and west of the centerline. From this figure one can see that the relative

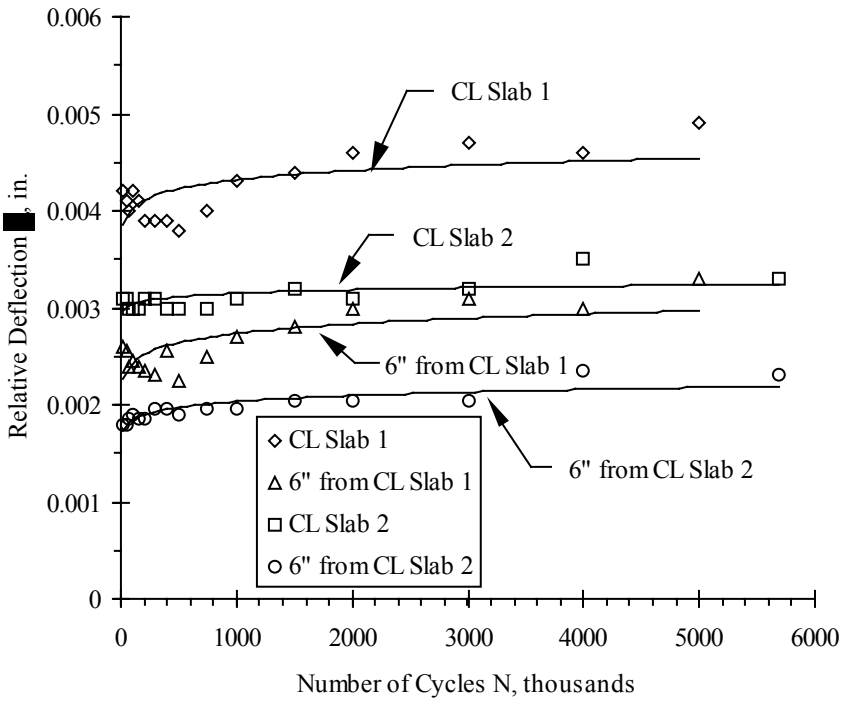

Figure 6.7 Relative deflection versus number of cycles comparison

displacements for Slab 1 were higher than those for Slab 2. Large relative displacements result in pumping, which leads to the faulting and cracking of pavement slabs. Therefore, Slab 1 is more likely to have problems with faulting and cracking than Slab 2.

From Figure 6.6, one can also see that the trendlines for Slab 2 are flatter than those for Slab 1. The flatter trendlines are the result of lower bearing stresses in the concrete around the dowels of Slab 2, which agrees with the theoretical results presented in Section 5.2.2.2. High bearing stresses lead to the erosion of concrete around the dowel resulting in an increase in relative displacements as the number of load repetitions increase. Since this is the type of behavior displayed by the trendlines for Slab 1, the authors conclude that the bearing stresses in the concrete around the dowels in Slab 1

were too high. The higher bearing stresses can be attributed to the larger spacing of dowels for Slab 1.

7.0 CONCLUSIONS AND RECOMMENDATIONS

7.1 Elemental Tests

The results from the elemental direct shear tests and the elemental fatigue test showed a direct relationship between a larger diameter bar resulting in lower bearing stresses at the face of the joint. This relationship, however, was not the case seen with the shaved dowel bars used in the fatigue testing. The shaved dowel bars were developed to create a large bearing surface for the concrete while using a smaller cross-sectional area. The flaw in the design of the shaved dowel bar is that in order to create the shape desired four corners are created, two on the top and two on the bottom. The corners are in the stress region of the dowel bars and create stress concentrations. The stress concentrations created by the shaved dowel bars actually caused the bearing stress to increase. On the other hand, the elliptical dowel bars do show a decrease in bearing stress. However, this lower stress was not as low as past elliptical dowel bar research has indicated. The area of the GFRP elliptical dowel bars was near the halfway point between the 1.875”ϕ and 1.5”ϕ GFRP dowel bars. The bearing stress returned for the elliptical dowel bars was also near the halfway point. Compared to previous research with elliptical steel dowel bars the GFRP elliptical dowel bars lose many of their advantages over the round dowel bars.

The change in behavior seen with the GFRP elliptical dowel bars is most likely due to voids that were seen in the GFRP elliptical dowel bars. These voids were created in the pultrusion process used to create the GFRP dowel bars. When creating an elliptical shape there are different distances from one face of the bar to the center compared to another face, minor axis versus major axis. These different distances create the

opportunity for differential cooling of the material during the pultrusion process. This differential cooling created visible voids and creases in the GFRP elliptical dowel bars. These voids and creases create weak points in the GFRP elliptical dowel bars. Thus, allowing more deflection at the joint and higher bearing stresses on the concrete.

There was also an increase in the modulus of dowel support with increasing age of the concrete. The aged specimens had a higher concrete strength and therefore should have had a lower relative deflection. The lower relative deflection of the aged specimens was indicated in the data from the elemental direct shear tests. This decrease in deflection causes an increase in the modulus of dowel support. However, the elemental fatigue tests indicated a different result, which will be discussed in the next section.

7.2 Testing Procedure for the determination of K_o

As was discussed in Section 4.1.3, the decision was made to use a modified AASHTO test method over the previous Iosipescu method. During the coarse of testing, a few problems developed for which additional changes to the test procedure are recommended. The recommended changes to the elemental direct shear test procedure consist of the following:

1) to replace the uniform load with two point loads, which are located near each end of the center block;
2) to ensure that no rotation of the end blocks occur, special clamping is necessary and the end blocks should be monitored for movement during testing,
3) special care should be taken to ensure that the end blocks bear evenly on their supports and, therefore, should be cast in a special bearing support material.

The above suggestions where taken into account and tested on another research project. The procedures used to verify items two and three above consisted of two additional details during testing. Rotation was monitored by setting up DCDTs on the end blocks of the specimens. The DCDTs where set on the end blocks opposite the center block. The purpose of these DCDTs were to check for movement of the specimens end blocks during testing. To ensure that the specimens were bearing evenly during testing a leveling dental plaster was used. The dental plaster was an 8000 psi product with the trade name Labstone. Initially, the tests were conducted without the use of Labstone and movement of the end blocks occurred. This movement was due to

unevenness in the bottom of the specimens caused during casting and a possible lack of an identical horizontal plane between the specimen end blocks. By casting the specimens in Labstone and then testing, the movement of the end blocks was eliminated.

This newly discovered movement of the specimens is believed to cause the discrepancy of the results between aged versus unaged specimens during the elemental fatigue testing. The rotation of the end blocks usually creates an increased relative deflection, which can have a dramatic effect on the calculation of the modulus of dowel support. The authors believe that an implementation of the above changes will provide more accurate and consistent results.

7.3 Design Implications

Since the results from the theoretical and experimental investigations indicate that the current design guideline for epoxy coated steel dowels is not appropriate for use with GFRP dowels, a new standard for the design of GFRP dowels is warranted. A design procedure based on solving theoretical equations is dependent upon a test that would give consistent results for the modulus of dowel support. As pointed out in Section 2.2.3, the modulus of dowel support was found to be highly variable in the previous research [11,13,14,15]. Therefore, for a theoretical based design procedure to work, a sound experimental or theoretical procedure needs to be found for determining the modulus of dowel support. In addition to the results from any theoretical investigation, knowledge gained through field studies and laboratory testing is also essential to the development of a new design standard for GFRP dowels.

Besides past research at ISU and the research described herein, the authors are aware of only one additional laboratory study that has investigated the fatigue

performance of concrete pavements containing GFRP dowels. This was the study conducted at the University of Manitoba on 10-inch thick concrete pavements containing GFRP dowels [32]. Researchers at the University of Manitoba demonstrated that for a 10-inch thick pavement slab subjected to 1 million cycles of a 29,200 pound wheel load, the 1.5-inch diameter GFRP dowels compared favorably to the 1.25-inch diameter steel dowels. The results of up to 10 million cycles of laboratory fatigue testing previously performed at ISU [11] on a total of four full-scale pavement slabs indicate that one possible GFRP dowel design for a 12-inch thick concrete pavement consists of 1.75-inch diameter dowels spaced at 8 inches on center. Another possible GFRP dowel design for a 12-inch thick concrete pavement based on the research described herein consists of 1.5-inch diameter dowels spaced at 6 inches on center. The implications of these results indicate that various combinations of diameter, spacing, number of cycles, and slab thickness are worthy of additional studies.

The authors note that the diameter of the GFRP dowels used in the study at the University of Manitoba on 10-inch thick concrete pavements was 1/4-inch larger than that recommended by AASHTO for an epoxy-coated steel dowel. However, previous research at ISU [11] indicates that GFRP dowels 1/4-inch larger than that recommended by AASHTO and spaced at the standard 12 inches will lead to larger deflections for a 12-inch thick concrete pavement. In a study entitled *Non-Corrosive Tie Reinforcing and Dowel Bars for Highway Pavement Slabs* [11], researchers at ISU tested one full-scale pavement slab containing 1.75-inch diameter GFRP dowels spaced at 12 inches on center. Figure 7.1 compares the relative displacements from this slab to those obtained from a slab containing 1.5-inch diameter steel dowels spaced at 12 inches on center,

which was tested in the same study. As shown by Figure 7.1, the relative displacements for the slab containing the 1.75-inch diameter GFRP dowels were higher than those for the slab containing the 1.5-inch diameter steel dowels. Since there was an increase in the relative displacements for the slab containing the 1.75-inch diameter GFRP dowels spaced at 12 inches on center, the slab has the potential for increased tensile stresses. With larger relative displacements there is also the increased potential for pumping and faulting of the slab. Therefore, GFRP dowels at 12 inches on center having a diameter 1/4-inch larger than that recommended by AASHTO need further investigation to be accepted as a design solution for 12-inch thick concrete pavements.

Intuitively, one would think that simply increasing the diameter of the dowel would also work for a 12-inch thick concrete pavement; however, this is not the case. The reason for this is due to the sensitivity of the relative deflection at smaller values of the modulus of dowel support as shown in Figure 7.2. Although there is a decrease in shear deflection, δ, due to selecting a larger diameter bar, this is offset by an increase in the deflection of the dowel at the face of the joint, y_o, as the result of a smaller modulus of dowel support for the larger diameter bar; therefore, the relative deflection may decrease only slightly if at all. In some instances the relative deflection may even increase for larger diameter bars, as shown in Table 5.8. Friberg [9] also noticed the increased sensitivity of the relative deflection at smaller values of the modulus of dowel support and recommended against using dowels having a modulus of dowel support less than 500,000 pci.

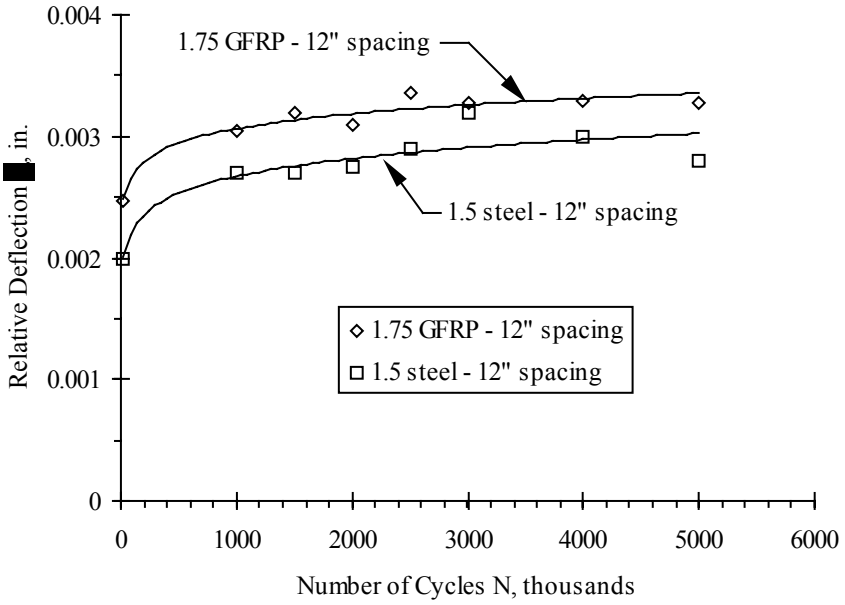

Figure 7.1 Relative deflection versus number of cycles for previous research at ISU

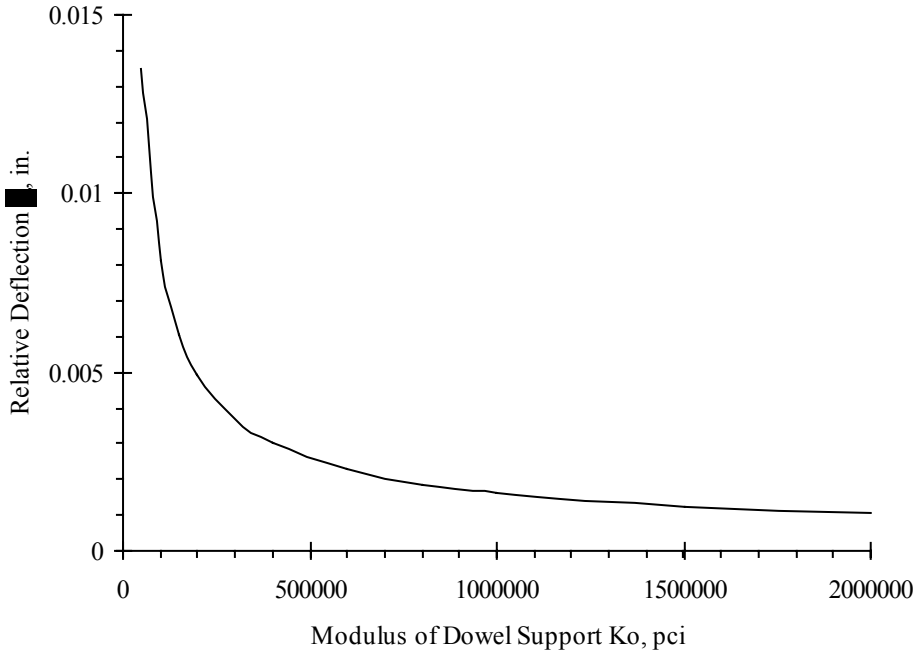

Figure 7.2 Relative deflection versus modulus of dowel support

Results from the research conducted at ISU indicate that for dowels greater than 1.5 inches in diameter, the decrease in relative displacement resulting from a larger diameter bar may be offset by the increase due to a smaller modulus of dowel support. Therefore, the appropriate design procedure for GFRP dowels appears to consist of spacing GFRP dowels at 12 inches on center having a diameter 1/4-inch larger than that recommended by AASHTO for pavements up to 10 inches thick. For pavements 12 inches thick (or possibly greater), 1.5-inch diameter dowels are suggested at a spacing of 6 inches on center. Other combinations of spacing and/or diameter may be possible; however, until further research is completed, the 1.5-inch diameter dowels at a spacing of 6 inches on center are recommended.

Although 2 million cycles of fatigue testing were performed on the 1.75-inch diameter GFRP dowels spaced at 8 inches on center, the performance parameter LTE was not evaluated for this dowel system. The dowel system was also tested in a pavement slab that had a transverse joint width of essentially zero. Since a joint width of 1/8-inch was determined to represent actual field conditions during the majority of a pavement's life, there is the potential for increased deflections above those that were observed in the previous research [11] if this dowel system is installed in highway pavements. Therefore, the authors suggest further testing of this dowel system in full-scale laboratory pavement slabs containing 1/8-inch transverse joints before this dowel system is used.

Based on the aforementioned methodology, a preliminary design guideline for GFRP dowels is proposed as shown in Table 7.1. The design guideline proposed is a preliminary guideline based on a small number of laboratory tests. Further research is

needed to confirm this proposed design standard, including the parameter variations of diameter, spacing, number of cycles, and slab thickness.

Table 7.1 Design guideline for GFRP dowels

Pavement Thickness h, in.	Diameter b, in.	Spacing, in.
14	1.5	6
12	1.5	6
10	1.5	12
8	1.25	12
6	1.0	12

7.4 Research Overview

7.4.1 Summary

Numerical, theoretical, and experimental investigations were conducted to determine the behavior of GFRP dowels. The numerical investigation consisted of the construction of two finite element models. Because of the lack of field data for the specific conditions of this research, a finite element model of a JPCP was created. To accurately model the behavior of a dowel embedded in concrete, two different dowel elements were developed. The dowel element representing a vertical spring was selected for use in the JPCP model. Deflections from the JPCP model were used to verify that the laboratory test setup simulated the behavior of an actual concrete highway pavement. A finite element model of the laboratory test setup was also constructed to determine a preliminary value for the modulus of subgrade reaction, which was used later in the theoretical investigation.

A theoretical investigation was carried out to determine the diameter and spacing of GFRP dowels that would result in a load transfer capacity equivalent to that of the currently recommended steel dowels. The more economical GFRP dowel system for equivalent load transfer from the research conducted to date consisted of 1.5-inch diameter GFRP dowels spaced at 6 inches on center.

Laboratory fatigue testing was performed on two full-scale specimens. The first specimen contained GFRP dowels having a diameter of 1.5 inches and spaced at 12 inches. This diameter and spacing was based on the current design standard for steel dowels. The second specimen contained the GFRP dowel system determined to be equivalent in load transfer capacity to that of the recommended steel dowels, which consisted of 1.5-inch diameter GFRP dowels spaced at 6 inches on center. Both specimens were subject to 5 million cycles of a 9,000 pound cyclic load. After only 582,000 cycles of load, the first specimen failed to transfer load effectively. However, based upon extrapolation, the second specimen would have still been effective in transferring load at 100 million cycles of load, which is the average number of ESALs a pavement is expected to accumulate over its design life.

Results from the fatigue testing conducted at ISU as well as from the University of Manitoba were used to develop a preliminary guideline for the design of GFRP dowels. The design guideline developed from this study suggests a 1/4-inch increase in the diameter recommended by AASHTO for pavements up to 10 inches thick. For pavements 12 inches thick or greater, the design guideline suggests a 1.5-inch diameter dowel placed at a reduced spacing of 6 inches on center.

7.4.2 Conclusions

The following conclusions were made with regard to the results of this research and pertain to contraction joints within concrete pavements. (These conclusions may not apply for expansion joints.)

- The JPCP model created for this study for full-scale slabs was successfully verified by comparing the results from the JPCP model for a pavement of assumed parameters to available theoretical and numerical solutions.

- The two dowel elements developed in this study accurately model the behavior of a dowel embedded in concrete.

- Actual field conditions are simulated by the laboratory test setup.

- All instrumentation, except for the strain gages attached to the dowel bars, was successful in collecting useful data for investigating the effectiveness of a GFRP dowel system in transferring load.

- The test procedure was effective in monitoring the fatigue performance of the GFRP dowels.

- The 1.5-inch diameter GFRP dowels spaced at 12 inches on center were inadequate in transferring load for the anticipated design life of the pavement.

- The 1.5-inch diameter GFRP dowels spaced at 6 inches on center were effective in transferring load over the anticipated design life of the pavement.

- The current design guideline for steel dowels cannot be applied to GFRP dowels.

7.4.3 Recommendations

The following are recommendations for further study.

- Additional laboratory testing is needed to confirm the design guideline proposed for GFRP dowels within contraction joints of concrete pavements. Further testing should include, as a minimum, tests on pavements of 6, 8, and 14 inches thick. Additional testing is also suggested on 12-inch thick concrete pavements containing 1.75-inch diameter GFRP dowels at spacings of 8 and 12 inches, respectively. Full-scale laboratory pavement specimens for these additional tests should contain a 1/8-inch wide transverse joint at midlength. Instrumentation for these tests should include strain gages embedded in the pavement for the determination of the tensile stresses in the pavement. Consideration should also be given to increasing the magnitude of the applied load to match that of the wheel loads of trucks on the road today.

- Additional experimental tests are needed to verify the observed increase in relative deflection with increased bar diameter for bar diameters greater than 1.5 inches. This testing could consist of elemental direct shear tests as

described by Porter et al. [14] or tests in accordance with modified AASHTO T-253.

- The polymer matrix of a fiber composite is hygroscopic, which means that it will absorb water. The absorption of water and subsequent swelling of GFRP dowels could possibly be detrimental to concrete pavements, therefore, this phenomenon should be investigated fully before GFRP dowels are implemented.

- With respect to design, the selection of the diameter and spacing of GFRP dowels to achieve a desired level of load transfer is a serviceability issue. A procedure for the design of GFRP dowels to resist the forces that develop in a dowel when transferring load is also needed. The authors recommend that the load resistance factor design method be used for the design of the dowels for strength. For this method, a reliability index will need to be determined and load and resistance factors selected to achieve this reliability index.

- Since expansion joints are placed in the roadway wherever the pavement meets a fixed structure, additional analysis, design, and testing of GFRP dowels within expansion joints is also needed. Additional research is needed for all types of joints to determine the effects of different sizes of gaps other than 1/8 inch. The additional effects of deflection due to flexure are needed for joints containing larger gaps.

- A new ASTM or AAHSTO standard test should be adopted to provide testing and to eliminate the errors of the current standard.

REFERENCES

1. American Society of Civil Engineers. New Report Card Reveals Little Improvement in Infrastructure. *Civil Engineering*, Vol. 71, No. 4, April 2001, pg. 30.

2. Ioannides, A.M., G.T. Korovesis. Analysis and Design of Doweled Slab-on-Grade Pavement Systems. *Journal of Transportation Engineering*, Vol. 118, No. 6, November/December 1992, pp. 745-768.

3. Brown, V.L. and C.L. Bartholomew. FRP Dowel Bars in Reinforced Concrete Pavements. *Proceedings of the International Symposium on FRP Reinforcement for Concrete Structures*, American Concrete Institute (ACI), Michigan, 1993.

4. American Concrete Pavement Association (ACPA). *Design and Construction of Joints for Concrete Highways*. ACPA, Skokie, Illinois, 1991.

5. American Association of State Highway and Transportation Officials (AASHTO). *AASHTO Guide for Design of Pavement Structures*. AASHTO, Washignton, D.C., 1993.

6. Huang, Y.H. *Pavement Analysis and Design*. Prentice Hall, Inc., New Jersey, 1993.

7. Teller, L.W. and H.D. Cashell. Performance of Doweled Joint Under Repetitive Loading. *PublicRoads*, Vol. 30, No.1, April 1958, pp. 1-24.

8. Timoshenko, S. and J.M. Lessels. *Applied Elasticity*. Westinghouse Technical Night School Press, Pennsylvania, 1925.

9. Friberg, B.F. Design of Dowels in Transverse Joints of Concrete Pavements. *Transactions, American Society of Civil Engineers*. Vol. 105, No. 2081, 1940.

10. Albertson, M.D. Fibersomposite and Steel Pavement Dowels. *Masters Thesis*. Iowa State University, 1992.

11. Porter, M.L., B. Barnes, B. Hughes, and K. Viswanath. Non-Corrosive Tie Reinforcing and Dowel Bars for Highway Pavement Slabs. *Final Report HR-343 Submitted to Highway Division of the Iowa Department of Transportation and Iowa Highway Research Board*. Ames, IA, November 1993.

12. Bradbury, R.D., Design of joints in concrete pavements. *Proceedings, 12th Annual Meeting of the Highway Research Board*, pp. 105-141, Washington D.C., 1932

13. Porter, M.L., D. Davis, and J. Rohner. Investigation of Glass Fiber Composite Dowel Bars for Highway Pavement Slabs. *Progress Report TR-408 Submitted to Project Development Division of the Iowa Department of Transportation and Iowa Highway Research Board*. Ames, IA, January 1999.

14. Porter, M.L., M.D. Albertson, B. Barnes, E. Lorenz, and K. Viswanath. Thermoset Composite Concrete Reinforcement. *Report HR-325 Submitted to Project Development Division of the Iowa Department of Transportation and Iowa Highway Research Board*. Ames, IA, May 1992.

15. Friberg, B.F., Load and deflection characteristics of dowels in transverse joints of concrete pavements. *Proceedings, 18th Annual Meeting of the Highway Research Board, National Research Council*, pp. 140-154, Washington D.C., 1938.

16. Grinter, L.E., Discussion of "Design of dowels in transverse joints of concrete pavements," by B.F. Friberg, *Transactions*, *American Society of Civil Engineers*. Vol. 105, pg. 1096-1101, New York, NY, 1940.

17. Yoder, E.J. and M.W. Witczak. *Principles of Pavement Design*. 2nd ed. John Wiley & Sons, Inc., New York, 1975.

18. ACI Committee 325. Structural Design Considerations for Pavement Joints. *Journal of the American Concrete Institute*, Vol. 28, No. 1, July 1956, pp. 1-28.

19. Westergaard, H.M. Computation of Stresses in Concrete Roads. *Proceedings, 5th Annual Meeting of the Highway Research Board*, Washington, D.C., 1925.

20. Tabatabaie, A.M., E.J. Barenburg, and R.E. Smith. *Longitudinal Joint Systems in Slipformed Rigid Pavements: Vol. II-Analysis of Load Transfer Systems for Concrete Pavements*. Report No. DOT/FAA.RD-79/4, Federal Aviation Administration, U.S. Department of Transportation, 1979.

21. SAS IP, Inc. *Ansys Elements Reference*. 8th ed. SAS IP, Inc., Pennsylvania, 1996.

22. Channakeshava, C., F. Barzegar, and G.Z. Voyiadjis. Nonlinear FE Analysis of Plain Concrete Pavements with Doweled Joints. *Journal of Transportation Engineering*, Vol. 119, No. 5, September/October 1993, pp. 763-781.

23. Brakke, C. Telephone conversation. Pavement Design Engineer, Iowa Department of Transportation, September 1999.

24. American Standard for Testing and Materials (ASTM). Annual Book of ASTM Standards. ASTM, Pennsylvania, 1986.

25. Auborg, P.F., and Wolf, W.W., Glass Fibers. *Advances in Ceramics*, Vol. 18, American Ceramic Society, Columbus, Ohio, pg. 51-78, 1986.

26. Ashland Chemicals, *Technical Data for AROPOL 7240 Isophthalic Polyester Resin*. Ashland Inc., Columbus, OH, July 1997.

27. Tsai, S.W., and Hahn, H.T., *Introduction to Composite Materials*. Technical Publishing Company, Inc., Lancaster, Pennsylvania, 1980.

28. Ugural, A.C., and Fenster, S.K., *Advanced Strength and Applied Elasticity, 3rd edition*. Prentice-Hall, Inc., Upper Saddle River, NJ, 1995.

29. Walrath, D.E., and Adams, D.F., The Iosipescu shear test as applied to composite materials. *Experimental Mechanics*, pg. 105-110, Brookfield Center, CT, March 1983.

30. Young, W.C., *Roark's Formulas for Stress and Strain, Sixth Edition*. McGraw-Hill, Inc., New York, NY, 1989.

31. ERES Consultants, Inc., *Falling Weight Deflectometer Testing for Iowa Field Evaluation of Alternate PCC Pavement Reinforcement Materials*, Reports 1-4, Champaign, Illinois, 1997-99.

32. Eddie D. Fibre Reinforced Polymer Dowels for Concrete Pavements. *Masters Thesis*. University of Manitoba, 1999.

ACKNOWLEDGEMENTS

The research described herein was conducted at the Iowa State University Structural Engineering Laboratories in the Department of Civil and Construction Engineering through the promising success of the Engineering Research Institute and sponsored by the Highway Division of the Iowa Department of Transportation (IDOT) and the Iowa Highway Research Board. The authors would like to thank the personnel at the IDOT who provided support through their experience and knowledge toward the project, namely Chris Brakke, Jim Grove, Vernon Marks and Mark Dunn. The cooperation from Dr. James Cable in the collection of data from a related project was also appreciated.

The authors would also like to recognize and thank several firms for providing materials services, and advice, including: Doug Gremel from Hughes Brothers, Inc. of Seward, Nebraska; James P. McCallion from RJD Industries, Inc. of Laguna Hills, California; and Technical Services, Inc. of Ames, Iowa.

The authors would like to acknowledge the support provided by Douglas L. Wood, Structural Engineering Laboratory Supervisor, for his expertise and assistance. Appreciation is also extended to the many laboratory assistants, without whom this work could not have been completed.

APPENDIX A

RECTILINEAR, SEMI-LOG, AND LOG-LOG PLOTS

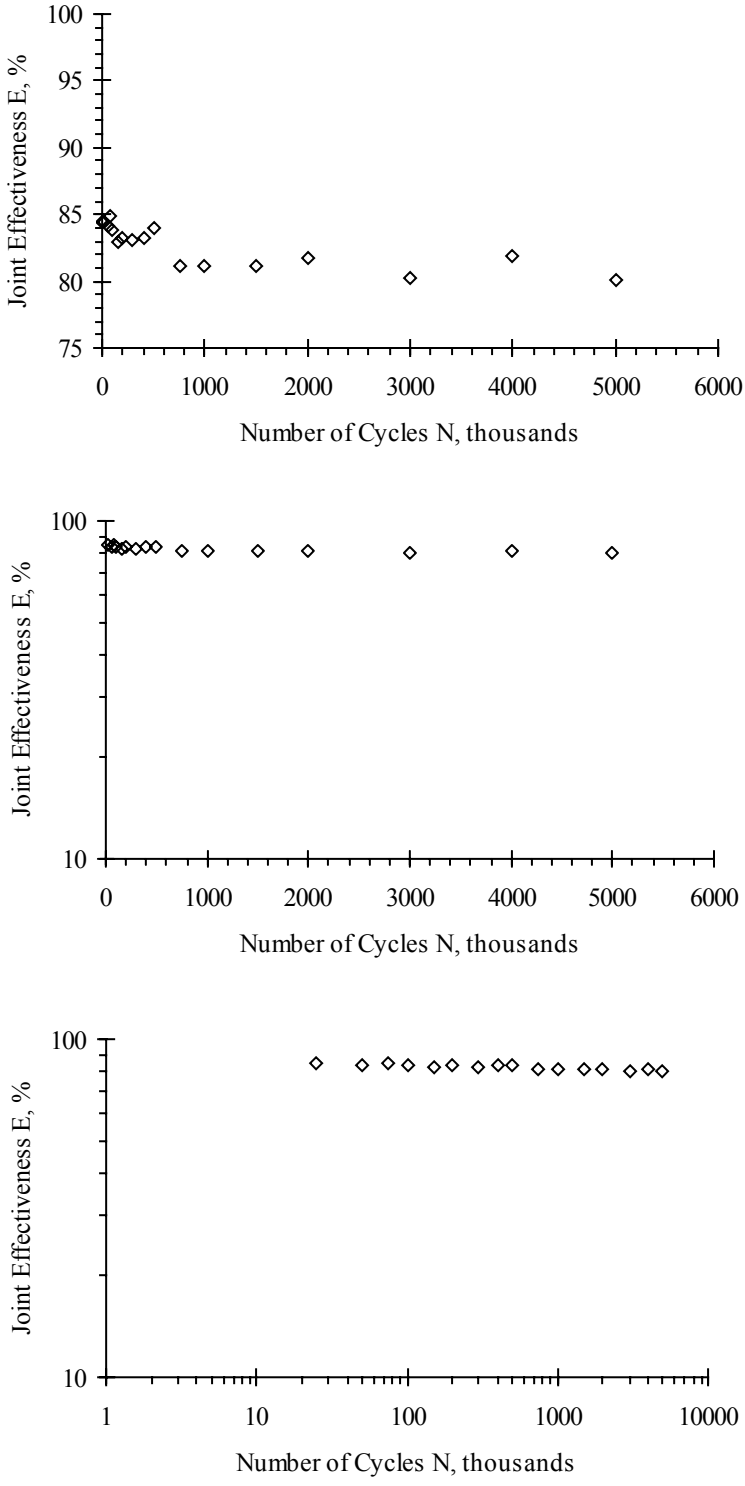

Figure A.1 Rectilinear, semi-log, and log-log plots of E vs. N for Slab 1

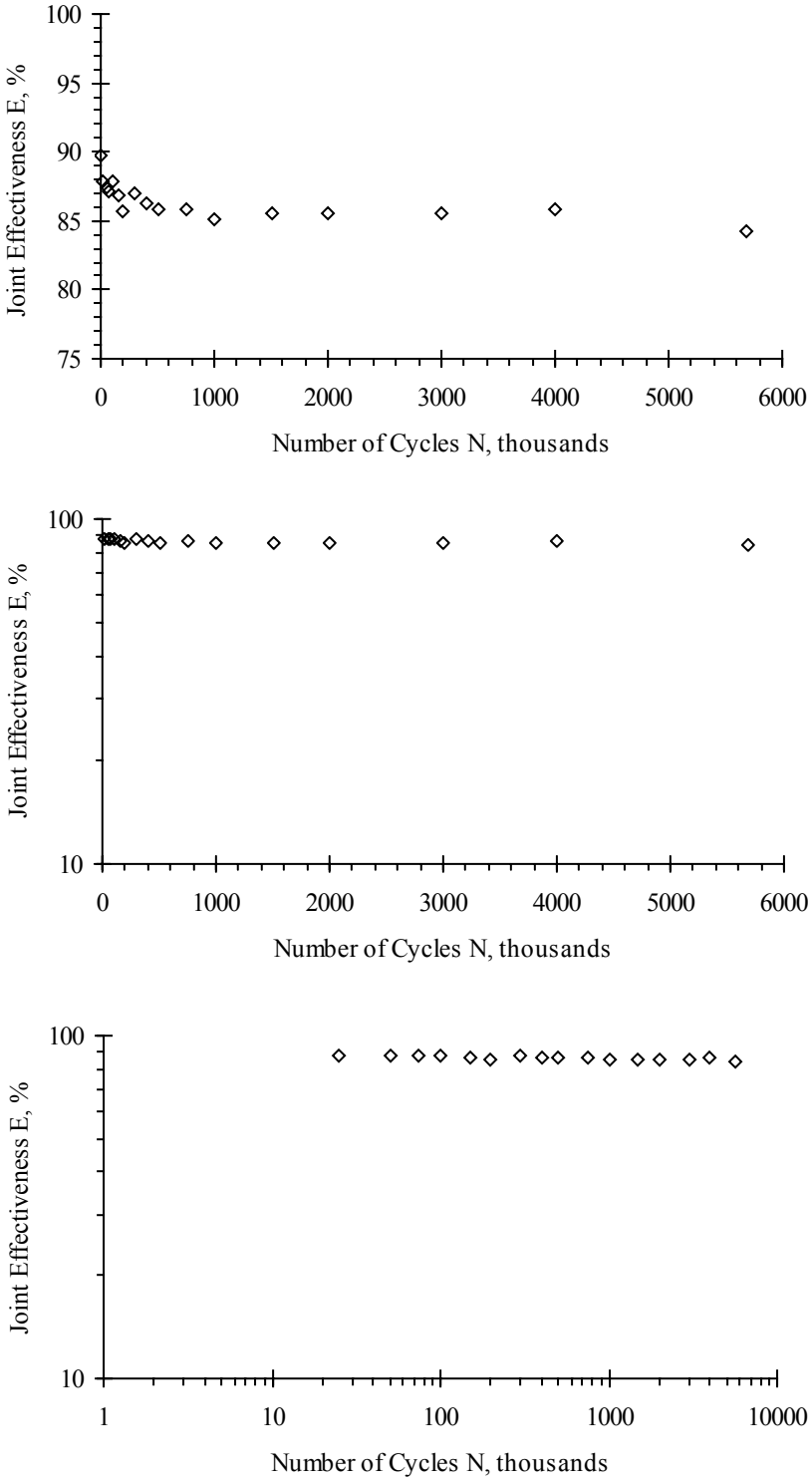

Figure A.2 Rectilinear, semi-log, and log-log plots of E vs. N for Slab 2

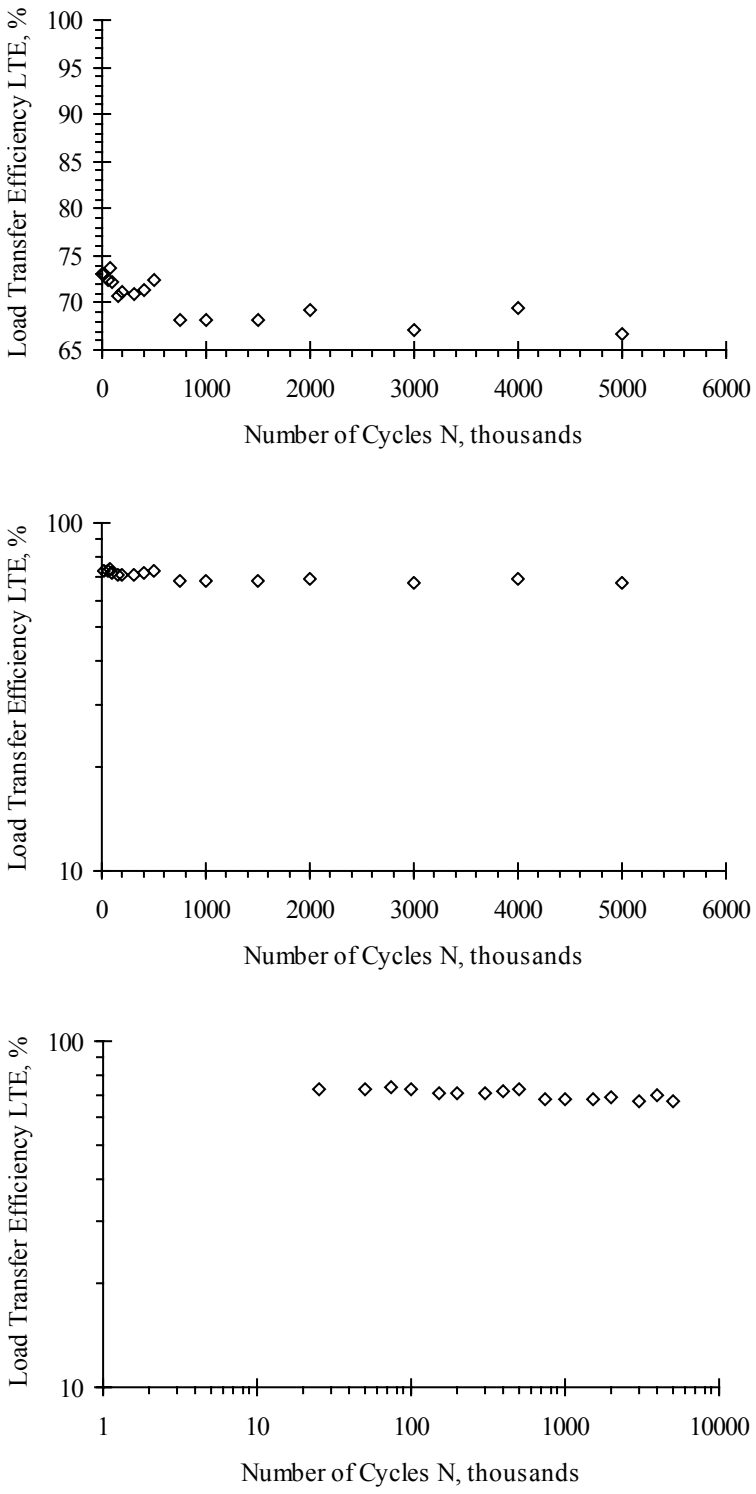

Figure A.3 Rectilinear, semi-log, and log-log plots of LTE vs. N for Slab 1

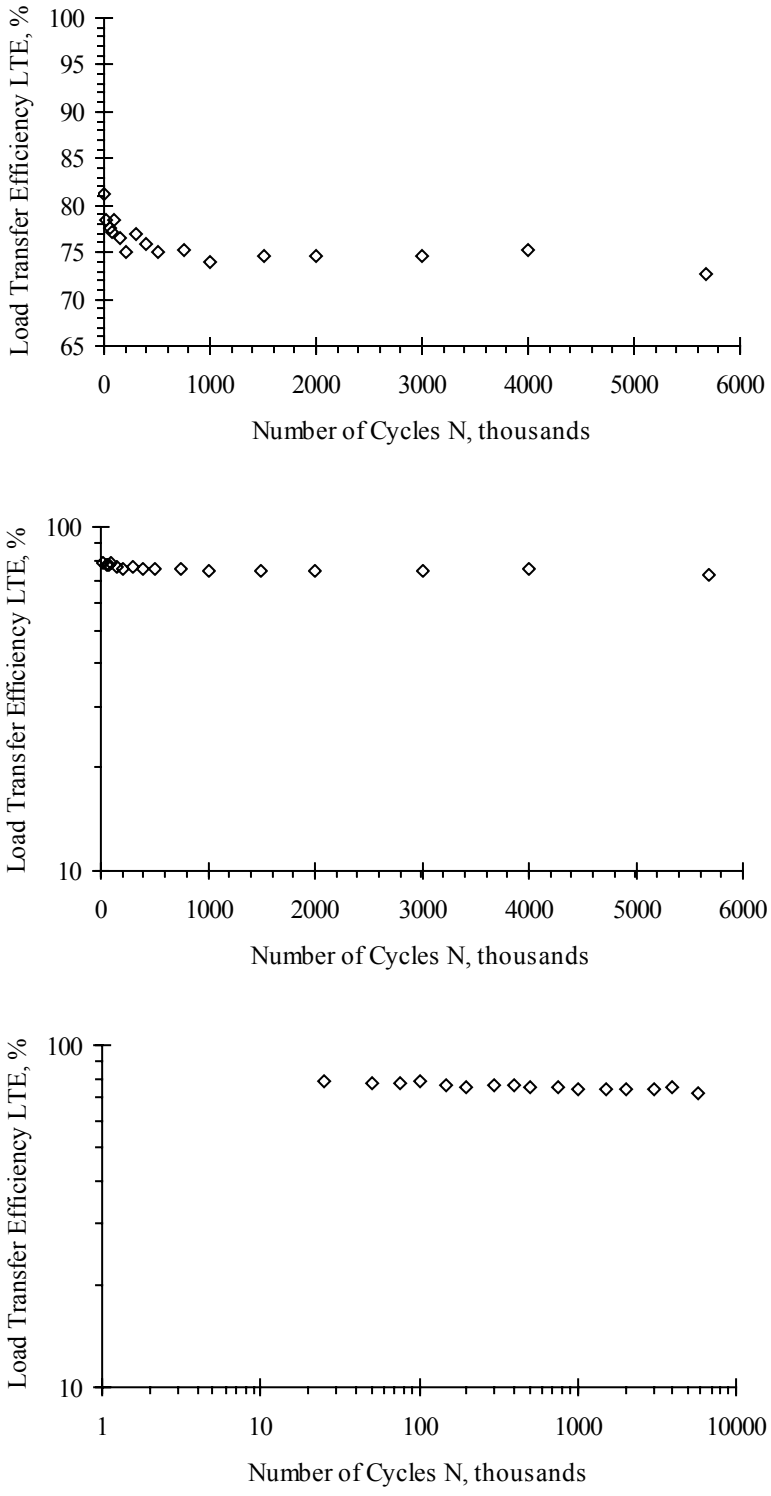

Figure A.4 Rectilinear, semi-log, and log-log plots of LTE vs. N for Slab 2

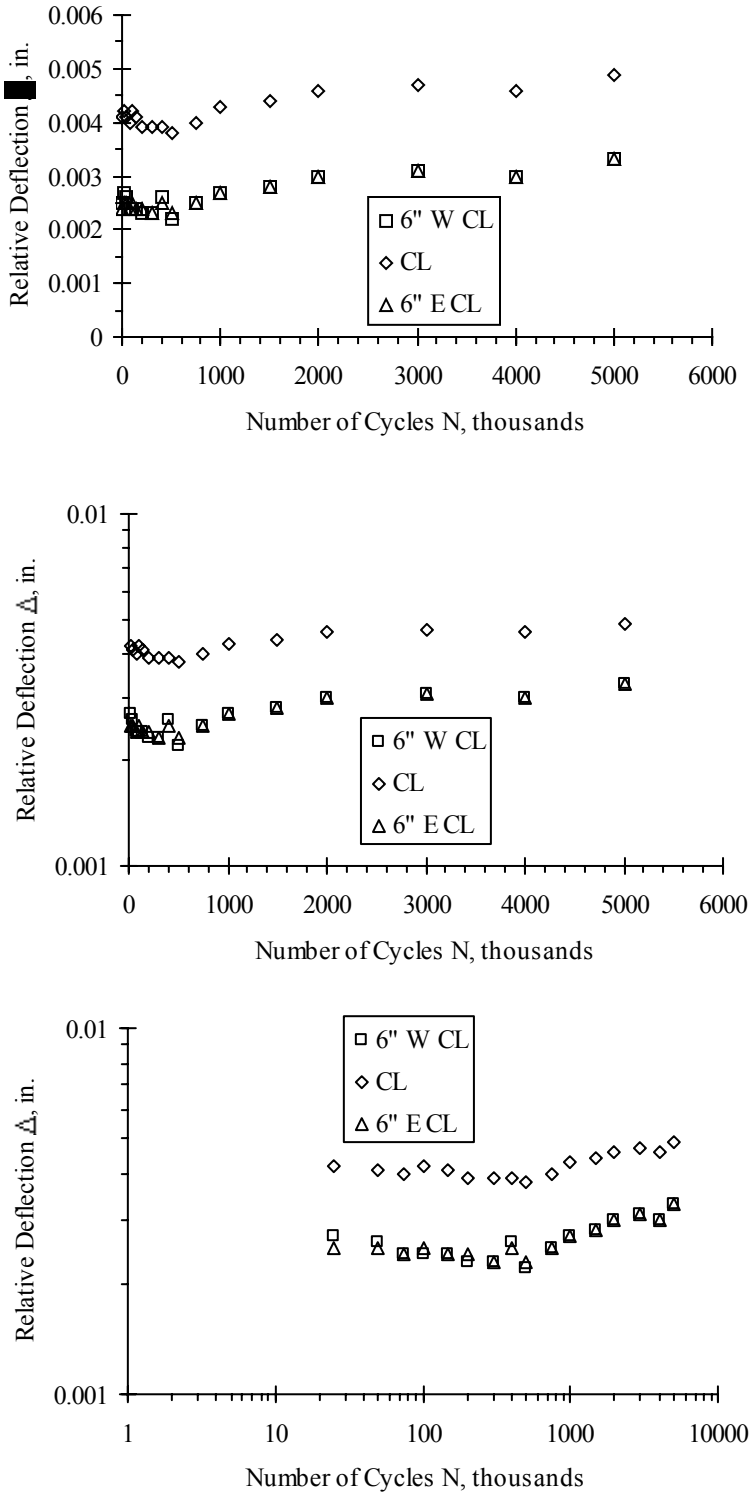

Figure A.5 Rectilinear, semi-log, and log-log plots of Δ vs. N for Slab 1

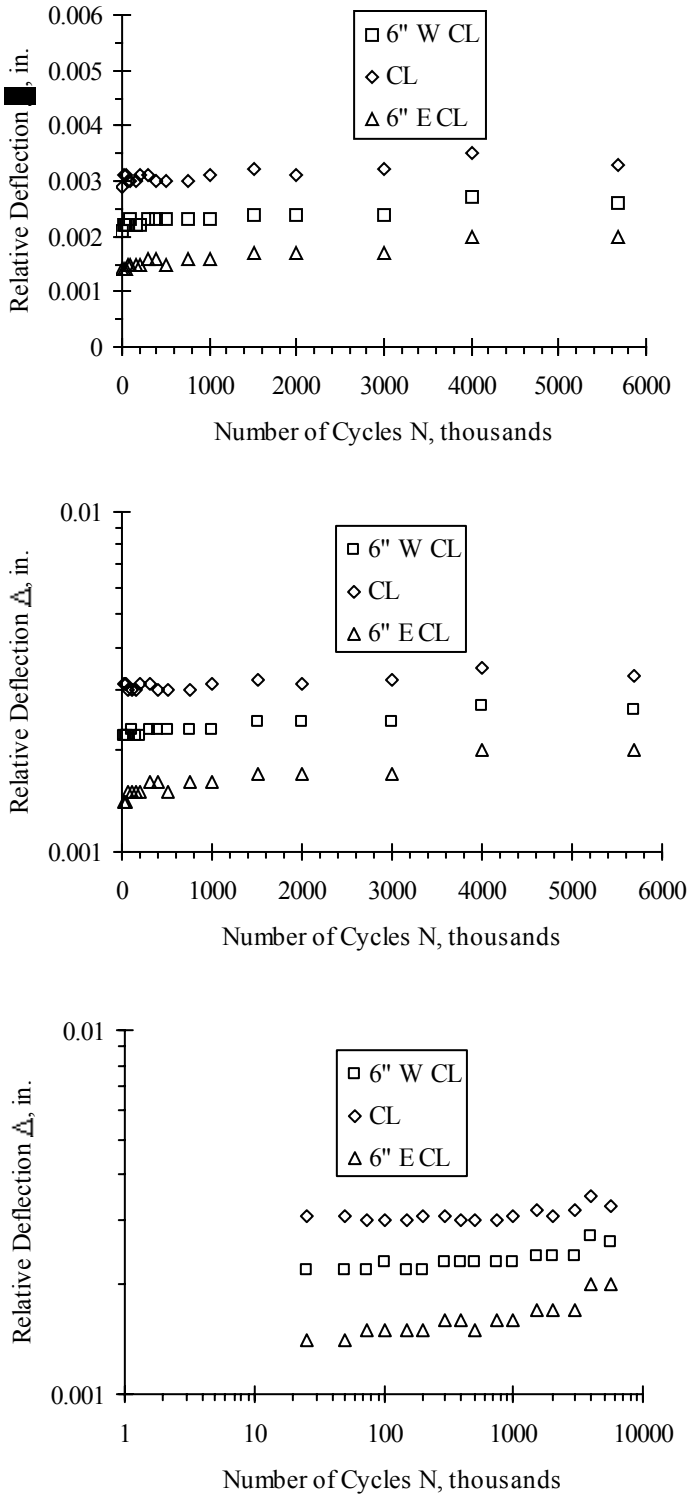

Figure A.6 Rectilinear, semi-log, and log-log plots of Δ vs. N for Slab 2

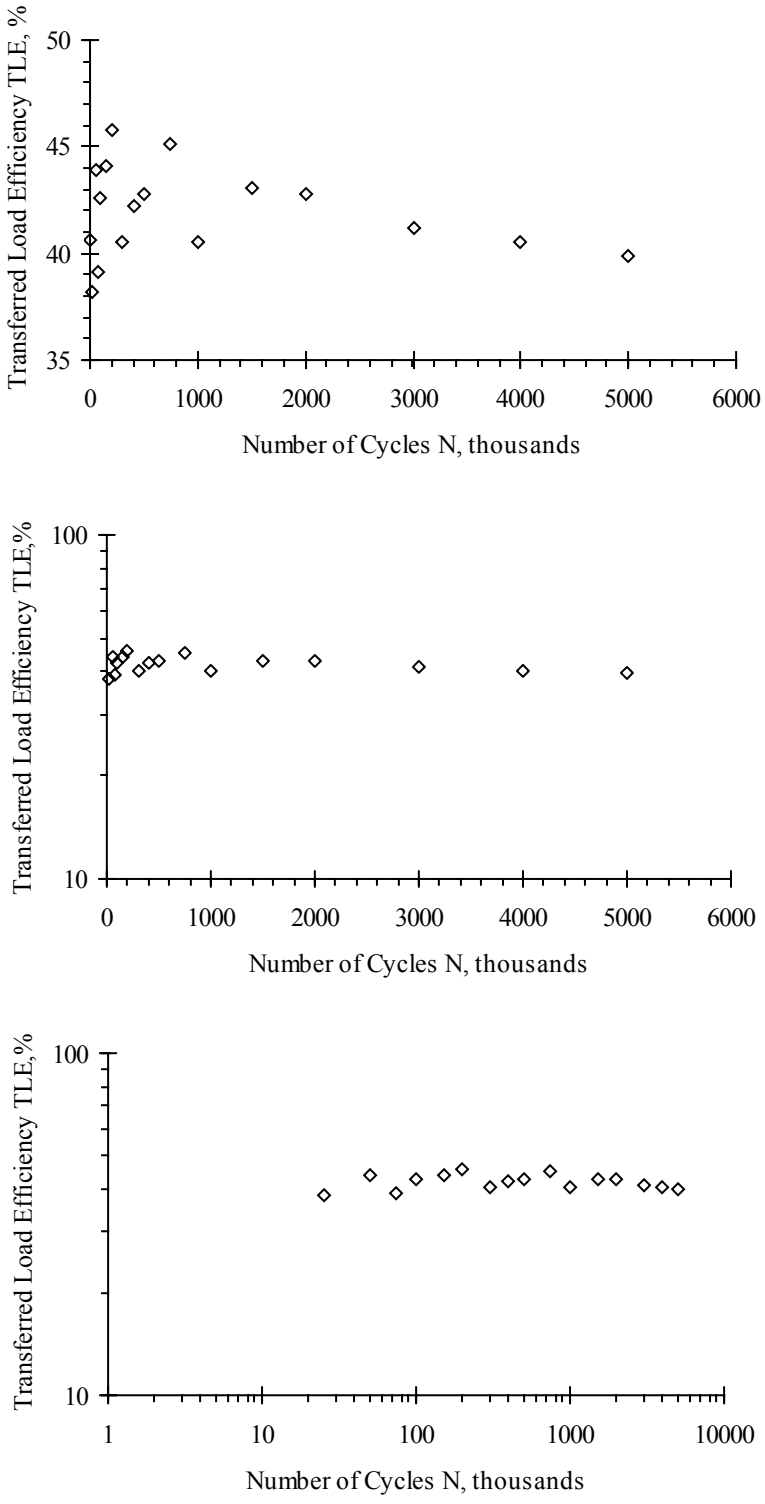

Figure A.7 Rectilinear, semi-log, and log-log plots of TLE vs. N for Slab 1

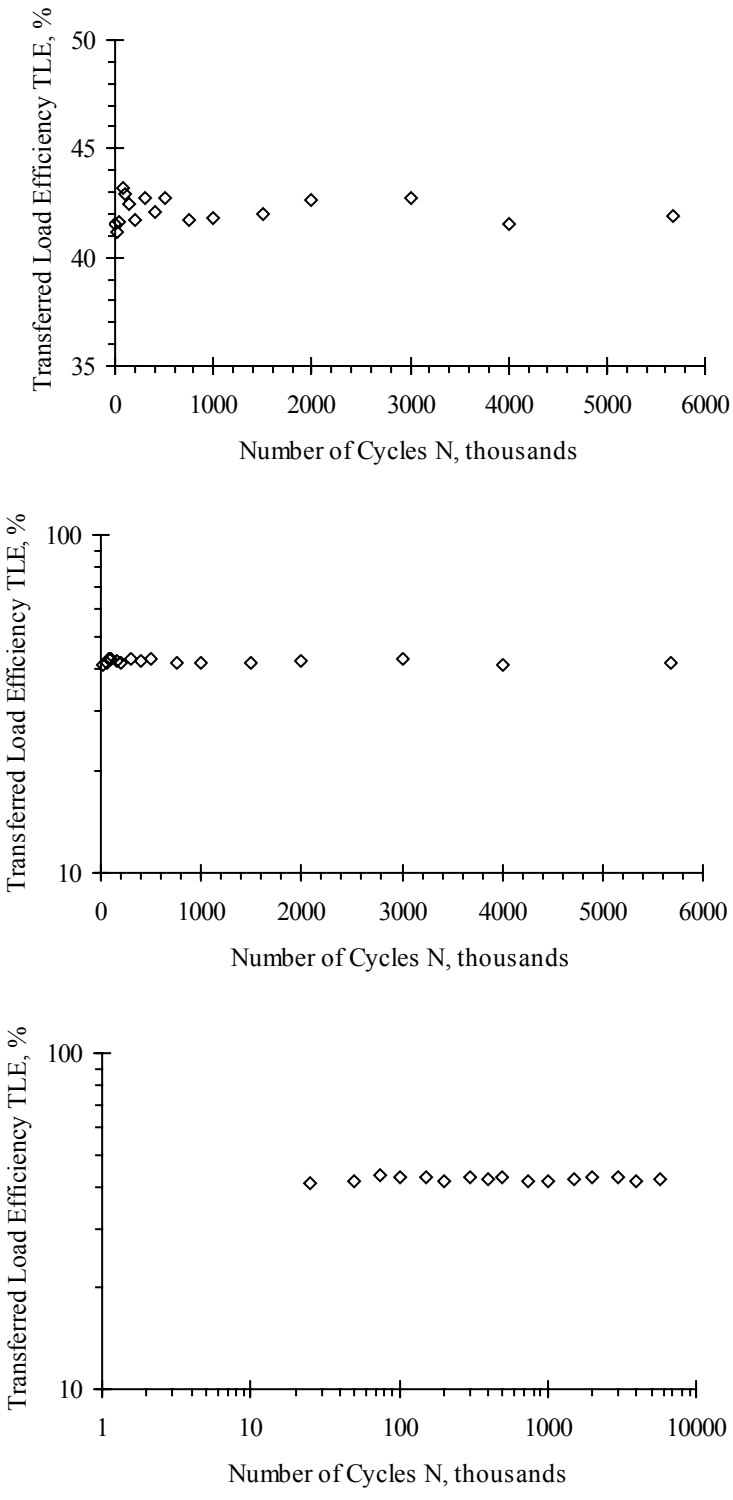

Figure A.8 Rectilinear, semi-log, and log-log plots of TLE vs. N for Slab 2

APPENDIX B

FORCE VS. STRAIN PLOTS FROM LOAD TESTS

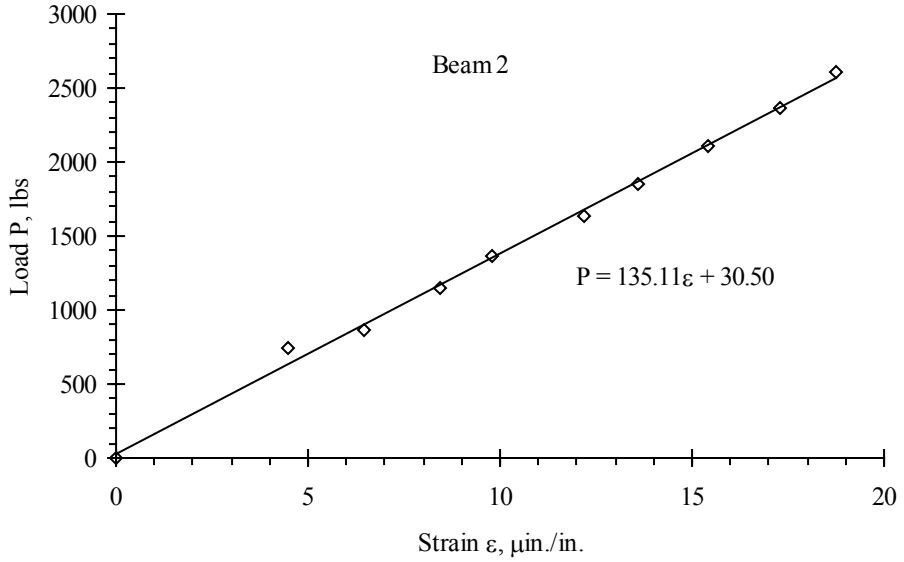

Figure B.1 Load vs. strain plot for Beam 2

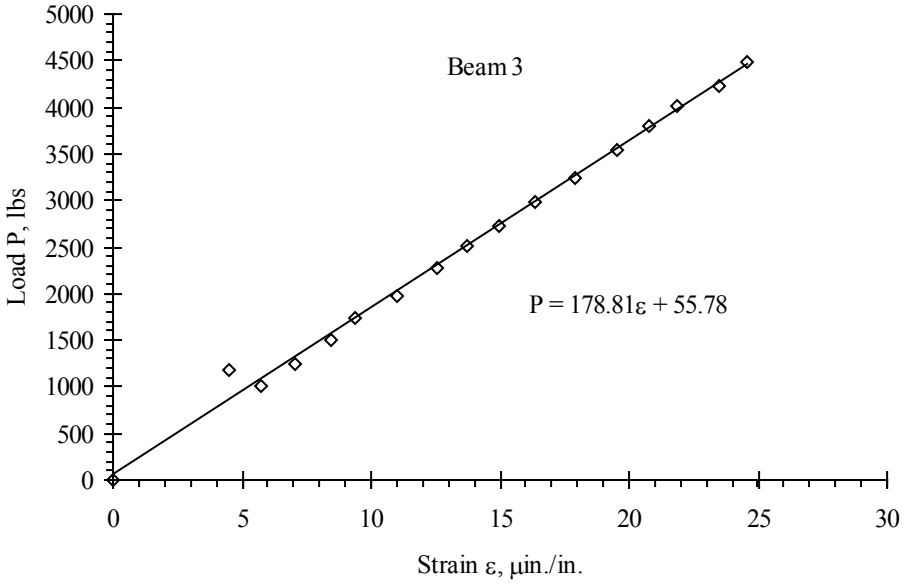

Figure B.2 Load vs. strain plot for Beam 3

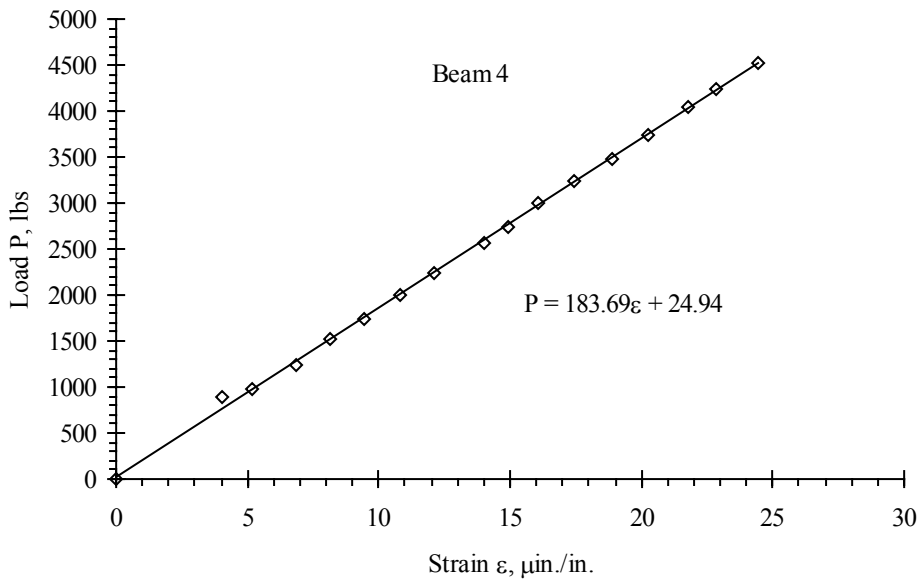

Figure B.3 Load vs. strain plot for Beam 4

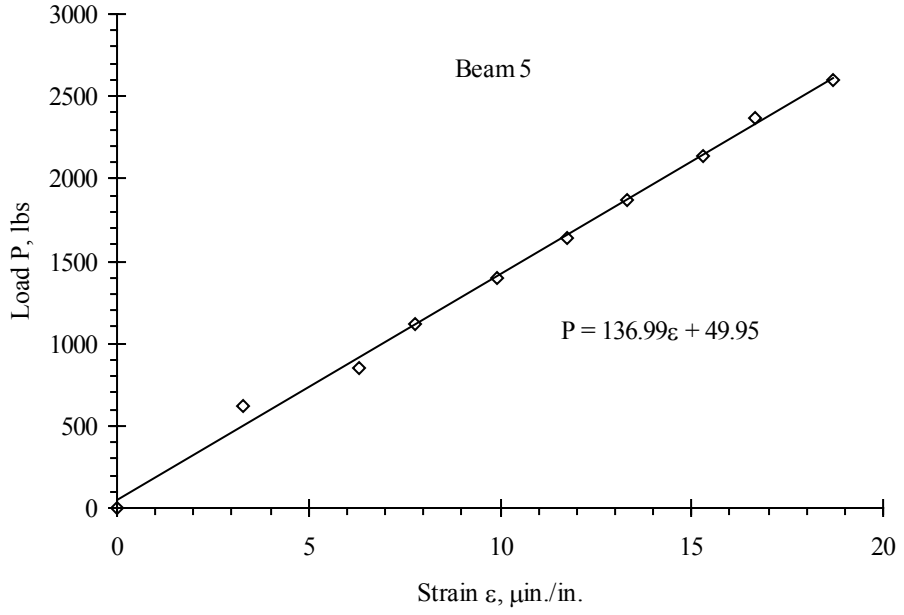

Figure B.4 Load vs. strain plot for Beam 5

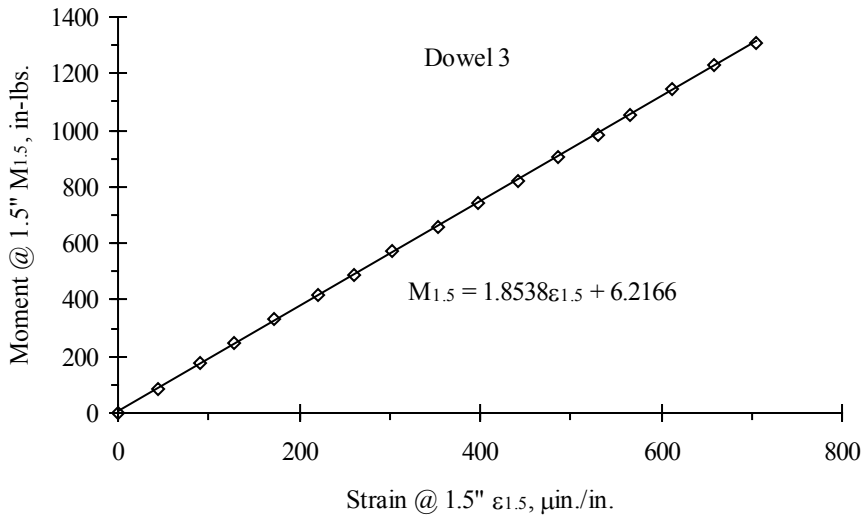

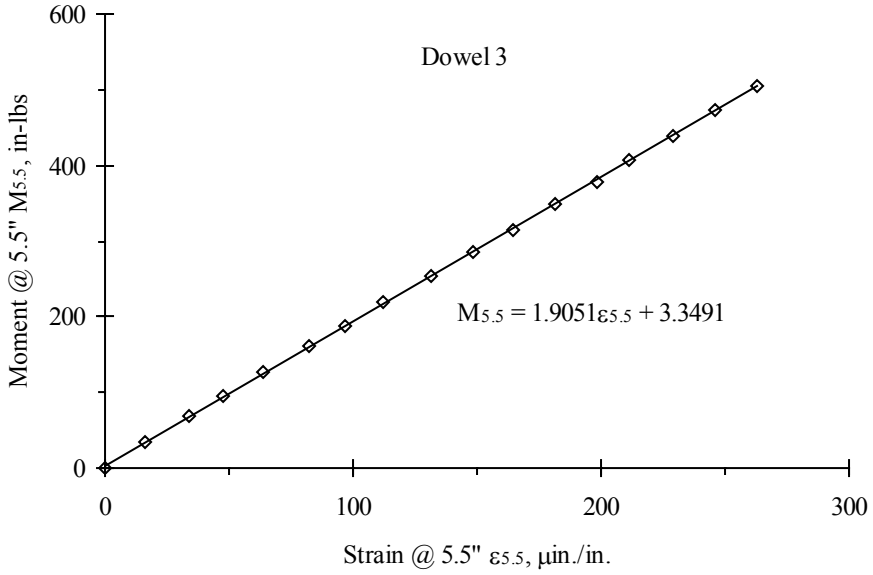

Figure B.5 Moment vs. strain plots for Dowel 3 in Slab 1

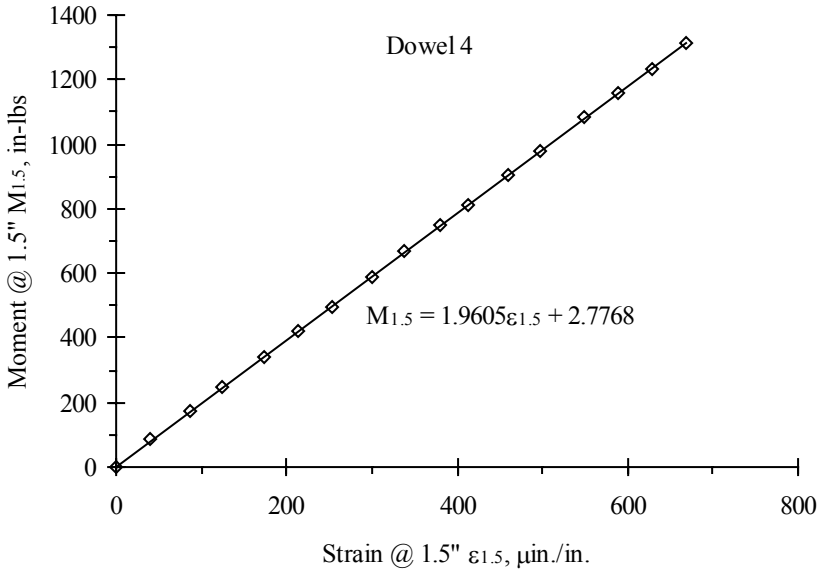

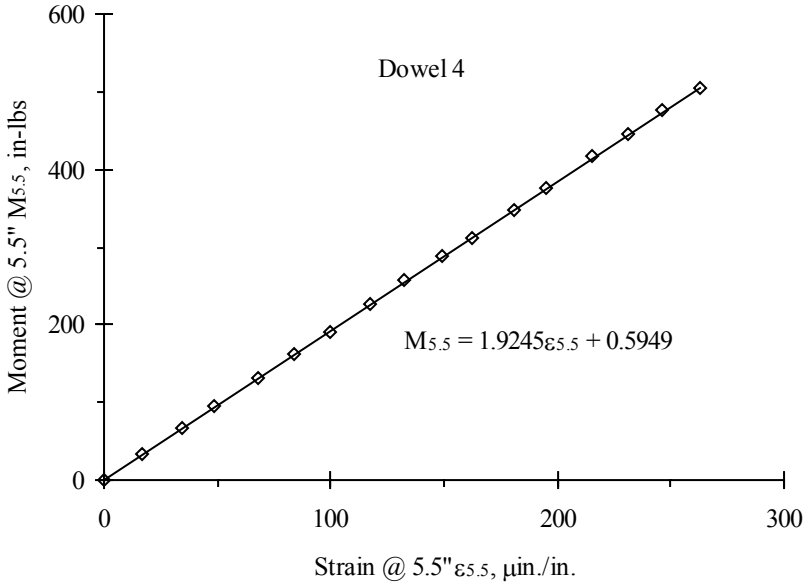

Figure B.6 Moment vs. strain plots for Dowel 4 in Slab 1

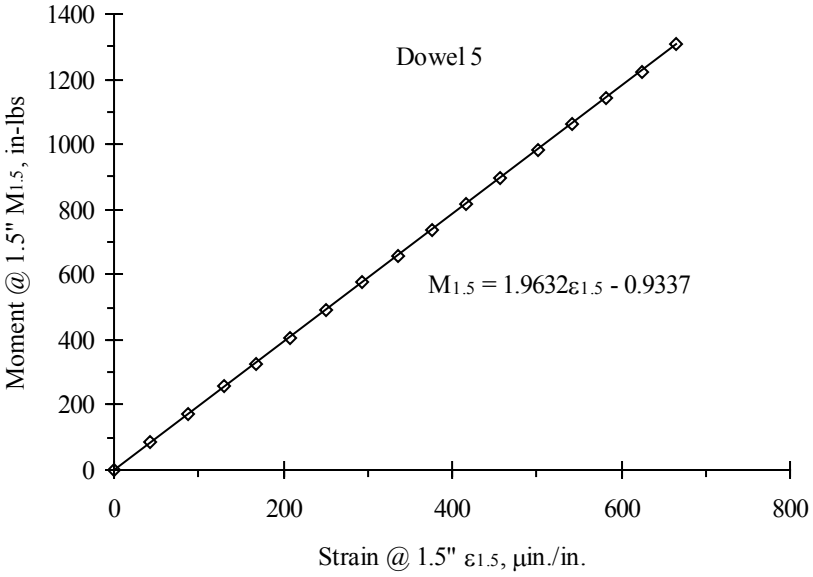

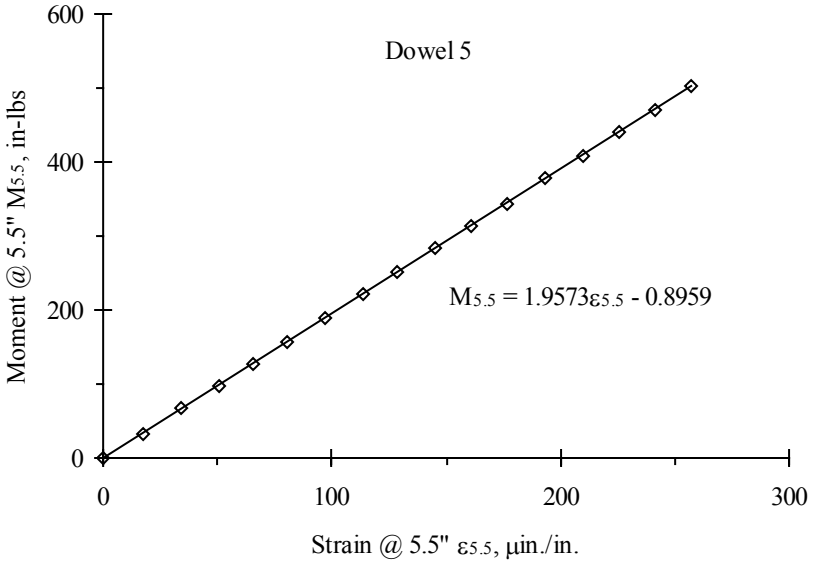

Figure B.7 Moment vs. strain plots for Dowel 5 in Slab 2

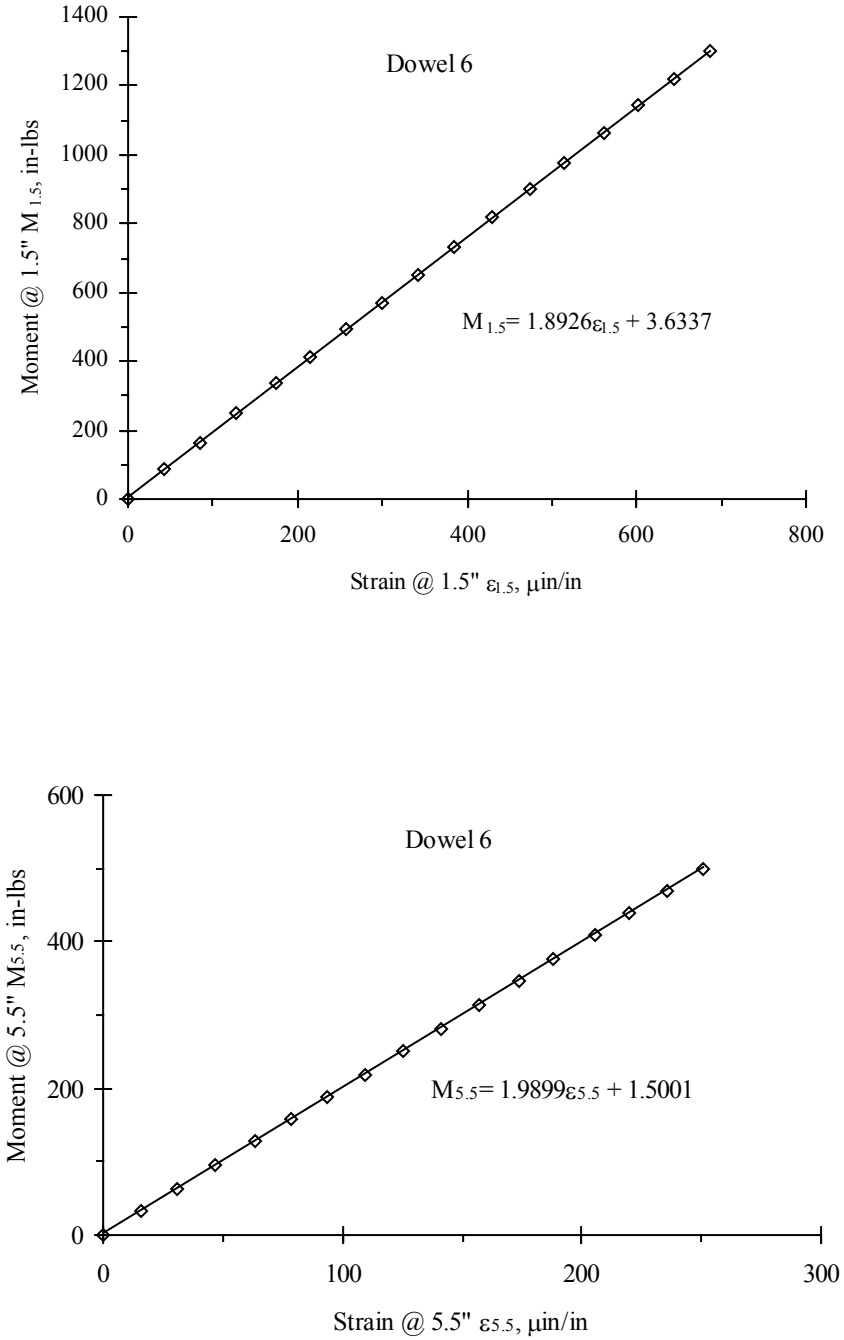

Figure B.8 Moment vs. strain plots for Dowel 6 in Slab 2

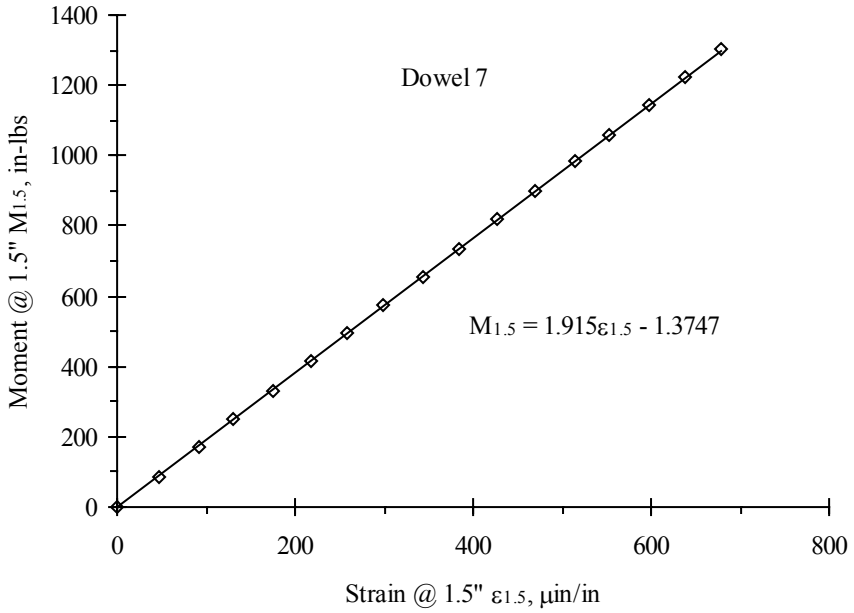

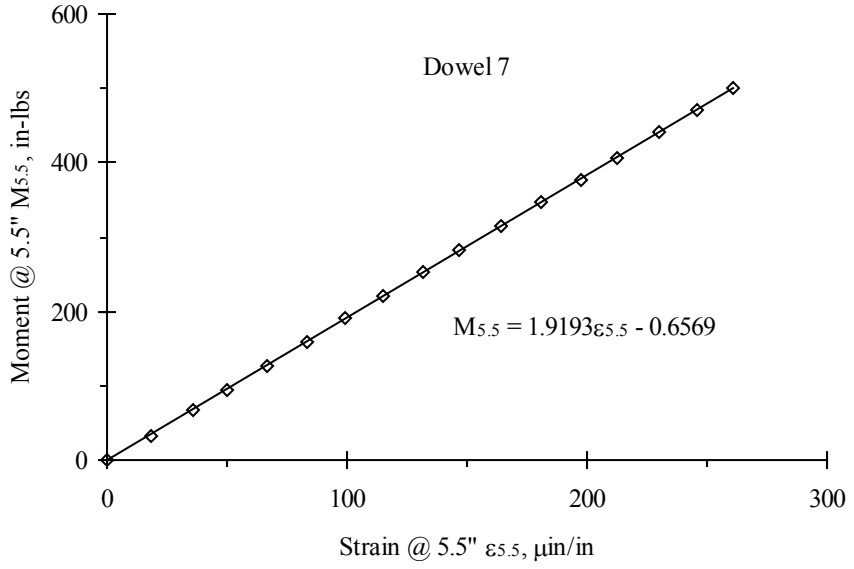

Figure B.9 Moment vs. strain plots for Dowel 7 in Slab 2